ISBN 978-82-326-4034-8 (printed version)
ISBN 978-82-326-4035-5 (electronic version)
ISSN 1503-8181

Doctoral Thesis

Einar Agnalt

2019:219

Einar Agnalt

Rotor Stator Interaction in Low-Specific Speed Francis Turbines

NTNU
Norwegian University of Science and Technology

2019:219

NTNU

NTNU
Norwegian University of
Science and Technology
Faculty of Engineering
Department of Energy and Process Engineering

NTNU
Norwegian University of
Science and Technology

Einar Agnalt

Rotor Stator Interaction in Low-Specific Speed Francis Turbines

Thesis for the degree of Philosophiae Doctor

Trondheim, September 2019

Norwegian University of Science and Technology
Faculty of Engineering
Department of Energy and Process Engineering

NTNU
Norwegian University of
Science and Technology

NTNU
Norwegian University of Science and Technology

Thesis for the degree of Philosophiae Doctor

Faculty of Engineering
Department of Energy and Process Engineering

ISBN 978-82-326-4034-8 (printed version)
ISBN 978-82-326-4035-5 (electronic version)
ISSN 1503-8181

2019:219

Printed by Skipnes Kommunikasjon as

Preface

This work has been conducted at the Waterpower Laboratory at the Norwegian University of Science and Technology in Trondheim. The research was carried out as a part of the HiFrancis research program sponsored by the Norwegian Research Counsil, The Norwegian Hydropower industry and the Norwegian Center for Hydropower.

Abstract

Several breakdowns in hydropower plants with low specific speed Francis runners have been reported. These breakdowns are understood to be related to pressure pulsations, vibration modulus and the combination of these. One of the main excitation forces in such runners is the pressure fluctuations originating from the rotor-stator interaction.

The primary objective for the thesis is to improve the understanding of the rotor-stator interaction to lower the risks of failure in future designs.

A setup for the investigation of the pressure pulsations related to the rotor-stator interaction is presented with the use of flush mounted pressure sensors, both onboard the runner and in the vaneless space. In addition, a position sensor is utilized to analyze the pressure data relative to the angular position of the runner.

The results from the onboard pressure measurements find that the phase of the guide vane passing pressure seen by the onboard pressure sensors are independent of the guide vane opening. Hence, the potential flow interaction is found to be the dominant effect and no evidence from the viscous wake effect is found on the onboard pressure. A clear resonance peak in the pressure field excited by the second harmonic of the guide vane passing frequency is found in the onboard measurements. The measured pressure is divided into the hydraulic effects and the effects from the Fluid Structure Interaction,

named the convective and acoustic pressure. The eigenfrequency and damping are estimated from the measurements. The convective pressure field seems to diminish almost linearly from inlet to outlet of the runner, while the acoustic pressure field has the highest amplitudes in the middle of the runner channel. At resonance, the acoustic pressure clearly dominates over the convective pressure.

In the vaneless space the pressure is known to be a combination of two effects; the rotating runner pressure and the throttling of the guide vane channels. The measured pressure is fitted to a theoretical pressure model to separate the two effects for two different runners. The main findings show that the pressure fluctuations in the guide vane cascade are controlled by throttling for low blade loading and the rotating runner pressure for higher blade loading.

The results are considered as a good reference for computational fluid dynamics validation and enables researchers to verify their codes and increase the accuracy in the calculation of new designs to reduce the risk of breakdowns in the future.

Keywords: Hydraulic turbine, Francis turbine, rotor-stator interactions, RSI, fluid-structure interaction, FSI, pressure pulsations

Acknowledgments

The work with this project would not have been possible without several contributors and partners. First of all, a special thanks to my supervisor Ole Gunnar Dahlhaug for his support and the never-ending belief in this project. My co-supervisor Pål-Tore Storli gave me a lot of fruitful discussions and ideas to confuse my mind. Also, a great thanks you to all colleagues at the Waterpower Laboratory and in the HiFrancis project for all the good discussions. I must also give an even more special thank you to Igor Iliev for all the discussions, both funny and technical topics, and all the shared knowledge.

Without the technical staff in the Laboratory, the experiments conducted in this work would never ended. Joar Grilstad, Trygve Oppland and Halvor Haukvik could not have been replaced by anybody to do this project better. I am most grateful to Halvor for the support during dark evenings with trouble, and for all the great technical solutions. I will also direct the attention to the EPT administration, Anita Yttersian and Wenche Johansen in particular. You have always been helpful and positive.

The final most grateful thanks is to my wife, Anna, for the support and for listening to the explanation of solutions and the frustrations through the project sometimes without the faintest idea of what I talked about.

List of publications

This thesis is a collection of papers found in Part II. The main papers focus on the measurements and the physics related to the Rotor-stator Interaction. Additional papers related to the measurement work in the thesis is presented with the abstract and comments about the relevance to the thesis in Part III.

Papers main research

A. Agnalt, Einar; Solemslie, Bjørn Winther; Dahlhaug, Ole Gunnar. (2019) *Onboard measurements of pressure pulsations in a high head Francis model runner.* IOP Conference Series: Earth and Environment. vol. 240.

B. Agnalt, Einar; Solemslie, Bjørn Winther; Dahlhaug, Ole Gunnar. *The rotor-stator interaction onboard a low specific speed Francis turbine.* – International journal of fluid machinery and systems: For review

C. Agnalt, Einar; Iliev, Igor; Solemslie, Bjørn Winther; Dahlhaug, Ole Gunnar. (2019) *On the Rotor Stator Interaction Effects of Low Specific Speed Francis Turbines*. International Journal of Rotating Machinery. vol. 2019.

D. Agnalt, Einar; Østby, Petter Thorvald Krogh; Solemslie, Bjørn Winther; Dahlhaug, Ole Gunnar. (2018) *Experimental Study of a Low-Specific Speed Francis Model Runner during Resonance.* Shock and Vibration. vol. 2018.

Papers additional work

1. Trivedi, Chirag; Agnalt, Einar; Dahlhaug, Ole Gunnar. (2017) *Investigations of unsteady pressure loading in a Francis turbine during variable-speed operation.* Renewable Energy. vol. 113.

2. Trivedi, Chirag; Agnalt, Einar; Dahlhaug, Ole Gunnar. (2018) *Experimental study of a Francis turbine under variable-speed and discharge conditions.* Renewable Energy. vol. 119.

3. Trivedi, Chirag; Agnalt, Einar; Dahlhaug, Ole Gunnar. (2018) *Experimental investigation of a Francis turbine during exigent ramping and transition into total load rejection.* Journal of Hydraulic Engineering. vol. 144 (6).

4. Sannes, Daniel B.; Iliev, Igor; Agnalt, Einar; Dahlhaug, Ole Gunnar. (2018) *Pressure Pulsation in a High Head Francis Turbine Operating at Variable Speed.* Journal of Physics, Conference Series. vol. 1042 (1).

5. Trivedi, Chirag; Agnalt, Einar; Dahlhaug, Ole Gunnar; Brandåstrø, Bård Aslak. (2019) *Signature analysis of characteristic frequencies in a Francis turbine.* IOP Conference Series: Earth and Environment. vol. 240.

6. Iliev, Igor; Trivedi, Chirag; Agnalt, Einar; Dahlhaug, Ole Gunnar. (2019) *Variable-speed operation and pressure pulsations in a Francis turbine and a pump-turbine.* IOP Conference Series: Earth and Environment. vol. 240.

7. Solemslie, Bjørn Winther; Trivedi, Chirag; Agnalt, Einar; Dahlhaug, Ole Gunnar. (2019) *Pressure Pulsations and Fatigue Loads in High Head Francis Turbines.* IOP Conference Series: Earth and Environment. vol. 240.

8. Østby, Petter T. K., Agnalt, Einar, Haugen, Bjørn, Billdal, Jan Tore. (2019) *Fluid structure interaction of Francis-99 turbine and experimental validation.* Francis-99 Third workshop. To be published

Contents

Structure of the Thesis

The thesis is divided into three parts. Part I is describing the background and the available literature in the field of research to create the basis for the objectives of the thesis. Based on the available literature and the experience in the current work, some additional theory about the Rotor-stator Interaction is presented. Towards the end of the Part I, some details about the measurement procedure and uncertainty analysis utilized in the papers can be found before the papers are summarized. The final words are used to present the conclusions and the recommendations for further work.

In Part II and Part III, papers are presented. Part II is the main first author work, which is the base of the current thesis. In Part III, the abstracts and comments about additional papers written in collaboration with the team at the Waterpower Laboratory are presented. The experimental data in the papers is from the same measurement setup as presented in the thesis, but the scope and objective is different.

List of figures

List of symbols

Latin symbols

g	gravitational acceleration [ms^{-2}]
H	Head [m]
k	number of diametrical modes [-]
m	arbitrary integer [-]
n	harmonic number [-]
N	rotational speed [s^{-1}]
N_{QE}	specific speed [-]
$\tilde{p}_E$	Fluctuating pressure as percentage of specific energy [%]
Q	Discharge [m^3s^{-1}]
Z_g	number of guide vanes [-]
Z_r	number of runner blades [-]

Abbreviations

3D	Three dimensions
BEP	Best Efficiency Point
CFD	Computational Fluid Dynamics
DAQ	Data Acquisition
EPT	The Department of Energy and Process Engineering
FSI	Fluid-Structure Interaction

HP	High Pressure
IEC	International Electrotechnical Commission
ISO	International Organization for Standardization
LP	Low Pressure
ND	Nodal Diameter
NTNU	Norwegian University of Science and Technology
RMS	Root-mean-square
RSI	Rotor-stator Interaction
STFFT	Short Time Fast Fourier Transform

Part I – Summary

1. Introduction

1.1 Motivation

The high focus on the environment and green energy along with an aging Norwegian Hydropower industry, leads to refurbishment of the power plants and the construction of new turbines. Some new installed Francis runners have experienced breakdown after a few running hours, which gives concerns to the validity of the calculations and simulations behind the design of the runners. The connection between the water and the structure in the runner, the fluid structure interaction (FSI) is believed to be one of the root causes for the failures. The pressure pulsations in the fluid and its relations to the resonance frequencies in the runner are of main interest. Historical data for 368 investigated Francis units is shown in Figure 1. Units from 450m Head had the highest historical possibility of cracking.

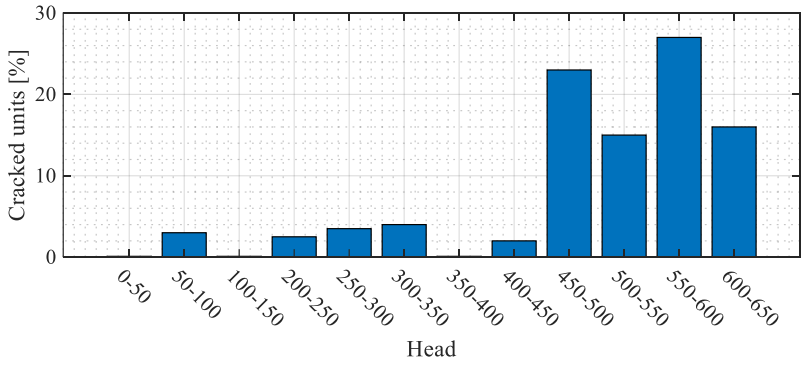

Figure 1 Cracks in Francis runners before 2009. Data from 368 turbines[1].

In the literature, the classification of a turbine is usually done with a parameter named the specific speed. Several definitions exist, but the recommendation in IEC62097[2] is proportional to rotational speed and discharge and inverse proportional to the head giving

$$N_{QE} = \frac{NQ_1^{0.5}}{(gH)^{0.75}} \quad (1)$$

where N is rotational speed, Q is discharge, g is gravitational acceleration, and H is head.

For the data in Figure 1, the turbines with the higher head will be found in the lower range of the specific speed. The design of Francis runners is a complex optimization where the efficiency and durability in the range of operation are balanced with cost. Several parameters are evaluated as size, submergence, cavitation, water velocities, rotational speed and structural strength. The usual design for low specific speed runners is with longer blades in the meridional view and small radial gap between the guide vanes and the leading edge of the runner blades as shown in Figure 2. The smaller gap gives higher influence on the runner from the pressure in the guide vane cascade and higher influence on the guide vane cascade from the runner. This two-way influence is known as the rotor-stator interaction.

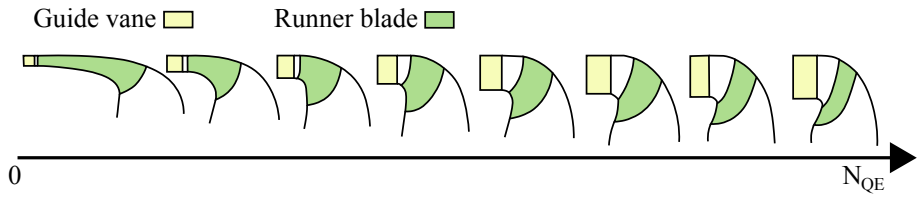

Figure 2 Radial view of Francis runners with increasing specific speed[3]

Today's runners are design with the use of computers. To improve the quality and reliability of the calculations and simulations, verifications based on experimental data must be performed. This requires access to a runner and the full geometry, preferably a prototype runner. Due to proprietary rights, the access to a prototype runner and the 3D geometry is restricted, hence in this study, measurements on the open access Francis 99 runner is performed to provide data for the verification of calculations and simulations.

1.2 Background

The following section focus on previous work related to onboard measurements in turbines, the rotor-stator interaction and the frequency response of runners.

Onboard measurements

Measurements including moving fluids and transient properties, as pressure pulsations, could be severely influenced by the mounting method of the sensor [4,5]. Today, pressure sensors with high accuracy and small sizes are available with flush mounted diaphragm. For applications where accurate flush mounting is possible, the uncertainty related to the hole size, the transmission tubes and the cavities will be removed[6]. Already in the 80s, miniature flush mounted sensors were utilized to analyze the onboard pressure in an axial-flow compressor as shown in Figure 3[7]. The sensors were flush mounted on both stator and rotor blades. Later, several studies utilized onboard measurements with flush mounted miniature sensors in rotating domains. Perrig et.al[8] did measurements in a Pelton bucket, Jansson and Cervantes[9] on a Kaplan runner, Berten et.al in a centrifugal pump impeller[10] and Münsterjohann and Becker[11] did pressure measurements in the rotating domain of a side channel blower.

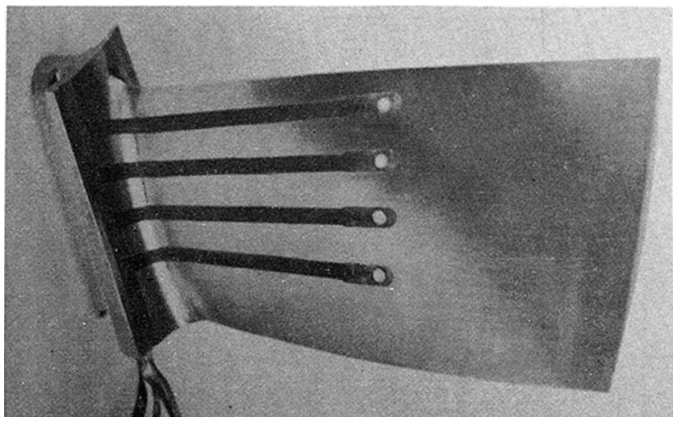

Figure 3 Onboard measurements in an axial-flow compressor[7].

In hydropower research related to Francis runners, Avellan et.al[12], Fahrat et.al[13] and Lowys et.al[14] presented a setup for onboard measurements in a low head Francis runner. Duparchy et.al [15] analyzed the onboard pressure influence from the vortex rope

in a similar setup. Gao et.al [16] did an analysis of the correlation between onboard and surrounding pressure where the experimental setup included pressure sensors on the surface of the blades. Kobro et.al did onboard measurements on the same runner as in the current thesis, but the complexity of the setup and durability of the sensors were not satisfactory[17]. Hasmatuchi[18] did a study, which aimed to improve the understanding of pressure fluctuations due to the Rotor-stator interaction (RSI) in high head pump turbines. The experimental setup was designed to collect data from wall pressure measurements in both the stationary and the rotating domain. The setup included pressure transducers in two consecutive impeller channels, with sensors mounted on both pressure and suction sides of the impeller blades as shown in Figure 4. The hub and shroud surfaces were also monitored.

The acquisition of data in the rotating domain was found with different methods in the literature, including telemetry, slip-ring, onboard acquisition and a combination of onboard acquisition and digital transfer with a slip-ring.

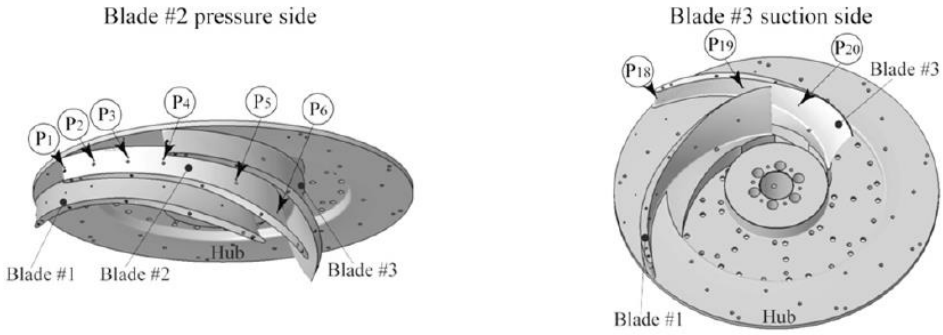

Figure 4 Onboard pressure transducers on impeller blades[18].

A description of the onboard measurements in the current thesis is covered in paper A.

The rotor-stator interaction

The rotor-stator interaction (RSI) is the main excitation force on a low specific speed runner[19]. With higher head and material savings in the runners, the RSI was known to be the root cause for several blade cracks and breakdowns in low specific speed Francis turbines

and pump turbines [20,21]. The nature of the RSI is commonly divided into potential flow interaction and viscous wake interaction[7,22–24]. The effect from potential flow interaction is related to the lift on the guide vanes and the accelerated flow in the cascade, which creates a low and high pressure side of the guide vanes[25]. The viscous wake effect is the defects in the flow field affecting the velocity distribution at the runner inlet[26]. Kobro[17] focused on the pressure fluctuations in the channel but the details in the RSI physiscs were not covered. Similar onboard studies were conducted by Zobeiri[27] and Hasmatuchi[18] in a pump turbine. Lewis et.al[28] showed that the use of distributor vane jets effected the torque fluctuations in the runner. Possibly, the potential effect was reduced by disturbing the guide vane trailing edge stagnation point. Moreover, several numerical studies of the RSI are available[29–31]. Nennemann et.al[32] showed how the non-uniform potential pressure and the velocity in the vaneless space created phase shifted torque variations on the blades as shown in Figure 5.

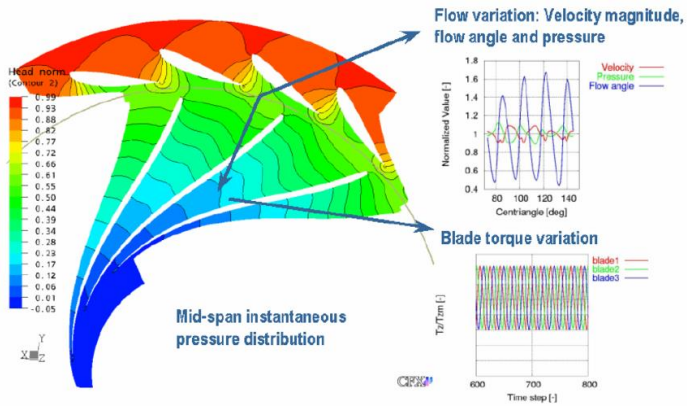

Figure 5 Rotor-stator interaction in a Francis turbine[32]. The potential interaction creates torque variations on the blades due to pressure and velocity fluctuations.

Several studies focus on how the RSI fluctuations in Francis and pump runners effect the surroundings of the runner and how to predict the pressure fluctuations. Zobeiri et.al [33] focused on the pressure propagation of the RSI in the guide vane cascade and the spiral casing in a pump-turbine. Yonezawa et.al [34] showed how the RSI interacted with the penstock waves and created a resonance condition. Ciocan and Kueny [35] and Hasmatuchi [18] did detailed studies of the velocity field in the vaneless space and the guide vane

cascade. Major findings were how the runner blades created a blockage of the flow in the guide vane channels and thereby creating a velocity fluctuation in the entire guide vane cascade.

More details about the rotor-stator interaction onboard the runner and in the vaneless space can be found in paper B and C.

The frequency response and mode shape of a runner

The knowledge about frequency response of turbines originates from the early days of steam turbines and bursting of turbine disks[36]. Several one-dimensional attempts were made to solve the problem. The first known modal vibration analysis, where both the group of frequencies and shapes were determined, were published in 1948[37]. In hydropower, some incidents with noise from turbines have been reported[20,38]. Tanaka et.al [21] reproduced the work of Tyler and Sofrin[39] to describe problems with high head reversible turbines and showed that the hydraulic excitation of the runner and the structural frequency response coincided in both frequency and modal shape. The discussion included the change in resonance frequency when the runner is submerged, denoted the added mass effect, and details about the design profile of the runner and the gap between the runner and the surrounding structure. Valentín et.al[40] analyzed the influence of the boundary conditions further and found the radial gaps as the most affecting factors on the resonance frequencies and mode shapes.

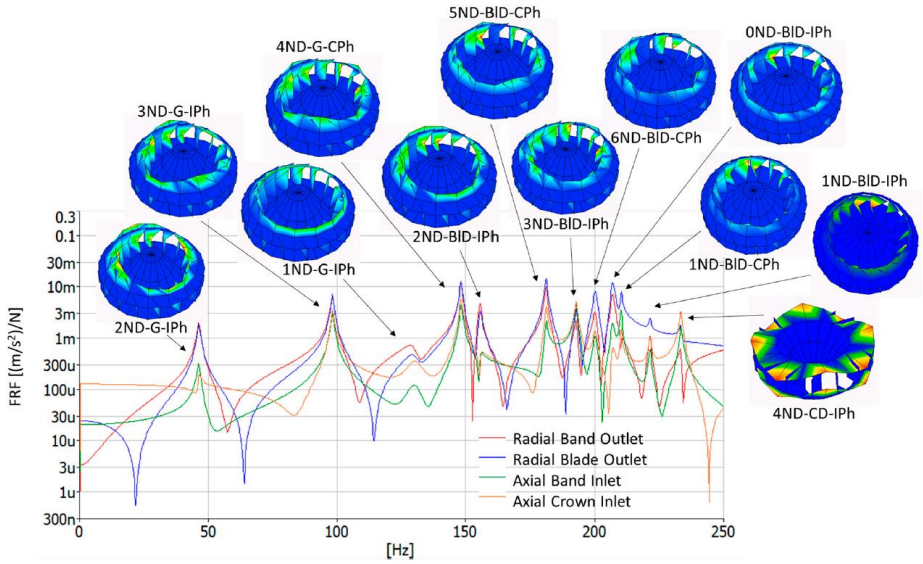

Figure 6 The modes of a runner[41]

The surrounding structure of the runner has a large impact on the natural frequencies and damping, hence the analysis should preferably be carried out with the runner mounted in the housing[21,42]. Presas et.al analyzed the frequency response of a pump turbine while mounted in the housing, but the use of two electronic muscles were not sufficient to excite all modes[43]. Østby et.al did similar experiment but with six patches on a six bladed model with good results. Major findings included that the modes with large movement of the hub and shroud, the global modes, disappeared when the runner was mounted in the housing. The blade modes were minimally affected by the housing[44]. Valentín et.al analyzed the natural frequencies of a prototype turbine through impact excitation in air, and later, pressure field excitation while in operation as shown in Figure 6. The results included natural frequencies excited during startup and frequencies excited by random phenomena's in part load and high load. By utilizing the excitation which naturally occurs in the operation of the runner, excitation complexity is reduced[41]. Several other studies focused on the frequency response and the added mass effect, mainly with measurements carried out with the runner not mounted in the turbine housing[42,45–51].

An analysis of the onboard pressure during resonance can be found in paper D.

1.3 Objective

The primary objective for the thesis is to improve the understanding of the physics in a low specific speed Francis runner in order to lower the risks of failure in future designs.

Secondary objectives:

- Analysis of the fluid influence on the runner with focus on rotor-stator interaction (RSI).
- Evaluation of the modal shape, its frequencies and the relation to the RSI.

The scope of the thesis is to design and perform model measurements on the Francis 99 model runner. The measurements include pressure inside and around the runner. The work is limited to steady state operation on three main operational points. The measurement data will be available for comparison with computational fluid dynamics (CFD) and structural simulations with the aim to improve simulation procedures and accuracy in the HiFrancis research project.

1.4 Main activities

The research was carried out with the following main activities

1. Literature review with the focus on onboard measurements and the rotor-stator interaction.
2. Design of a measurement setup for onboard measurements and a measurement of the runner position.
3. Preparations in the laboratory with machining of the runner and electronics for the measurement chain.
4. Measurement campaign.
5. Data analysis with focus on the rotor-stator interaction onboard the runner and the correlation with the runner vibration.

2. The Rotor-stator Interaction Pressure Field

Noise problems in turbomachinery were the first challenge leading to the analysis of the pressure field arising from the RSI[39]. The RSI effects on the runner are a result of the upstream flow condition from the guide vane cascade. The runner is surrounded by a repetitive pattern with zones of higher and lower pressure. When the runner rotates, each runner channel is experiencing a varying pressure and velocity field depending on the position relative to the guide vanes. This variation of the inlet condition to the runner channels is the source of the fluctuation pressure found onboard the runner. Due to different number of runner channels and guide vanes, the fluctuating pressure in different runner channels is phase shifted. As a result, the overall pressure onboard the runner, and thereby the forces acting on the runner, gets zones of higher and lower pressure, velocity and torque. The overall pressure field is known as the modal pressure field. The connection between the nodal diameters k, number of blades Z_r, number of guide vanes Z_g and harmonics n is[39]:

$$mZ_g + k = nZ_r \tag{2}$$

where m is arbitrary integer. The runner in the current study is equipped with 28 guide vanes and 30 runner blades. With Eq. 2, the mode shape of the fundamental frequency includes 2 nodal diameters with the integer $m=1$. This excitation force from the fundamental guide vane passing frequency can be illustrated by dividing a 28 period signal into 30 segments as shown in Figure 7. The intersection line for each segment represents the pressure in each of the 30 runner channels at one instant of time. By plotting a curve through the intersection points the overall pressure with two nodal diameters appears.

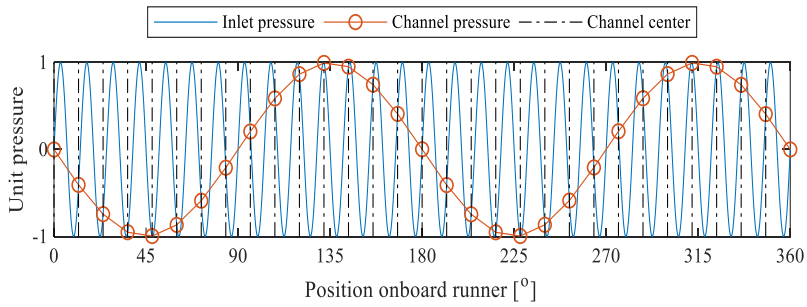

Figure 7 Illustration of the ND2 excitation.

The second harmonic of the guide vane passing frequency is shown in Figure 8. This corresponds to *n=2* in Eq. 2. The integer *m* which gives the lowest number of nodal diameters is *m=2*, giving *k=4*. A sinusoidal signal with 2*28 periods is divided into 30 equal segments. The intersection line for each segment represents the pressure in each of the 30 runner channels. By plotting a curve through the intersection points, the overall pressure with four nodal diameters appears.

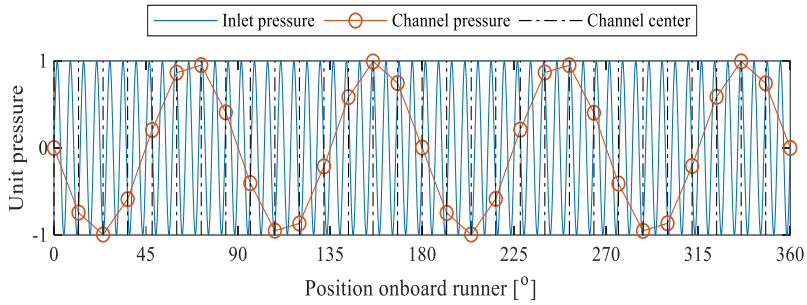

Figure 8 Illustration of the ND4 excitation.

The pulsating pressure field in each channel also creates a pulsation in the torque on each blade. The flow enters the runner radially and leaves the runner vertically, hence the pressure will have a component in the vertical direction of the runner and the pulsations creates bending forces on the runner as shown in Figure 9. With two nodal diameters in the pressure field, zones with higher and lower bending force will be as shown in Figure 10.

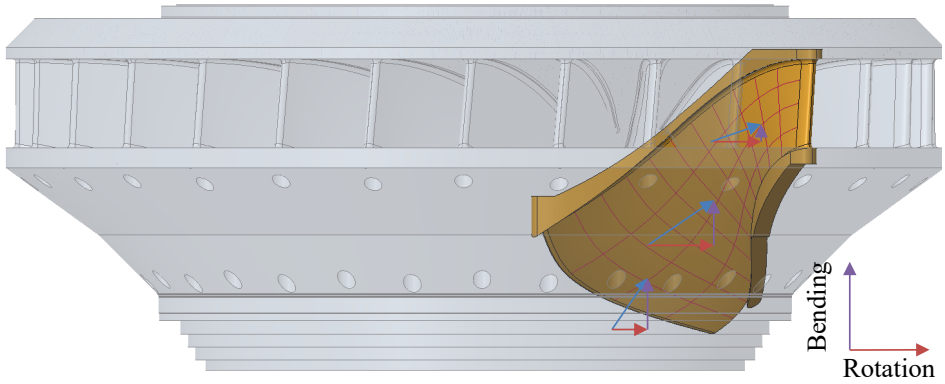

Figure 9 Illustration of the bending and rotational forces

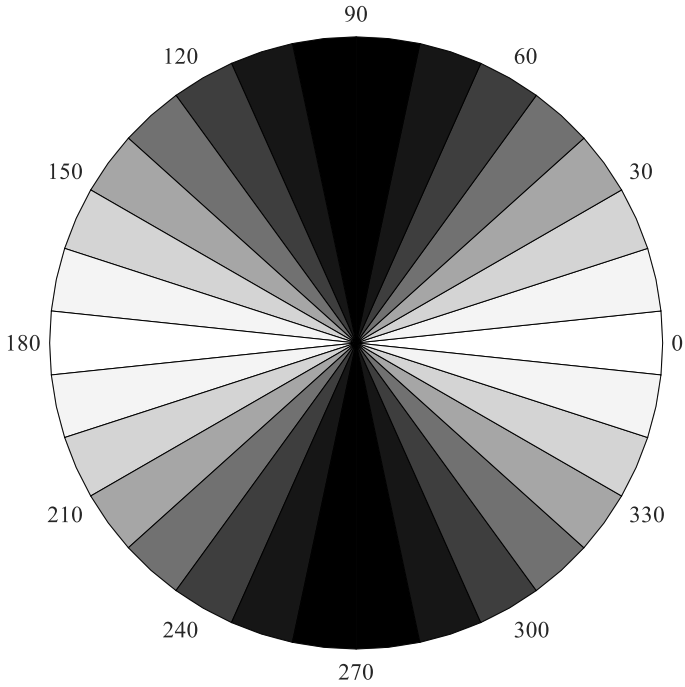

Figure 10 Illustration of a runner with an overall pressure with 2 nodal diameters. The bending of the runner will be higher where the pressure is higher.

The bending force with nodal 4 nodal diameters is utilized to excite the runner in paper D.

"If theory predicted everything exactly, there would be no need for experiments. NASA planners could spend an afternoon drawing up a mission with their perfect computer models and then launch a flawlessly executed mission that evening (of course, what would be the point of the mission, since the models could already predict behavior in space anyway?)."

(A. Manella)

3. Measurement Procedure

The main goal of an experiment is to investigate a process and record the results. The process is physically changed and the results are being recorded to identify the variables of the process. The variables are classified as independent, dependent or extraneous. Extraneous variables are the ones that cannot be controlled but affects the measurements. The usual way of doing experiments is to manipulate the independent variables and measure and record the dependent variables. However, in most experiments it is difficult to identify all variables and control or measure them accurately. To get a good evaluation of the results in such experiments, the use of repeatability and statistics is necessary[52].

3.1 Calibration and uncertainty

To quantify the value of a variable, a sensor must be used. The variables can be steady or varying in time. Regardless, the sensor will always measure the variable with some uncertainty. The purpose of a calibration is to quantify the uncertainty. For accurate quantification, the calibration must be performed with a known reference source, and the calibration process must represent the process in the experiment[52]. If the experiment is designed to measure a steady pressure, the calibration and uncertainty must be accordingly while an experiment with the purpose of finding pressure fluctuations where the mean value is subtracted must have a different procedure for both calibration and uncertainty evaluation.

The variables in the work presented here were both steady and time-dependent. The pressure sensors were initially calibrated in the estimated pressure range of the measurements with a GE P3000 Series pneumatic deadweight tester as the primary

reference as shown in Figure 11. The analysis of the calibration data was done following the guidelines of German Calibration Service for the quantification of the uncertainty in the mean pressure [53]. This guideline is according to the ISO guide for the uncertainty of measurements[54]. To ensure accuracy, the whole measurement chain was taken into account in the calibration, in accordance with the recommendations in IEC 60193[2].

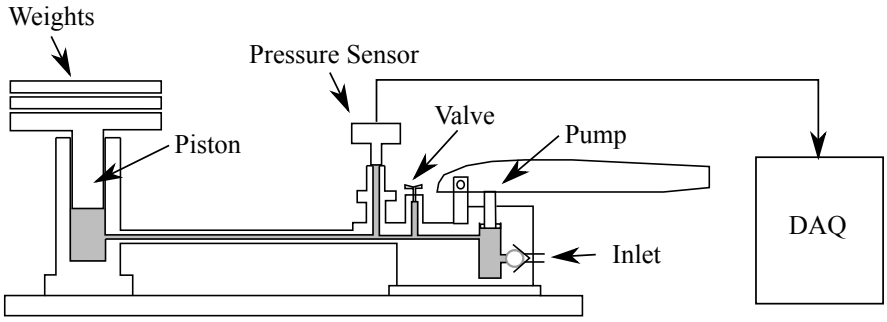

Figure 11 Experimental setup for the static calibration

The effect of runner rotation was tested in air by spinning the runner at rated speed, but no influence was found on the overall uncertainty and therefore not included in the calculations. The calibration constants for each sensor were found with linear regression and the deviation between the calibration reference and the sensor output was used for the estimation of uncertainty.

To evaluate the long-time stability and temperature sensitivity of the sensors, substitute calibration was conducted in zero flow conditions at the start up and stop each measurement day as shown in Figure 12. The substitute sensor was calibrated and mounted on the draft tube cone. Figure 13 shows the calibration results for pressure sensor R1. The uncertainty stems is the uncertainty from initial static calibration. Upper and lower limits includes the long-time repeatability of the sensor related to the reference sensor mounted in the draft tube cone and manufacturer uncertainty is for reference. The total uncertainty for the mean should be in the same range as stated by the manufacturer.

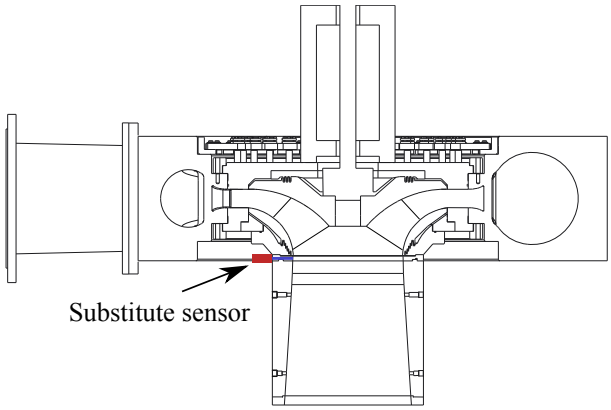

Figure 12 Experimental setup for the substitute calibration

A summary of the calibrated expanded uncertainties for R1 pressure sensor is found in Table 1 for BEP. The expanded uncertainties were calculated with a coverage factor of two which for a measurand with normal distribution represents a coverage probability of approximately 95%.

Table 1. Uncertainty budget for mean pressure, BEP

	Mean pressure [kPa]	Expanded calibrated uncertainty [kPa]	Expanded long time stability [kPa]	Expanded measurement repeatability [kPa]	Total Expanded uncertainty [kPa]
R1	128	0.8	2.1	2.6	3.4 (2.7%)

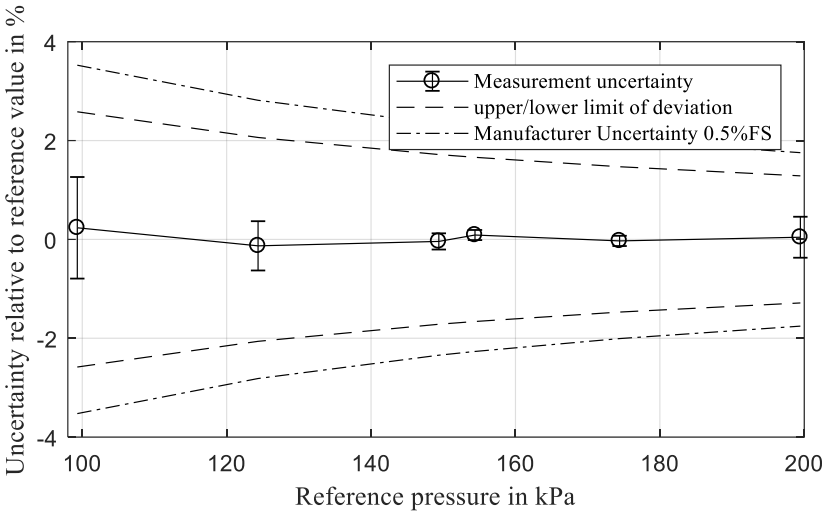

Figure 13 Static calibration result for R1.

As evaluation of pressure amplitudes is a dynamic quantity, dynamic uncertainty must be addressed. All components in the current pressure measurement chain, from the sensors to the data acquisition, are stated to have resonance frequencies above 10kHz, hence the dynamic uncertainty is assumed to be neglectable and only repeatability and hysteresis from static calibration remain in the uncertainty evaluation [52]. A repeatability test was conducted at 1 Hz with a pressure alternating between 100kPa and 90kPa absolute pressure. A high pressure and low-pressure source was used with two valves alternating the pressure. The setup for the calibration is shown in Figure 14. The uncertainty budget for the RSI amplitudes measured with the sensor R1 is shown in Table 2.

Table 2. Uncertainty budget for RSI amplitudes, BEP 12m head

	Repeatability [kPa]	Amplitude RMS of fundamental frequency RSI [kPa]	Relative Uncertainty [%]	Amplitude RMS of first harmonic RSI [kPa]	Relative Uncertainty [%]
R1	0.01	1.17	0.85	0.08	13

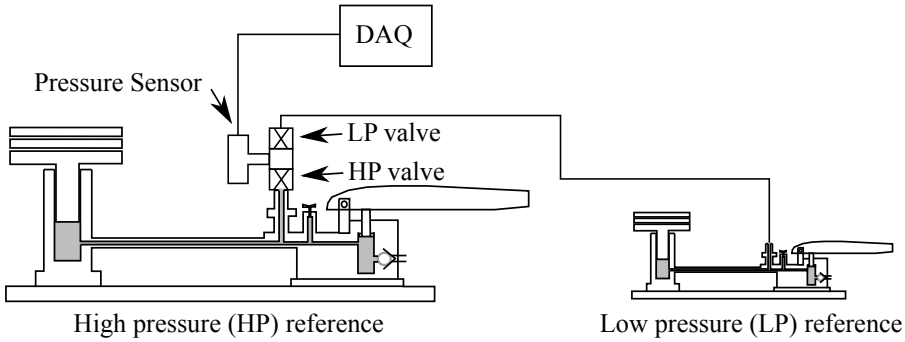

Figure 14 Experimental setup for the repeatability calibration.

A vibration test with the runner in air was conducted to analyze the pressure sensors vibration sensitivity. The results did not give any additional uncertainty. More details can be found in paper D. To analyze the variation of the blade passing amplitude for each sensor, a short time fast Fourier transform (STFFT) was used. The analysis was performed with window length equal to 100 periods of the RSI signal and with 50% overlap. The amplitudes were found to be normally distributed, and a 95% probability interval was calculated. The STFFT calculation is shown in Figure 15.

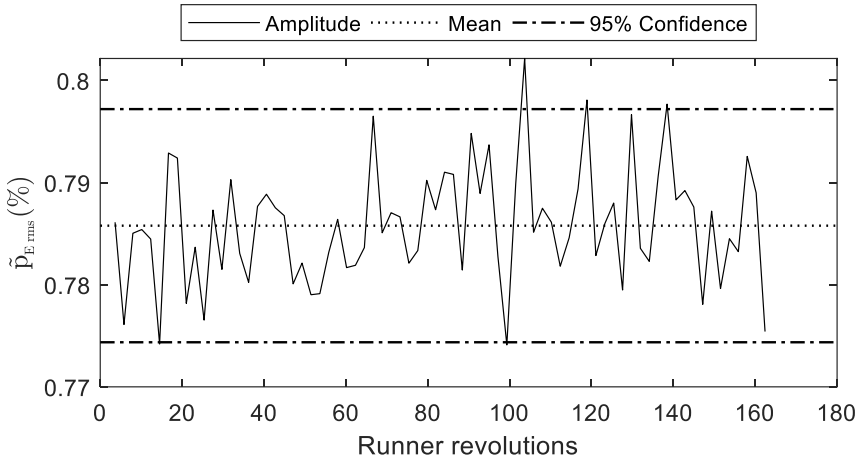

Figure 15 Calculation of the amplitude repeatability with STFFT

To analyze the repeatability of the experiments and the test rig, BEP was recorded at the beginning and end of each measurement day. The 95% probability limits of the difference between the reference and each sensor were calculated as presented for the flow sensor in Table 5

The uncertainty of the position measurement is related to linearity of the position sensor (0.05º), conversion rate of the digital analog converter (~0) and signal noise and the post-processing filtering (0.4º). The uncertainty related to signal noise and post-processing were found from the difference in the raw signal and filtered signal. In addition, the anti-aliasing filter of all other sensors gave a time-delay, which gave an added uncertainty as a function of rotational speed (0.2º at 380 rpm). The total maximum absolute position uncertainty was 0.45º.

Table 3. Uncertainty budget for operational sensors, BEP

Description [unit]	Sensor	Mean Value	Expanded calibrated uncertainty	Expanded long time stability	Expanded measurement repeatability	Total Expanded uncertainty
Flow [m^3/s]	FTQ1	0.203	$0.3 \cdot 10^{-3}$	$0.01 \cdot 10^{-3}$	$1.1 \cdot 10^{-3}$	0.001 (0.56%)

The uncertainty evaluation steps:

1. Evaluation of the mean pressure:
    a. Static calibration
    b. Zero repeatability and temperature shift with substitute calibration
2. Evaluation of the pressure amplitudes:
    a. Sensor repeatability calibration
    b. Amplitude repeatability in the measurements
3. Evaluation of the test rig repeatability
    a. Repeated BEP measurements

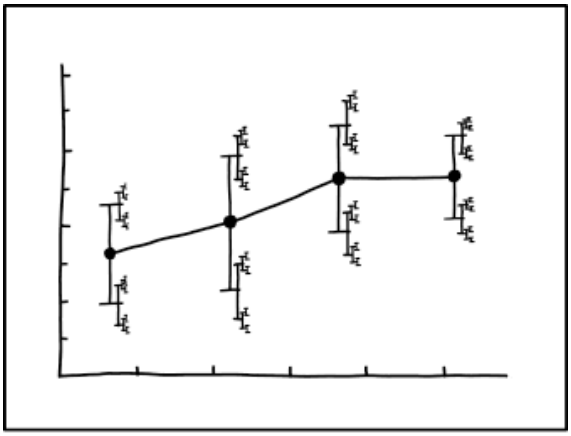

I DON'T KNOW HOW TO PROPAGATE ERROR CORRECTLY, SO I JUST PUT ERROR BARS ON ALL MY ERROR BARS.

“Nothing is too wonderful to be true, if it be consistent with the laws of nature and in such things as these, experiment is the best test of such consistency”

(Michael Faraday, 1849, Royal Institution London)

4. Summary of Papers

Paper A: *Onboard measurements of pressure pulsations in a low specific speed Francis model runner*

The paper is written as a presentation of the onboard measurement with the hub mounted pressure sensors. In addition, the use of a position sensor and the conversion to a position referenced analysis of the data are presented. The setup is considered to be a good way of measuring onboard pressure and pressure fluctuations for the verification of computational fluid dynamics. The knowledge of the absolute position of the runner enabled analysis of the pressure in sectors around the runner.

Paper B: *The rotor-stator interaction onboard a low specific speed Francis turbine.*

The paper focuses on the main excitation force in low specific speed runners, the rotor-stator interaction. The pressure from the guide vanes is divided into the effect from potential flow interaction and the effect from the guide vane viscous wake. The potential flow interaction is found to be the dominant effect, and no evidence from the viscous wake effect is found on the onboard pressure.

Paper C: *Experimental study of the rotor-stator interaction in a low specific speed Francis turbine and pump-turbine*

The paper focuses on the rotor-stator interaction as seen in the vaneless space and the guide vane channels. From the literature, the pressure in this area is known to be a combination of throttling effects and the rotating runner pressure. A mathematical model is developed to distinguish between the two effects. Measurements from two runners are analyzed, and the main findings show that the pressure fluctuations in the guide vane cascade are mainly controlled by throttling for a low blade loading case and the rotating runner pressure for a higher blade loading case.

Paper D: *Experimental study of a low specific speed Francis model runner during resonance*

An analysis of the pressure in a runner channel of a low specific speed Francis model runner during resonance is presented. The analysis includes experiments and the development of a pressure model to estimate both the convective and acoustic pressure field during resonance. Previous studies in the literature focus on the convective pressure from the rotor-stator interaction and utilizes separate sensors for the analysis of the runner vibration. New analysis possibilities are enabled by analyzing both effects from the pressure measurements. The measurements find a clear resonance peak in the pressure field excited by the second harmonic of the guide vane passing frequency. The convective pressure field diminishes close to linearly from inlet to outlet of the runner, while the acoustic pressure field has the highest amplitudes in the middle of the runner channel. At resonance, the acoustic pressure clearly dominates over the convective pressure.

5. Conclusion

The results presented in this thesis, gives more details about the physics in the rotor-stator interaction in low specific speed Francis turbines and increases the understanding of the main excitation source in low specific speed turbines. This could lead to better predictions and design considerations to reduce the risk for resonance and cracks in the future.

The main findings can be divided into three categories; the mechanisms of the pressure onboard the runner, the mechanisms of the pressure around the runner in the guide vane cascade and the vaneless space and technical findings related to the measurement setup.

A resonance in the runner is found with the use of onboard pressure sensors:

- By separating the measured pressure amplitudes into an acoustic and a convective pressure field, their individual shapes together with the eigenfrequency and the damping are estimated. Previous studies focused on the convective part and separate measurements for the analysis of eigenfrequency and damping.
- The convective pressure field diminishes close to linearly from the inlet to the outlet, while the acoustic pressure field has the highest amplitudes in the middle of the runner channel.
- At resonance the acoustic pressure clearly dominates over the convective pressure. For the comparison with numerical results, the convective pressure represents the output from computational fluid dynamics (CFD) and the acoustic pressure, resonance frequency and damping represent the output from simulations as modal and flutter analysis.

- The pressure in the runner is found to be highly dependent on the potential pressure in the guide vane cascade and there is no clear evidence of any effect on the pressure in the runner channel from the viscous wake.

The pressure in the guide vane cascade and the vaneless space is controlled by two effects: throttling and the rotating runner pressure:

- With low blade loading in the runner, the main influence of the pressure field in the guide vane cascade and vaneless space is found to be the pressure disturbance from the runner introducing a throttling effect in the guide vane channel, resulting in fluctuation in the potential pressure in the guide vane cascade.
- With higher blade loading and few blades, the pressure in the vaneless space is found to be a direct measurement of the rotating pressure field from the runner and smaller influence from the throttling.
- The difference in the measured pressure amplitudes in the vaneless space is caused by the phase shift between the throttling effect and the rotating runner pressure.

Measurement setup and calibration:

- The position resampled signal increases the accuracy of the measurement analysis and gives an addition perspective on experimental data.
- For the mean pressure, the uncertainty of the measurements is mostly affected by the zero stability of the sensors and the repeatability of the measurements.
- The evaluation of fluctuating quantities must be done with representative methods, and the uncertainty is the repeatability of the sensors and the repeatability of the amplitudes in the measurements.

6. Further Work

The measurement setup presented in paper A with reference to the absolute position of the runner should be investigated further. For any turbine, the details in the analysis of all runner speed dependent pressure fluctuations can be increased and the presented sector analysis can be a valuable addition to already established analysis methods. The use of onboard custom built amplifiers is not recommended in future projects due to the complexity. The amplifiers should preferably be mounted on the runner shaft for easy access during measurements.

Steady state measurements with onboard data is presented in paper A. Also load changes were performed in the same measurement campaign reported in the HiFrancis project. Future onboard pressure measurements should include starts and stops for the numerical verification.

In paper B and C, the rotor-stator interaction is investigated in both the rotating and the stationary domain. Similar analysis should be repeated for different runners and preferably on prototypes to verify the method and further increase the details in the knowledge of the RSI. It is also suggested to investigate the RSI with the presented method while varying the gap between the runner blades leading edge and the guide vane trailing edge. One possible approach could be to lengthen the leading edges of the runner blades.

The frequency response analysis presented in paper D should be repeated with a geometry with less complex assembly for easier numerical analysis. The use of

pressure measurement in modal analysis is highly recommended in future project since this additional data gives more information for the verification of the numerical results. In addition, the use of strain gauges in the frequency analysis should be evaluated, preferably with a non-bolted runner to reduce the numerical modelling complexity and uncertainty.

The experience of the work in the current thesis can be summarized in the following recommendations for future work.

Primary

- Reduce the complexity of the measurement chain.
    - Preferably amplifiers available in the market.
- Design a runner for the operation at resonance condition without bolts, preferably with resonance from the fundamental guide vane passing frequency as a reference case for the verification of structural simulations.
    - Natural excitation from the pressure field and full modal analysis with excitation from external sources, as electronic muscles.

Secondary

- Similar measurements and analysis for other runner designs to verify the findings related to the RSI, both onboard and in the vaneless space.
- Modal measurement in both pressure and strain domain for more geometries to verify the findings in the pressure field during resonance for other runner designs.
- Similar measurement on prototypes
- Onboard measurements during starts and stops. Preferably with scalable rotating mass compared to prototype.

7. References

[1] Bjarne Børresen 2009 Sprekker i løpehjul. analyser, forebygging og erfaringer

[2] IEC 1999 *NEK IEC 60193 Hydraulic turbines, storage pumps and pump-turbines Model acceptance tests*

[3] Bovet T 1961 *Contribution to the study of Francis-Turbine Runner design* (New York: The American Soc. of Mechanical Engineers)

[4] Rayle R E 1949 *An investigation of the influence of orifice geometry on static pressure measurements* Master Thesis (Cambridge, Massachusetts, USA: Massachusetts Institute of Technology)

[5] H.Bergh and H.Tijdeman 1965 *Theoretical and experimental results for the dynamic response of pressure measuring systems* (Nationaal Lucht- En Ruimtevaartlaboratorium Report)

[6] Franklin R e. and Wallace J M 1970 Absolute measurements of static-hole error using flush transducers *J. Fluid Mech.* **42** 33–48

[7] Gallus H E, Lambertz J and Wallmann T 1980 Blade-Row Interaction in an Axial-Flow Subsonic Compressor Stage *J. Eng. Power* **102** 169–77

[8] Perrig A, Avellan F, Kueny J-L, Farhat M and Parkinson E 2005 Flow in a Pelton Turbine Bucket: Numerical and Experimental Investigations *J. Fluids Eng.* **128** 350–8

[9] Jansson I and Cervantes M 2007 A method to flush mount replaceable pressure sensors on a 9.3 MW prototype of a Kaplan runner *Proceedings of the 2nd IAHR International Meeting of the Workgroup on Cavitation and Dynamic Problems in Hydraulic Machinery and Systems,* IAHR International Meeting of the

Workgroup on Cavitation and Dynamic Problems in Hydraulic Machinery and Systems : 24/10/2007 - 26/10/2007 pp 299–304

[10] Berten S, Hentschel S, Kieselbach K and Dupont P 2011 Experimental and Numerical Analysis of Pressure Pulsations and Mechanical Deformations in a Centrifugal Pump Impeller *Proceedings of the ASME-JSME-KSME 2011 Joint Fluids Engineering Conference* AJK-Fluids2011 vol 1 (Hamamatsu, Shizuoka, Japan: JSME) pp 297–306

[11] Münsterjohann S and Becker S 2018 Wall Pressure and Blade Surface Pressure in a Side Channel Blower *Int. J. Rotating Mach.*

[12] Avellan F, Etter S, Gummer J H and Seidel U 2000 Dynamic pressure measurements on a model turbine runner and their use in preventing runner fatigue failure *Proceedings of the 20th IAHR Symposium, Charlotte, North Carolina, USA, August*

[13] Farhat M, Natal S, Avellan F, Paquet F, Lowys P Y and Couston M 2002 Onboard Measurements of Pressure and Strain Fluctuations in a Model of low Head Francis Turbine. Part 1 : Instrumentation *Proc. 21st IAHR Symp. Hydraul. Mach. Syst.* 865–72

[14] Pierre-Yves Lowys, Jean-Loup Deniau, Eric Gaudin, Pierre Leroy and Mohand Djatout 2006 On-board model runner dynamic measurements HydroVision (Portland: HCI Publications)

[15] Duparchy F, Favrel A, Lowys P-Y, Landry C, Müller A, Yamamoto K and Avellan F 2015 Analysis of the part load helical vortex rope of a Francis turbine using on-board sensors *J. Phys. Conf. Ser.* **656** 012061

[16] Gao Z, Zhu W, Meng L, Zhang J, Zhang F, Pan L and Lu L 2017 Experimental Study of the Francis Turbine Pressure Fluctuations and the Pressure Fluctuations Superposition Phenomenon Inside the Runner *J. Fluids Eng.* **140** 041208-041208–9

[17] Kobro E 2010 *Measurement of pressure pulsations in Francis turbines* Ph. D. (Norwegian University of Science and Technology, Trondheim)

[18] Hasmatuchi V 2012 *Hydrodynamics of a pump-turbine operating at off-design conditions in generating mode* Doctoral Thesis (Lausanne, Switzerland: Ecode Polytechnique Federale de Lausanne)

[19] Seidel U, Hübner B, Löfflad J and Faigle P 2012 Evaluation of RSI-induced stresses in Francis runners *IOP Conf. Ser. Earth Environ. Sci.* **15** 052010

[20] Brekke H 2010 A Review on Oscillatory Problems in Francis Turbine *New Trends in Technologies: Devices, Computer, Communication and Industrial Systems* (InTech)

[21] Tanaka H 2011 Vibration Behavior and Dynamic Stress of Runners of Very High Head Reversible Pump-turbines *Int. J. Fluid Mach. Syst.* **4** 289–306

[22] D. Y. Li, R. Z. Gong, H. J. Wang, X. Z. Wei, Z. S. Liu and D. Q. Qin 2016 Analysis of Rotor-Stator Interaction in Turbine Mode of a Pump-Turbine Model *J. Appl. Fluid Mech.* **9** 2559–68

[23] Arndt N, Acosta A, Brennen C E and Caughey T K 1989 Rotor-stator interaction in a diffuser pump *ASME J. Turbomach.* **111** 213–21

[24] Dring R P, Joslyn H D, Hardin L W and Wagner J H 1982 Turbine Rotor-Stator Interaction *J. Eng. Power* **104** 729–42

[25] Østby P T K, Billdal J T, Haugen B and Dahlhaug O G 2017 On the relation between friction losses and pressure pulsations caused by Rotor Stator interaction on the Francis-99 turbine *J. Phys. Conf. Ser.* **782** 012010

[26] Antonsen Ø 2007 *Unsteady flow in wicket gate and runner with focus on static and dynamic load on runner* Doctoral Thesis (Trondheim, Norway: Norwegian University of Science and Technology)

[27] Zobeiri A 2009 *Investigations of Time Dependent Flow Phenomena in a Turbine and Pump-Turbine of Francis Type: Rotor-Stator Interactions and Precessing Vortex Rope* (Lausanne: EPFL)

[28] Lewis B J, Cimbala J M and Wouden A M 2014 Wicket gate trailing-edge blowing: A method for improving off-design hydroturbine performance by adjusting the runner inlet swirl angle *IOP Conf. Ser. Earth Environ. Sci.* **22** 012021

[29] Li Z, Wang Z, Wei X and Qin D 2016 Flow Similarity in the Rotor–Stator Interaction Affected Region in Prototype and Model Francis Pump-Turbines in Generating Mode *J. Fluids Eng.* **138** 061201–061201

[30] Trivedi C, Cervantes M J, Gandhi B K and Dahlhaug O G 2013 Experimental and Numerical Studies for a High Head Francis Turbine at Several Operating Points *J. Fluids Eng.* **135** 111102–111102

[31] Yan J, Koutnik J, Seidel U and Hübner B 2010 Compressible simulation of rotor-stator interaction in pump-turbines *IOP Conf. Ser. Earth Environ. Sci.* **12** 012008

[32] Nennemann B, Vu T C and Farhat M 2005 CFD prediction of unsteady wicket gate-runner interaction in Francis turbines: A new standard hydraulic design procedure *HYDRO 2005*

[33] Zobeiri A, Kueny J-L, Farhat M and Avellan F 2006 Pump-turbine rotor-stator interactions in generating mode: pressure fluctuation in distributor channel *23rd IAHR Symposium on Hydraulic Machinery and Systems*

[34] Yonezawa K, Toyahara S, Motoki S, Tanaka H, Doerfler P and Tsujimoto Y 2014 Phase Resonance in Centrifugal Fluid Machinery *Int. J. Fluid Mach. Syst.* **7** 42–53

[35] Ciocan G D and Kueny J L 2006 Experimental Analysis of Rotor Stator Interaction in a Pump-Turbine *23rd IAHR Symposium on Hydraulic Machinery and Systems* (Yokohama, Japan)

[36] Rieger N F *Progress With the Solution of Vibration Problems of Steam Turbine Blades*

[37] Rao J S 2011 Bladed Disks *History of Rotating Machinery Dynamics* History of Mechanism and Machine Science (Springer, Dordrecht) pp 299–325

[38] Ohashi H 1994 Case Study of Pump Failure Due to Rotor-Stator Interaction *Int. J. Rotating Mach.*

[39] Tyler J M and Sofrin T G 1962 *Axial Flow Compressor Noise Studies* (Warrendale, PA: SAE International)

[40] Valentin D, Ramos D, Bossio M, Presas A, Egusquiza E and Valero C 2016 Influence of the boundary conditions on the natural frequencies of a Francis turbine *IOP Conf. Ser. Earth Environ. Sci.* **49** 072004

[41] Valentín D, Presas A, Bossio M, Egusquiza M, Egusquiza E and Valero C 2018 Feasibility of Detecting Natural Frequencies of Hydraulic Turbines While in Operation, Using Strain Gauges *Sensors* **18** 174

[42] Valentín D, Ramos D, Bossio M, Presas A, Egusquiza E and Valero C 2016 Influence of the boundary conditions on the natural frequencies of a Francis turbine *IOP Conf. Ser. Earth Environ. Sci.* **49** 072004

[43] Presas A, Valero C, Huang X, Egusquiza E, Farhat M and Avellan F 2012 Analysis of the dynamic response of pump-turbine runners-Part I: Experiment *IOP Conf. Ser. Earth Environ. Sci.* **15** 052015

[44] Østby P T K, Sivertsen K, Billdal J T and Haugen B 2019 Experimental investigation on the effect off near walls on the eigen frequency of a low specific speed francis runner *Mech. Syst. Signal Process.* **118** 757–66

[45] Lais S, Liang Q, Henggeler U, Weiss T, Escaler X and Egusquiza E 2009 Dynamic analysis of Francis runners-experiment and numerical simulation *Int. J. Fluid Mach. Syst.* **2** 303–314

[46] Kurosawa S, Matsumoto K, Miyagi J, He L and Wang Z 2015 Fluid-Structure Interaction Analysis for Resonance Investigation of Pump-Turbine Runner *ASME/JSME/KSME 2015 Joint Fluids Engineering Conference* vol 1A: Symposia, Part 2 (Seoul, South Korea) p V01AT12A002

[47] Kushner F 2004 Rotating Component Modal Analysis And Resonance Avoidance Recommendations. *Proceeding of the thirty-third turbomachinery symposium* Turbomachinery Symposium ; 33; 2004; Houston, Tex. (George R. Brown Convention Center, Houston, Texas: Turbomachinery Laboratory) pp 143–62

[48] Egusquiza E, Valero C, Liang Q, Coussirat M and Seidel U 2009 Fluid added mass effect in the modal response of a pump-turbine impeller *ASME 2009 International Design Engineering Technical Conferences and Computers and Information in Engineering Conference* (San Diego, California, USA: American Society of Mechanical Engineers) pp 715–724

[49] Rodriguez C G, Egusquiza E, Escaler X, Liang Q W and Avellan F 2006 Experimental investigation of added mass effects on a Francis turbine runner in still water *J. Fluids Struct.* **22** 699–712

[50] Valentín D, Presas A, Egusquiza E, Valero C and Bossio M 2017 Dynamic response of the MICA runner. Experiment and simulation *J. Phys. Conf. Ser.* **813** 012036

[51] MAO Z and WANG Z 2016 Structural Characteristic in Prototype Runner of Francis Turbine Analysis

[52] Dunn P F 2014 *Measurement and Data Analysis for Engineering and Science, Third Edition* (CRC Press)

[53] Physikalisch-Technische Bundesanstalt (PTB) and German Calibration Service (DKD) 2014 Guideline DKD-R 6-1 Calibration of Pressure Gauges

[54] ISO/IEC GUIDE 98-3:2008(E) Guide to the expression of uncertainty in measurement (GUM:1995)

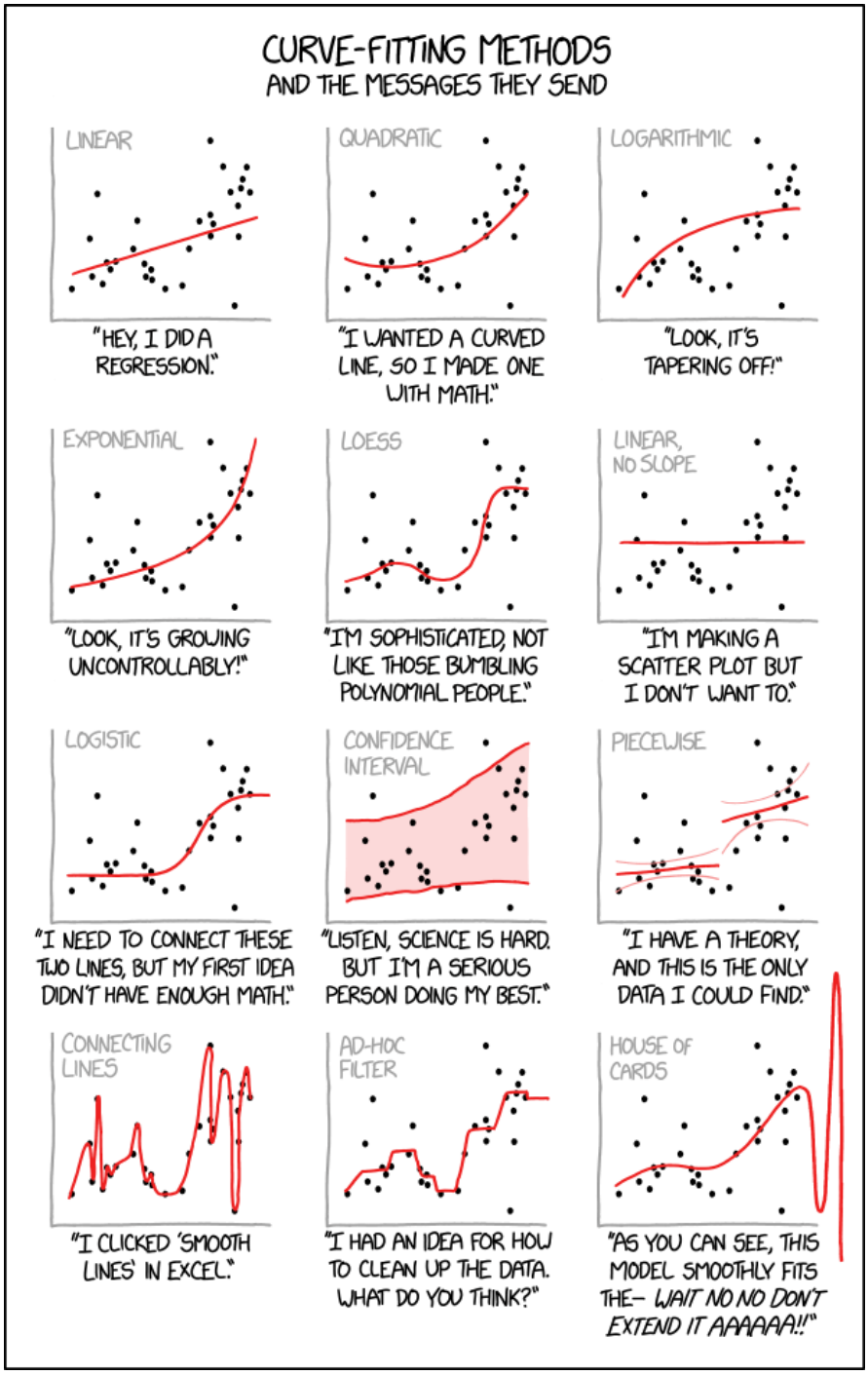

(CC BY 2.5) www.xkcd.com

Part II – Papers

“Measures are more than a creation of society, they create society”

(Ken Alder, 2002)

Onboard measurements of pressure pulsations in a low specific speed Francis model runner

E Agnalt, B W Solemslie, O G Dahlhaug

Waterpower Laboratory, Department of Energy and Process Engineering, NTNU - Norwegian University of Science and Technology, Trondheim, Norway

E-mail: einar.agnalt@ntnu.no

Abstract. Over the last years, there have been several incidents with cracks in high head Francis turbines. These cracks are understood to be related to pressure pulsations, vibration modulus and the combination of these. In this paper, a setup for the investigation of pressure pulsations in a low specific speed model turbine is presented with the use of onboard pressure sensors. Earlier onboard measurements have mainly utilized blade-mounted sensors. In this paper, a setup with hub-mounted pressure sensors is described. In addition, a position sensor is utilized to analyse the pressure data relative to the angular position of the runner. The setup is considered as a good reference for computational fluid dynamics validation and is considered less extensive for evaluating the onboard pressure pulsations compared to blade-mounted sensors.

Onboard measurements of pressure pulsations in a low specific speed Francis model runner

1. Introduction

Some new power plants with installed Francis turbines have experienced a breakdown after few hours of operation. The design and calculations of Francis runners are based on numerical analysis, but the main problem is the validation of the results regarding fluid structure interaction in the runner. For a better understanding of the physics behind this problem, measurements must be performed for the validation of the numerical results.

Measurements including moving fluids and transient properties, as pressure pulsations, could be severely influenced by the mounting method of the sensor [1,2]. Today, pressure sensors with high accuracy and small sizes are available with flush mounted diaphragm. For application where accurate flush mounting is possible, the uncertainty from mounting related to hole size, transmission tubes and cavities will be removed[3]. The time and frequency response for the measurements are only related to dynamic properties of the diaphragm and the acquisition chain as described in the ISA standard "A Guide for the Dynamic Calibration of Pressure sensors"[4]. In the current measurements, flush mounting of the sensors was selected to reduce uncertainty related to the mounting method.

To analyze the pressure in the runner channel, the main method found for onboard pressure measurements, are with the use of miniature blade-mounted sensors. Several studies utilized onboard measurements with blade-mounted miniature sensors [5–11]. Kobro et.al did onboard measurements on the same runner as described in this paper, but the complexity of the setup and durability of the sensors were not satisfactory[12]. Another concern is the possibility for mechanical influence on the pressure sensors if mounted on thin blades. The setup presented utilizes a measurement method with hub-mounted pressure sensors to analyze the pressure pulsations onboard a low specific speed Francis model runner.

The data acquisition in the rotating domain can be done with different methods including telemetry, slip-ring, onboard acquisition and a combination of onboard

acquisition and digital transfer with a slip-ring. In the presented setup, a parallel sampling data acquisition system for all measurements were selected to avoid uncertainties related to time synchronization, hence a multi-channel analog slip-ring system was used.

In addition to the onboard pressure measurements, a setup for continuous angular position measurement of the runner is presented. The objective of the measurements is the analysis of onboard pressure.

2. Methods

2.1. Experimental setup

The Francis test-rig available at the Waterpower Laboratory, at Norwegian University of Science and Technology was used for the experimental studies[13,14]. The Francis turbine in the test-rig is shown in Figure 16.

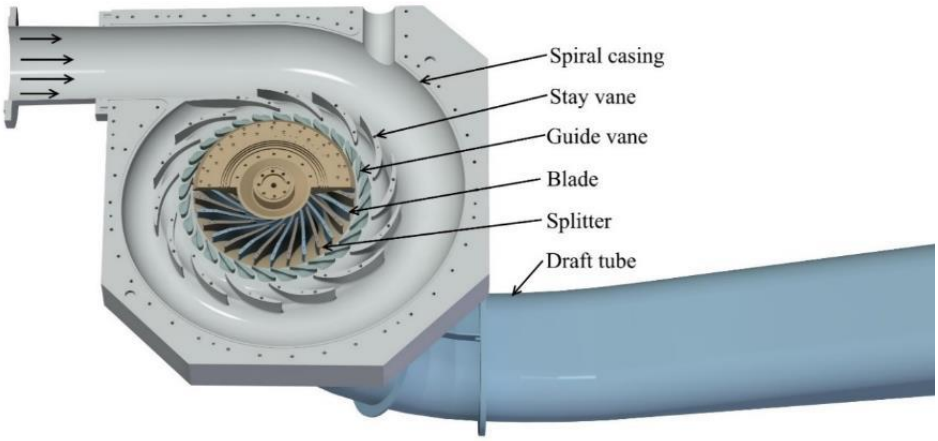

Figure 16 Three-dimensional view of the investigated Francis turbine.

The Francis turbine was equipped with all required instruments to conduct model testing according to IEC 60193[15]. The total number of pressure taps in the experimental setup was 24. In this paper, the focus was on four sensors mounted in the runner. Figure

17 shows the locations of the onboard pressure sensors in the turbine (R1, R2, R3 and R4). The onboard sensors were mounted in the runner crown. Due to space restriction and the number of channels in the slip ring, custom amplifiers were built and mounted onboard the runner.

To analyze the pressure values onboard the runner relative to the stationary frame, a position sensor (Z) was added to the shaft. The sensor was a digital encoder with 13 bit resolution. The digital position signal was converted to analog +/-10V saw tooth to reduce the number of leads in the cable, and for easier synchronization of other analog values in the DAQ system. The position sensor is shown in Figure 18

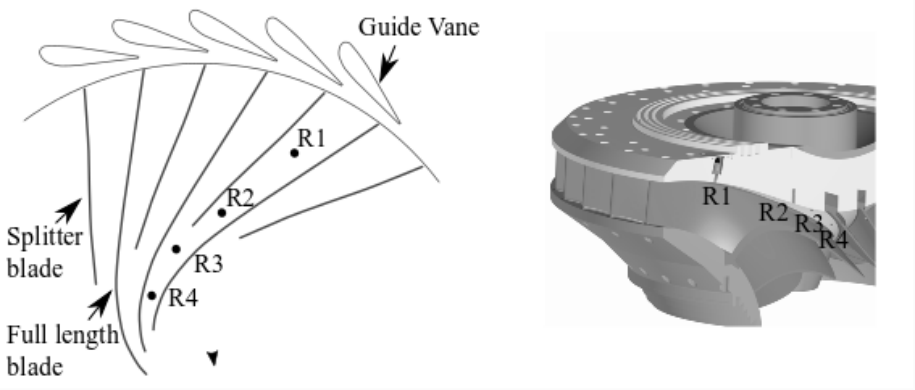

Figure 17 Onboard pressure sensors R1 to R4

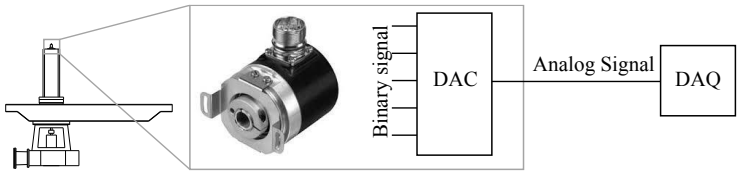

Figure 18 Position sensor Z. A digital absolute encoder measures the angular position with binary output. The binary signal is converted to analog value with a digital to analog converter (DAC).

2.2. Data acquisition

The data acquisition system (DAQ) for the onboard measurements, was built with the use of slip-ring. This was chosen to enable full time-synchronisation between the stationary and rotating domain, which was of great importance when relating the onboard measurement to runner position measured in the stationary domain. This approach does however introduce longer signal transfer with analog voltage and is therefore more susceptible to noise. This could be reduced with differential signal transfer, but with limited number of channels in the slip-ring, single ended data transfer were selected with common ground. A differential signal transfer, where each channel has signal and reference, would be more noise resistant. A comparison between a single ended and differential signal transfer confirmed this. Nevertheless, in the uncertainty analysis, the added noise did not affect the total uncertainty in the measurements. The input to the DAQ system had low-pass filters for anti-aliasing, and the total number of channels in the measurement campaign were 50.

The onboard amplifiers were design with programmable gain instrumentation amplifiers and a precision voltage reference for excitation voltage to the sensors. The amplifiers were design with dual power supply to utilize the full range of the +/-10V input to the DAQ system. One amplifier and a connector board is shown in Figure 19. The amplifiers were mounted inside the runner, i.e. as close as possible to the signal source, to improve noise resistance.

Figure 19 Onboard amplifiers, single card and two amplifiers mounted in a connector. The connector with the amplifiers were mounted inside the runner.

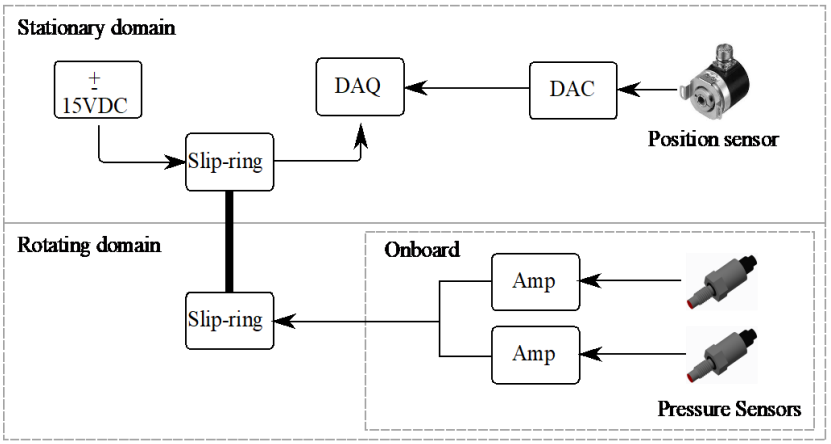

Figure 20 Data acquisition setup

2.3. Measurements

The setup presented in this paper, was utilized for several measurements and operational conditions. The results for this paper are based on the measurements presented in Table 4.

Table 4. Measurement summary. Alpha is guide vane opening.

Description	N_{ED}	Q_{ED}	Head	Alpha	Speed
Best Efficiency Point (BEP)	0.180	0.154	15.6 m	10 º	382.7 rpm

2.4. Post processing methods

The position sensor was used to analyse the onboard measurements relative to the stationary domain. The raw signal from the position sensor was +- 10V saw tooth signal representing one revolution of the runner as presented in Figure 21. The digital to analog conversion of the position from the encoder was operation in a transparent mode, meaning all changes of position was continuously updated on the analog output. This gave glitches on the signal which needed to be filtered. A local regression smoothing filter was used.

The signal was then converted to a continuous increasing position vector and the first derivative was calculated to find the speed vector.

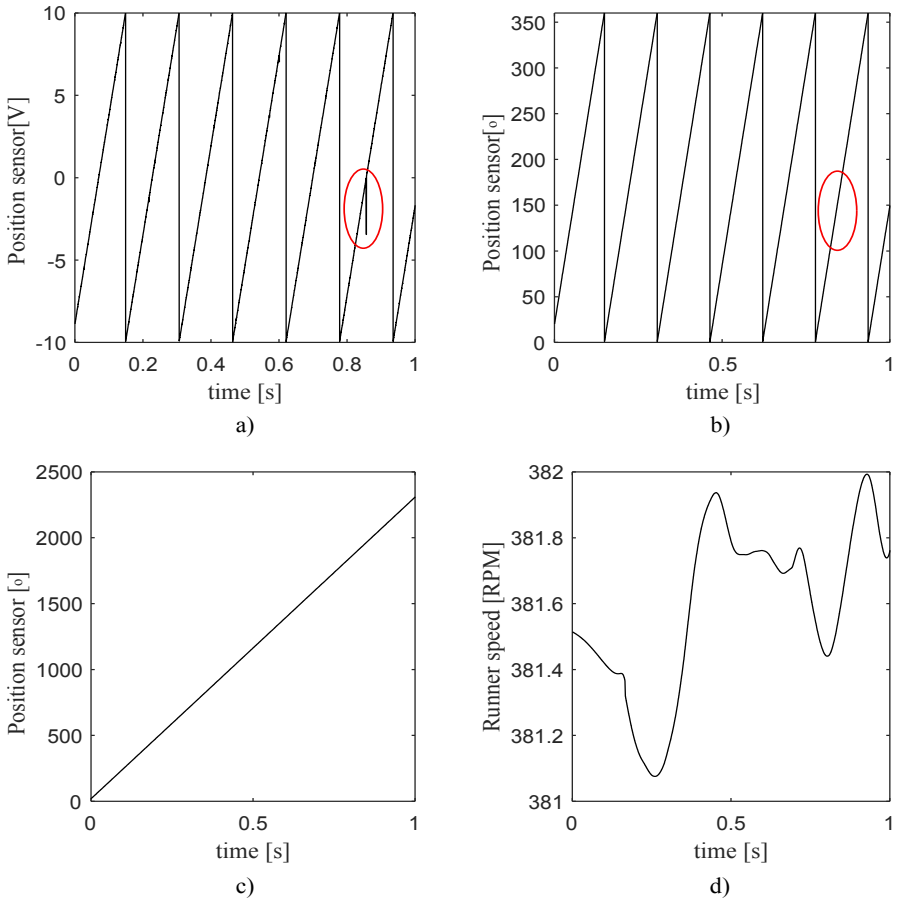

Figure 21 Position sensor signal processing. a) Saw tooth raw data from sensor. The signal includes some noise and glitches from the digital to analog conversion (circled). b) The signal is filtered using local regression smoothing. c) A continuous vector is created from the saw tooth signal by adding 360º for each drop. d) First derivative of the signal gives the speed vector.

2.5. Calibration and uncertainty

The pressure sensors were initially calibrated in the estimated pressure range for the measurements using the guidelines of German Calibration Service [16]. This guideline is according to the ISO guide to uncertainty of measurements[17]. To ensure accuracy, the whole measurement chain is taken into account in the calibration, in accordance with the recommendations in IEC 60193[15]. For practical reasons, the slip ring was not spinning during calibration, but a separate test was performed with a constant precision voltage source without any added uncertainty. The effect of runner rotation was tested in air by spinning the runner at rated speed, but the influence was found to be neglectable. The calibration constants for each sensor were found with linear regression and the deviation between the calibration reference and the sensor output was used for the estimation of uncertainty. To further evaluate the long-time stability and temperature sensitivity of the sensors, substitute calibration were conducted in zero flow conditions at startup and stop each measurement day. The substitute sensor was calibrated and mounted on the draft tube cone. Figure 22 shows the calibration results for pressure sensor R1 and the limits of deviation including the long-time stability. A summary of the calibrated expanded uncertainties for all pressure sensors is found in Table 5 for BEP. The expanded uncertainties are calculated with a coverage factor of two which for a measurand with normal distribution represents a coverage probability of approximately 95%.

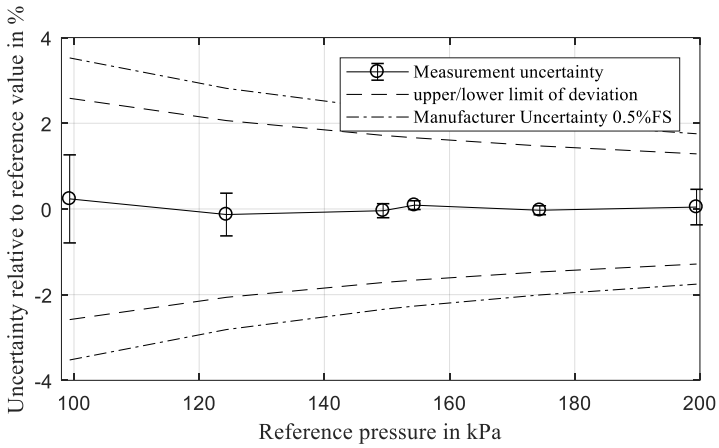

Figure 22 Calibration result for R1. Measurement uncertainty is uncertainty from initial calibration. Upper and lower limits includes the long-time repeatability of the sensor related to the reference sensor mounted in the draft tube cone. Manufacturer uncertainty is shown for reference.

For the evaluation of amplitudes, which is a dynamic property, the static calibration may not be valid[18]. If the frequency response function of the system is known, the dynamic uncertainty could be modelled[19]. In the current measurement setup, all sensors are stated to have resonance frequencies above 25kHz. Frequencies of interest are below 1,2% of resonance, hence it is assumed that the dynamic uncertainty is neglectable and only repeatability and hysteresis from static calibration remains in the uncertainty evaluation due to covariance[20]. In Figure 23, the 95% absolute repeatability in kPa for the calibrated points for the sensor R1 are presented.

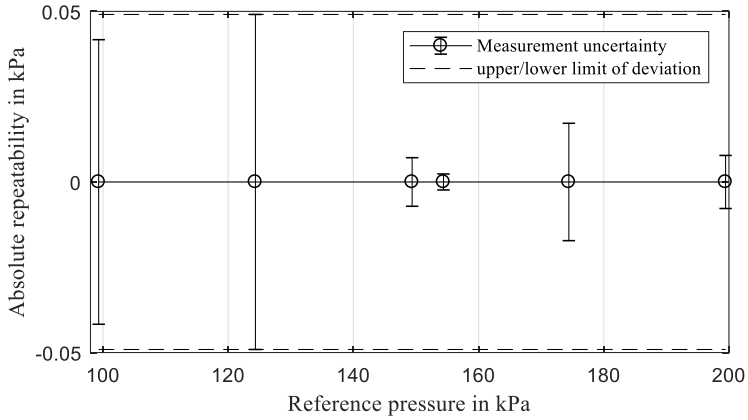

Figure 23 Repeatability calibration result for sensor R1

To analyse the repeatability of the experiments and the test rig, BEP was recorded at the beginning and end of each day the measurements were performed. The 95% probability limits of the difference between reference and each sensor were calculated as presented in Table 5

Table 5. Uncertainty budget for mean pressure, BEP

Location	Type / Full scale range	Mean pressure [kPa]	Expanded calibrated uncertainty [kPa]	Expanded long time stability [kPa]	Expanded measurement repeatability [kPa]	Total Expanded uncertainty [kPa]
R1	Entran/7bara	128	0.8	2.1	2.6	3.0 (2.3%)
R2	Entran/7bara	101	1.2	3.0	2.2	3.7 (3.7%)
R3	XP5/2bara	88	0.6	1.1	0.7	1.3 (1.5%)
R4	XP5/2bara	80	0.2	0.9	1.0	1.3 (1.6%)

Uncertainty budget for the amplitudes RSI amplitudes is presented in Table 6

Table 6. Uncertainty budget for RSI amplitudes, BEP

Location	Type/Fs	Repeatability [kPa]	Amplitude RMS of fundamental frequency RSI [kPa]	Relative Uncertainty [%]	Amplitude RMS of first harmonic RSI [kPa]	Relative Uncertainty [%]
R1	Entran/7bara	0.05	1.17	4.3	0.08	63
R2	Entran/7bara	0.05	0.88	5.7	0.06	83
R3	XP5/2bara	0.02	0.67	3.0	0.04	50
R4	XP5/2bara	0.02	0.39	5.1	0.02	100

The uncertainty of the position measurement is related to linearity of the position sensor (0.05º), conversion rate of the digital analog converter (neglectable) and signal noise and the post-processing filtering (0.4º). The uncertainty related to signal noise and post-processing was found from the difference in the raw signal and filtered signal. In addition, the anti-aliasing filter of all other sensors gave a time-delay which gave an added uncertainty as a function of rotational speed (0.2º at 380 rpm). The total maximum absolute position uncertainty was 0.45º.

3. Results and discussion

The small speed variation in Figure 21d will in a fast Fourier transform give possible spectral leakage if not properly configured. To remove the effect of small changes in the rotational speed, the measured onboard signals were resampled to a fixed rate position signal. With small speed variation, rotational steps of the position vector were nonuniform. The nonuniform steps are represented by the speed vector in Figure 21d, since speed is first derivative of position. The resample process interpolates the measurands to a fixed number of equally spaced sample points per revolution. To verify the resampling process, FFTs of the signal were calculated before and after resampling. Figure 24a is for reference with ten flat-top windows overlapping with 50%. The results give good amplitude prediction for both signals, but the frequency resolution is low. It is well known that longer windows in FFT will give higher frequency resolution, but varying frequencies will give spectral leakage and thereby reduce amplitude accuracy[20]. This is shown in Figure 24b, where a single window is used for a 30-second measurement. As seen in the figure, the resampled signal is unaffected by the leakage and maintains the correct amplitude. The conversion to the positional domain is therefore considered particularly useful if evaluating speed dependent frequencies in variable speed measurements with short time FFT.

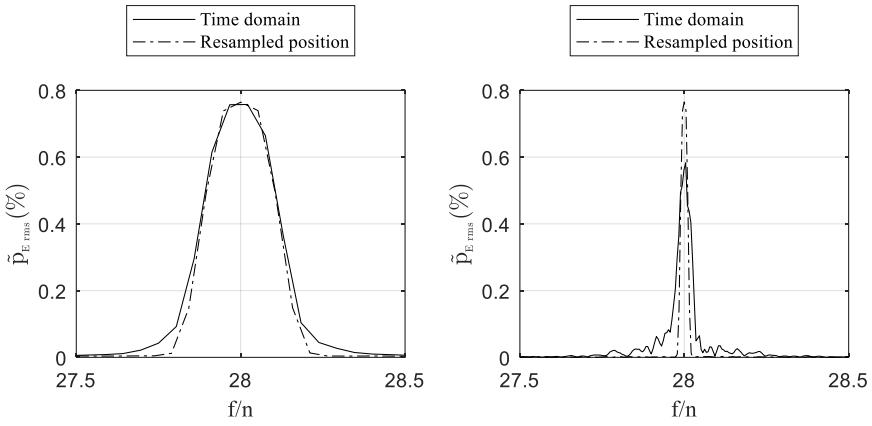

Figure 24 FFT comparison of time domain data and resampled position domain data for guide vane passing fundamental frequency. a) Reference calculation to show unaltered amplitude prediction b) Longer windows for higher frequency resolution, unaffected amplitude accuracy for resampled signal.

Figure 25 shows the measured pressure for R1-R4 for one revolution of the runner. A moving average was calculated for each sensor with window length equal to ten revolutions of the runner to avoid filtering of the frequency content of the signal. An uncertainty band was added according to the uncertainties presented in Table 5.

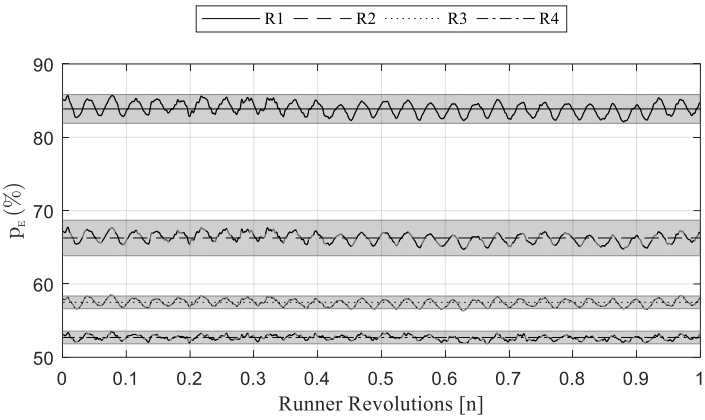

Figure 25 Measured pressure in position R1 to R4. A moving average is calculated for each sensor. The shaded area represents the uncertainty of the moving mean.

To analyse the frequencies in the signals, Fast Fourier Transform (FFT) with Welch method was used. The frequency with predominant amplitude is the guide vane passing frequency as shown in Figure 26.

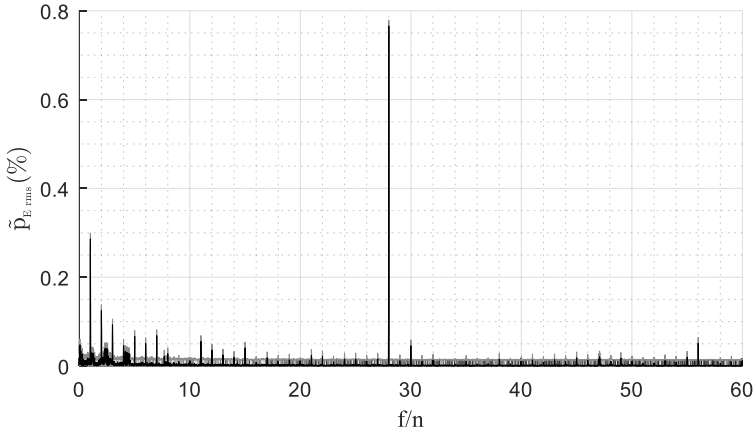

Figure 26 FFT R1 in time domain normalized to runner frequency. Grey shaded area represents uncertainty according to **Table 6**.

By dividing the angular position into 360 sectors, the pressure for each rotational degree of the runner was analysed. In Figure 27, the mean pressure in each sector for 191 revolutions is presented for the sensor R1. The standard deviation for each sector was also calculated and indicated as a 95% interval. This analysis provides information of the pressure for both random and systematic quantities.

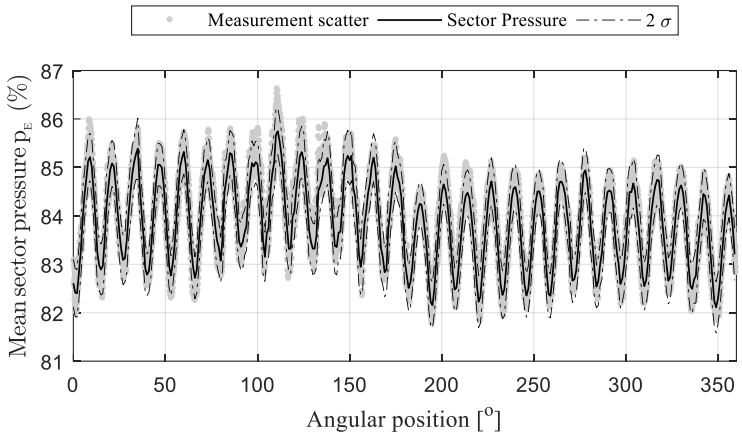

Figure 27 Mean pressure of R1 in one degree angular sectors, calculated from 191 revolutions of the runner.

4. Conclusion

The measurement setup is considered to give valuable data for CFD verification and the study of onboard pressure in the runner. Combined with a CFD analysis, this could provide valuable information for explaining the physics in the runner channel. The position resampled signal is considered to increase the accuracy of measurement analysis. For the mean pressure, the uncertainty of the measurements was mostly affected by the zero stability of the sensors and the repeatability of the measurements. The evaluation of fluctuating quantities is less affected by the uncertainties in the mean pressure. The RSI frequency is found to be the frequency with predominant amplitude in the channel.

References

[1] Rayle R E 1949 *An investigation of the influence of orifice geometry on static pressure measurements* Thesis (Massachusetts Institute of Technology)

[2] H.Bergh and H.Tijdeman 1965 *Theoretical and experimental results for the dynamic response of pressure measuring systems* (Nationaal Lucht- En Ruimtevaartlaboratorium Report)

[3] Franklin R e. and Wallace J M 1970 Absolute measurements of static-hole error using flush transducers *J. Fluid Mech.* **42** 33–48

[4] ISA 2002 *A guide for the dynamic calibration of pressure transducers* (67 Alexander Drive, P. O. Box 12277, Research Triangle Park, North Carolina 27709: ISA)

[5] Farhat M, Natal S, Avellan F, Paquet F, Lowys P Y and Couston M 2002 Onboard Measurements of Pressure and Strain Fluctuations in a Model of low Head Francis Turbine. Part 1 : Instrumentation *Proc. 21st IAHR Symp. Hydraul. Mach. Syst.* 865–72

[6] Perrig A, Avellan F, Kueny J-L, Farhat M and Parkinson E 2005 Flow in a Pelton Turbine Bucket: Numerical and Experimental Investigations *J. Fluids Eng.* **128** 350–8

[7] Pierre-Yves Lowys, Jean-Loup Deniau, Eric Gaudin, Pierre Leroy and Mohand Djatout 2006 On-board model runner dynamic measurements HydroVision (Portland: HCI Publications)

[8] Jansson I and Cervantes M 2007 A method to flush mount replaceable pressure sensors on a 9.3 MW prototype of a Kaplan runner *Proceedings of the 2nd IAHR International Meeting of the Workgroup on Cavitation and Dynamic Problems in Hydraulic Machinery and Systems,* IAHR International Meeting of the Workgroup on Cavitation and Dynamic Problems in Hydraulic Machinery and Systems : 24/10/2007 - 26/10/2007 pp 299–304

[9] Berten S, Hentschel S, Kieselbach K and Dupont P 2011 Experimental and Numerical Analysis of Pressure Pulsations and Mechanical Deformations in a

Centrifugal Pump Impeller *Proceedings of the ASME-JSME-KSME 2011 Joint Fluids Engineering Conference* AJK-Fluids2011 vol 1 (Hamamatsu, Shizuoka, Japan: JSME) pp 297–306

[10] Duparchy F, Favrel A, Lowys P-Y, Landry C, Müller A, Yamamoto K and Avellan F 2015 Analysis of the part load helical vortex rope of a Francis turbine using on-board sensors *J. Phys. Conf. Ser.* **656** 012061

[11] Gao Z, Zhu W, Meng L, Zhang J, Zhang F, Pan L and Lu L 2017 Experimental Study of the Francis Turbine Pressure Fluctuations and the Pressure Fluctuations Superposition Phenomenon Inside the Runner *J. Fluids Eng.* **140** 041208-041208–9

[12] Kobro E 2010 *Measurement of pressure pulsations in Francis turbines* Ph. D. (Norwegian University of Science and Technology, Trondheim)

[13] Trivedi C, Agnalt E and Dahlhaug O G 2018 Experimental study of a Francis turbine under variable-speed and discharge conditions *Renew. Energy* **119** 447–58

[14] Bergan C, Goyal R, Cervantes M J and Dahlhaug O G 2016 Experimental Investigation of a High Head Model Francis Turbine During Steady-State Operation at Off-Design Conditions *IOP Conf. Ser. Earth Environ. Sci.* **49** 062018

[15] IEC 1999 *NEK IEC 60193 Hydraulic turbines, storage pumps and pump-turbines Model acceptance tests*

[16] Physikalisch-Technische Bundesanstalt (PTB) and German Calibration Service (DKD) 2014 Guideline DKD-R 6-1 Calibration of Pressure Gauges

[17] ISO/IEC GUIDE 98-3:2008(E) Guide to the expression of uncertainty in measurement (GUM:1995)

[18] Hessling J P 2006 A novel method of estimating dynamic measurement errors *Meas. Sci. Technol.* **17** 2740

[19] Elster C, Link A and Bruns T 2007 Analysis of dynamic measurements and determination of time-dependent measurement uncertainty using a second-order model *Meas. Sci. Technol.* **18** 3682

[20] Dunn P F 2014 *Measurement and Data Analysis for Engineering and Science, Third Edition* (CRC Press)

“You need a little bit of insanity to do great things”

(Henry Rollins)

The rotor-stator interaction onboard a low specific speed Francis model runner

E Agnalt[1], B W Solemslie[1], P T Storli[1] and O G Dahlhaug[1]

[1]Waterpower Laboratory, Department of Energy and Process Engineering, NTNU - Norwegian University of Science and Technology, Trondheim, Norway

E-mail: einar.agnalt@ntnu.no

Abstract. Over the last years, several breakdowns in hydropower plants with low specific speed Francis runners have been reported. One of the main excitation forces in such runners is the pressure fluctuations originating from the rotor-stator interaction. In this paper, the rotor-stator interaction has been analyzed utilizing pressure sensors onboard the runner. The pressure sensors were flush mounted in the hub of the runner, and the signals were transmitted through a slip-ring system. The measurements have been analyzed relative to the runner angular position by utilizing an angular position sensor mounted to the shaft end. Measurements with different guide vane angle have been compared in order to study the potential flow interaction and the viscous wake effects

for the pressure inside the runner. The results from the onboard pressure measurements found that the phase of the guide vane passing pressure seen by the onboard pressure sensors was independent of the guide vane opening. Hence, the potential flow interaction was found to be the dominant effect and no evidence from the viscous wake effect was found on the onboard pressure.

Index. Francis turbine, position measurement, pressure measurement, rotor-stator interaction

1. Introduction

In the recent years, multiple new power plants with installed Francis runner have experienced breakdown after few running hours[1]. In low specific speed runners, the rotor-stator interaction (RSI) is the main excitation force on the runner[2]. The nature of the rotor-stator interaction is well described in the literature and commonly divided into the effect from potential flow interaction and viscous wake interaction[3–6]. The potential flow effect is related to the accelerated flow in the cascade and the low and high-pressure side of the guide vanes[7]. The viscous wake effect is the defects in the flow field affecting the velocity distribution at the runner inlet[8]. To distinguish between the effect from the potential pressure and the viscous wake, a resource demanding numerical analysis or optical access to the vaneless space could be required[9].

With higher head and material savings in the runners, the RSI was early known to be the root cause for several blade cracks and breakdowns in Francis turbines and pump turbines [10, 11]. Tanaka et.al [11] used a known relation from the turbomachinery industry[12] to show that the hydraulic interference between a blade and a guide vane caused an excitation of the runner creating a global excitation pattern similar to the pattern of the frequency response of the runner. Measurements utilizing onboard sensors in the runner were performed by Kobro [13], with focus on the pressure fluctuations in the channel but the details in the RSI were not covered. Similar onboard studies were

conducted by Zobeiri [14] and Hasmatuchi [15] in a pump turbine. Lewis et.al [16] showed that the use of guide vane jets effected the torque fluctuations in the runner. Possibly, the potential effect was reduced by disturbing the guide vane trailing edge stagnation point. Moreover, numerical studies of the RSI are available[17–21], but the details in the interacting forces from the potential flow effects and the viscous wake are to the authors knowledge only available in the literature for compressible turbomachinery[3].

The current paper presents a method utilizing pressure measurements related to the guide vane angle and the runner angular position. By relating the onboard pressure measurements to the angular position of the runner, more details about the RSI can be found. Due to small angular rotation of the guide vanes, the angular distribution of the potential pressure is expected to be independent of the guide vane angle. The viscous wake interaction is expected to be dependent on the guide vane angle, as the wake follows the slipstream of the guide vane. Detailed knowledge about the driving forces of the RSI phenomena is crucial when designing future runners, avoiding operation at resonance conditions. The objective of the current study is to differentiate the effect from the potential pressure and the viscous wake on the pressure onboard a runner by relating the measurements to the absolute position of the runner.

2. Methods

2.1. Experimental setup

The Francis test-rig available at the Waterpower Laboratory, Norwegian University of Science and Technology was used for the experimental studies[22]. The Francis test-rig was equipped with all required instruments to conduct model testing according to IEC 60193[23]. The runner in current study was a 1:5.1 scale with dimensionless specific speed of 0.07. The design was based on the Tokke power plant in Norway. The runner in the current study was a bolted design with 15+15 splitter and full-length blades. The number of guide vanes was 28 and the spiral casing was bolted through 14 stay vanes. The draft tube of the test rig was an elbow-type. The Francis turbine in the test-rig is shown in Figure 28.

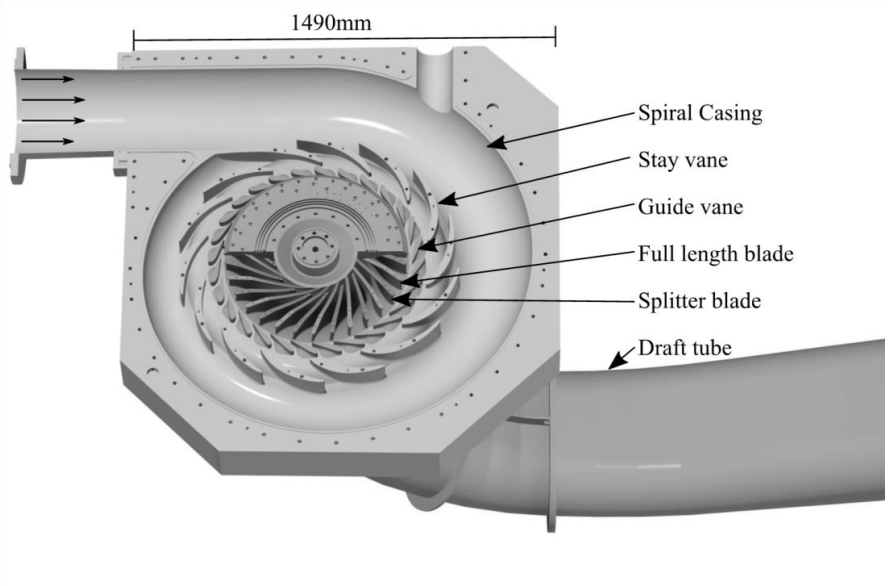

Figure 28 Three-dimensional view of the investigated Francis turbine.

The pressure from the guide vanes acting on the runner is a result of the upstream flow field and the guide vane cascade design. The center section of the guide vane design is shown in Figure 29. The figure indicates the free vortex streamlines from the stay vanes. The guide vanes have an angle of attack relative to the free vortex flow, hence lift and circulation is generated creating potential pressure effects[8]. The trailing edge shape is oblique, known to create weak vortices[24].

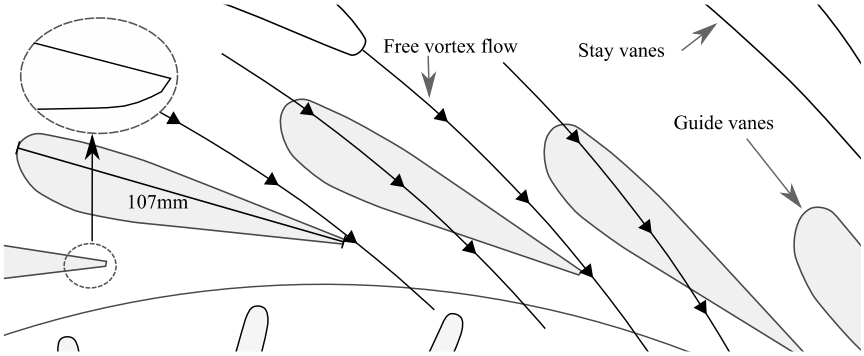

Figure 29 Guide vane design. The arrows indicates the path described by a free vortex flow. The guide vanes directs the flow creating lift and a pressure field

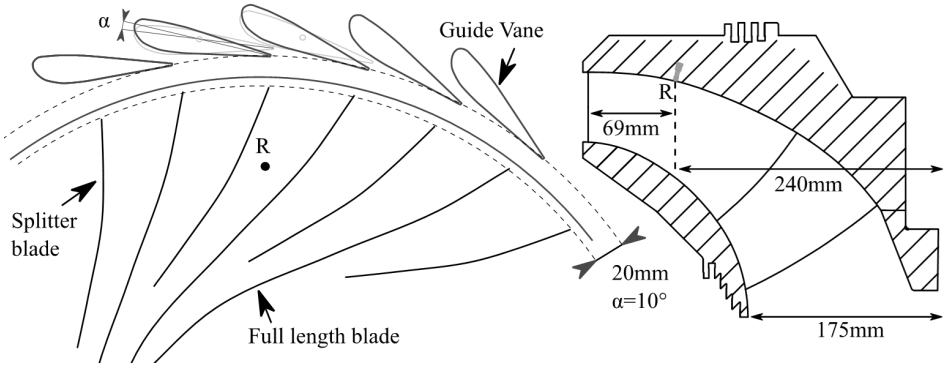

Figure 30 Onboard pressure sensor R

Measurements including moving fluids could be severely influenced by the mounting method of the sensor [25]. Recently, pressure sensors with high accuracy and small sizes have become available with flush mounted diaphragm. For application where accurate flush mounting is possible, the uncertainty from mounting i.e. related to hole size, transmission tubes and cavities will be neglectable[26]. The time and frequency response for the measurements is then only related to the dynamic properties of the diaphragm and

the data acquisition (DAQ) chain[27]. In the current measurements, flush mounted sensors were selected to reduce uncertainty related to mounting method.

Figure 30 shows the locations of the onboard pressure sensor in the turbine (R). The onboard sensor was mounted in the runner hub. The pressure signal was amplified onboard and then transmitted through a slip-ring before the connection to the DAQ system. A slip-ring was utilized to minimize the time synchronization uncertainty between rotating and stationary domain when relating the pressure to the angular position of the runner.

The position sensor was installed on the end of the shaft, above the generator as shown in Figure 31. For easier signal analysis and DAQ configuration, the signal was converted to analog +-10V before the DAQ system with a digital to analog converter (DAC).

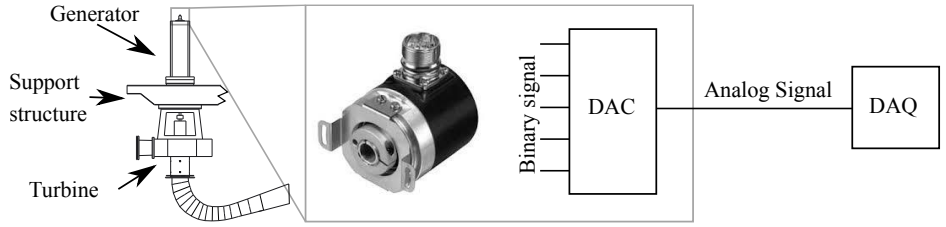

Figure 31 Position sensor on the shaft

2.2. Measurements

The results in this paper are based on the measurements at three operating points, presented in Table 7.

Table 7. Measurement summary. All parameters are defined according to the IEC60193[23]. α is guide vane opening.

Description	n_{ED}	Q_{ED}	Head	α	Speed
Best Efficiency Point (BEP)	0.180	0.154	15.6m	10º	382.7 rpm
Part Load (PL)	0.179	0.107	15.5m	6.7º	379.5 rpm
High Load (HL)	0.179	0.184	15.6m	12.4º	381.9 rpm

2.3. Calibration and uncertainty

Static calibration of the pressure sensors was initially done in an estimated pressure range for the measurements using the guidelines of German Calibration Service[28]. A pneumatic deadweight tester, GE P3000 Series, was used as the primary reference for the pressure calibration. As evaluation of pressure amplitudes is a dynamic quantity, dynamic uncertainty must be addressed. All components in the current pressure measurement chain, from the sensors to the data acquisition, are stated to have resonance frequencies above 10kHz, hence the dynamic uncertainty is assumed to be neglectable and only repeatability and hysteresis from static calibration remain in the uncertainty evaluation. A repeatability test was conducted at 1 Hz with a pressure alternating between 100kPa and 90kPa absolute pressure. The uncertainty budget for the RSI guide vane passing amplitudes at BEP is presented in Table 8

Table 8. Uncertainty budget for RSI amplitudes, BEP

	1Hz Repeatability [kPa]	Amplitude RMS of fundamental RSI [kPa]	Relative Uncertainty [%]	Amplitude RMS of first harmonic RSI [kPa]	Relative Uncertainty [%]
R	0.01	1.17	0.85	0.08	13

The uncertainty budget for the position sensor (Z) is summarized in Table 9. The uncertainties are based on the given data for the encoder and the DAC. A smoothing filter was utilized to filter the signal noise, and the noise uncertainty was calculated from the

difference in the raw signal and the filtered position signal used in the analysis. Timing uncertainties were converted to angular offset with the average of the speeds given in Table 7

Table 9. Uncertainty budget of position sensor

Encoder linearity [º]	DAC conversion rate [º]	Noise [º]	Time delay [º]	Total absolute uncertainty [º]
0,05	0	0,4	0,2	0,45

The position accuracy was verified with several measurements at BEP, at different rotational speed and head. The angular shift of the pressure was calculated with cross-correlation and was found to be within the stated total absolute uncertainty.

3. Results

All pressure values presented is calculated as percentage of potential energy (E=gH) and denoted pE(%) as recommended by the IEC60193[23]. H is net head. Fluctuating quantities are denoted with a tilde (~).

The analysis of the measurands relative to position was done with the use of angular sectors. Sector limits were defined, and measurands falling within the limits were added in a sector group. For all values in each sector group, the mean, standard deviation, minimum and maximum were calculated. The process is shown in Figure 32 where the sector steps are indicated by the minor grid lines. For good visibility of the sectors, the step is set to 2 degrees. In addition to the analysis in Figure 32, the distribution of values in each sector was calculated. The data was close to normally distributed for all sectors, hence the variation is believed to be of random nature.

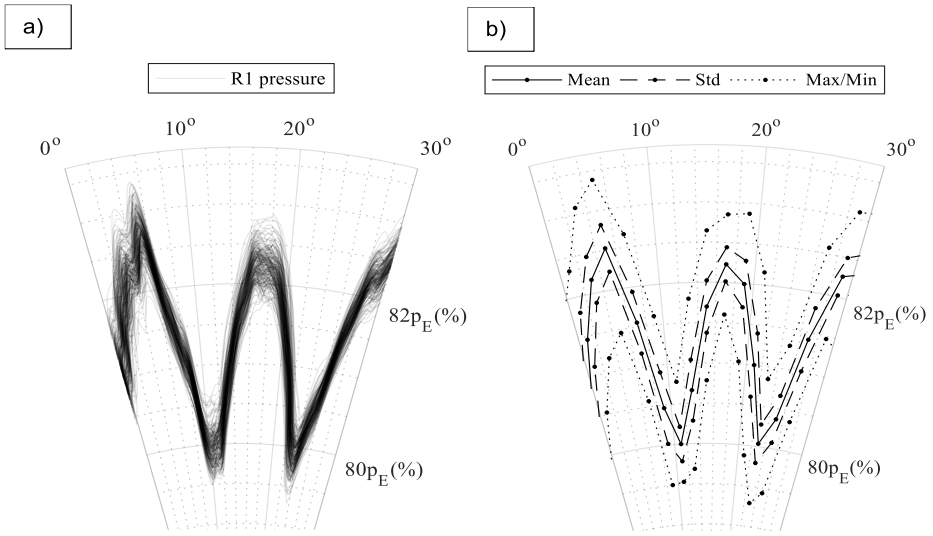

Figure 32 a) The measured pressure, with sensor R for 180 revolutions of the runner. The plot is made with semi-opaque lines, hence darker color indicate multiple overlapping lines. b) Calculation in each sector. Mean, standard deviation and maximum/minimum values.

The following results were analyzed in sectors for each 0.5 degrees for higher resolution and phase accuracy. In Figure 33 the mean pressure for each sector is shown for guide vane angle 6.7, 10.0 and 12.4 as presented in Table 7. A high-pass filter was used to increase the comparability by removing the low frequency content.

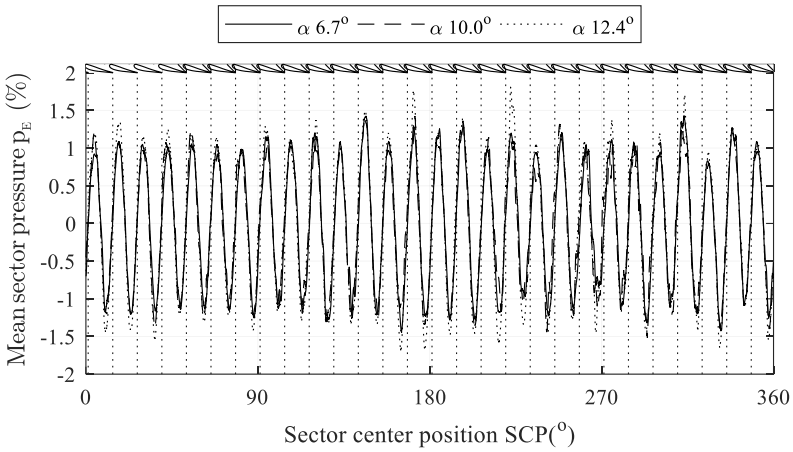

Figure 33 The mean pressure in the runner for all sectors. The mean is calculated from 180 full revolutions. The vertical lines indicates the distance between the guide vanes

To highlight the details, the sectors from 0º to 40º is shown in Figure 34.

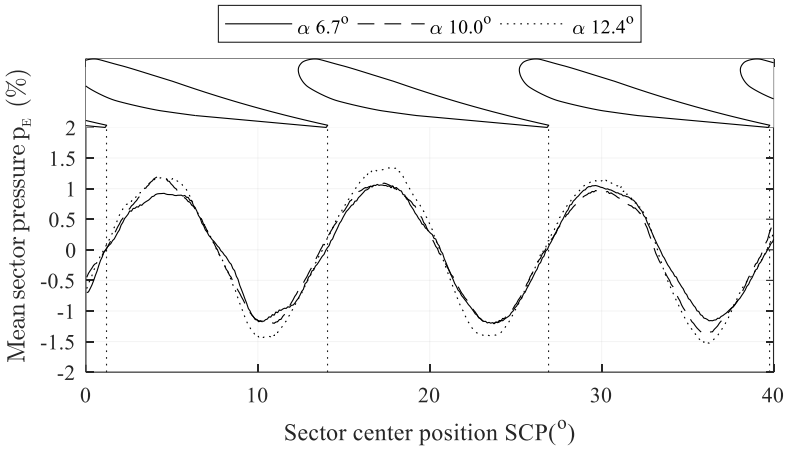

Figure 34 The mean pressure for the sectors in the range 0º to 40º. The mean is calculated from 180 full revolutions. The vertical lines indicates the distance between the guide vanes

Further details of the measured amplitudes were analyzed with the use of short time fast Fourier transform. The analysis was performed with window length equal to 100 periods of the RSI signal and with 50% overlap. The main component of the presented measurement in Figure 34 is the fundamental of the guide vane passing pressure. In Figure 35, the amplitudes of the guide vane passing pressure is shown. The uncertainty bars represent the 95% probability.

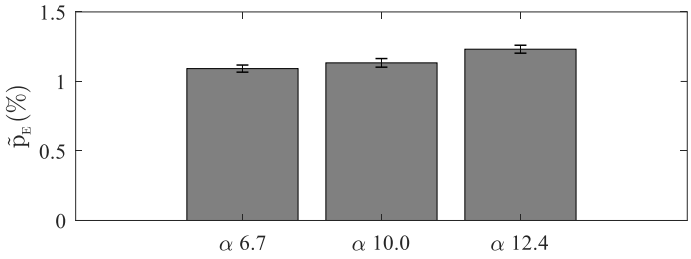

Figure 35 The fundamental guide vane passing frequency amplitude with 95% probability for the sensor R. The amplitude is percentage of head.

4. Discussion

The analysis of the rotor-stator interaction onboard the runner was carried out by analyzing the pressure in one runner channel measured with pressure sensor R. Three guide vane opening angles were investigated to analyze the pressure. It was expected to find a phase shift between the measurements with different guide vane opening relative to the runner position if the viscous wake was the main source for the pressure in the channel as illustrated in Figure 36. With increasing guide vane opening, the pressure should have a recognizable phase shift against the rotational direction of the runner. Also, from classical wake theory, the pressure amplitudes were expected to be lower since the viscous wake was expected to be weaker on lower guide vane openings, due to longer distance from the trailing edge of the guide vane to the impact point and lower flow velocity[29]. Contrarily, with larger guide vane openings, the wake was directed more on the runner, and the pressure effect from the viscous wake was expected to be more visible.

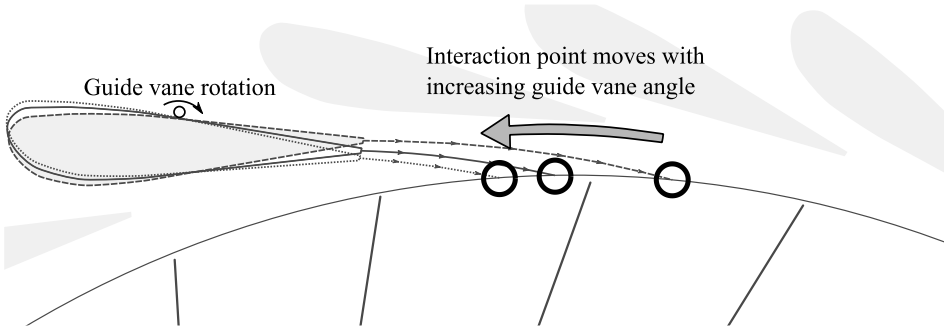

Figure 36 The viscous wake interaction point with the runner. The interaction point is expected to be dependent on the angular position of the guide vane. The indicated wake is assumed to follow a path described by a free vortex flow.

The dependency of the potential pressure to the guide vane angle was assumed neglectable compared to the viscous wake angular dependency. Due to the Kutta condition, the stagnation point will be located at the trailing edge for all measurements[30], and the trailing edge tangential movement around the runner is in the order of millimeters. At the outlet of the guide vane cascade, the expected pressure field is illustrated in Figure 37a. High-pressure zones are located around the trailing edge stagnation points. The angular position of the runner in Figure 37b illustrates the runner position when the channel with the sensor R is most effected by the high pressure zone. This corresponds to the position were the guide vane trailing edge stagnation point is in the middle of the channel.

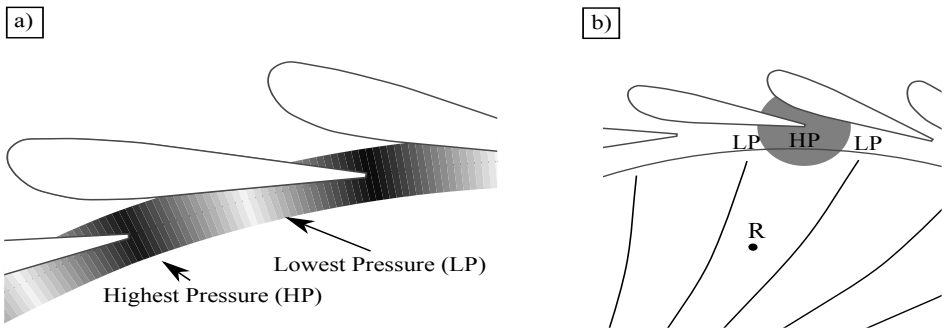

a b

Figure 37 a) Illustration of the potential pressure at the outlet of the guide vane cascade. b) The angular position of one runner channel relative to the guide vanes where the effect from potential pressure is expected to be at maximum.

With increasing guide vane angle, the potential pressure effect was expected to give higher pressure fluctuations in the runner, because the gap between the guide vanes to the runner was reduced, and because the strength of the pressure field was expected to increase due to higher flow. On the other hand, a decreasing factor was a possible reduction in the lift force since the guide vanes were more aligned with the free vortex flow from the stay vanes with increasing guide vane opening, as shown in Figure 29. From the amplitude analysis shown in Figure 35, there was an increasing trend in amplitude with increasing guide vane opening indicating the influence of the increasing factors.

From the results presented in Figure 33 and Figure 34, there is no evidence of a significant phase shift for the pressure in the runner channel relative to position. From the previous discussion about viscous wakes dependency of the guide vane angle and the expected phase shift in the pressure, no evidence of the viscous wake effect in the runner pressure is found. By comparing the assumed position of the highest pressure influence from the potential pressure shown in Figure 37b and the measured pressure shown in Figure 34, it is clear that the potential pressure is the source for the pressure fluctuations

in the runner channel. However, the RSI is highly dependent on the guide vane cascade design and flow conditions[31]. Hence, different lift conditions in the guide vane section and less favorable trailing edge design of the guide vanes will create different results.

5. Conclusion

Analysis of the influence from potential pressure and the viscous wake was done by varying the guide vane angle, hence moving the interaction point of the viscous wake on the runner. The pressure in the runner channel was monitored with a pressure sensor mounted in the runner hub. The analysis of the measurements did not find any phase shift in the pressure relative to the runner position for the investigated guide vane openings. Hence, the pressure in the runner was found to be highly dependent on the potential pressure in the guide vane cascade and there is no clear evidence of any effect on the pressure in the runner channel from the viscous wake. As the geometry in current study is open and available[32], the results could be used for numerical verification. The presented experimental method should be repeated for several designs with a large head range preferably on prototypes for validation.

References

[1] Østby, P. T. K., Billdal, J. T., Sivertsen, K., Haugen, B., and Dahlhaug, O. G., 2016, "Dynamic Stresses In High Head Francis Turbines," Hydropower & Dams, no. 3.

[2] Seidel, U., Hübner, B., Löfflad, J., and Faigle, P., 2012, "Evaluation of RSI-induced stresses in Francis runners," IOP Conference Series: Earth and Environmental Science, vol. 15, no. 5, p. 052010.

[3] Gallus, H. E., Lambertz, J., and Wallmann, T., 1980, "Blade-Row Interaction in an Axial-Flow Subsonic Compressor Stage," J. Eng. Power, vol. 102, no. 1, pp. 169–177.

[4] D. Y. Li, R. Z. Gong, H. J. Wang, X. Z. Wei, Z. S. Liu, and D. Q. Qin, 2016, "Analysis of Rotor-Stator Interaction in Turbine Mode of a Pump-Turbine Model," Journal of Applied Fluid Mechanics, vol. 9, no. 5, pp. 2559–2568.

[5] Arndt, N., Acosta, A., Brennen, C. E., and Caughey, T. K., 1989, "Rotor-stator interaction in a diffuser pump," ASME Journal of Turbomachinery, vol. 111, pp. 213–221.

[6] Dring, R. P., Joslyn, H. D., Hardin, L. W., and Wagner, J. H., 1982, "Turbine Rotor-Stator Interaction," J. Eng. Power, vol. 104, no. 4, pp. 729–742.

[7] Østby, P. T. K., Billdal, J. T., Haugen, B., and Dahlhaug, O. G., 2017, "On the relation between friction losses and pressure pulsations caused by Rotor-stator interaction on the Francis-99 turbine," J. Phys.: Conf. Ser., vol. 782, no. 1, p. 012010.

[8] Antonsen, Ø., 2007, "Unsteady flow in wicket gate and runner with focus on static and dynamic load on runner," Doctoral Thesis, Norwegian University of Science and Technology, Trondheim, Norway.

[9] Gagnon, J.-M., Ciocan, G. D., Deschenes, C., and Iliescu, M., 2008, "Numerical and Experimental Investigation of Rotor-Stator Interactions in an Axial Turbine: Numerical Interface Assessment," in Proceedings of FEDSM2008, Jacksonville, Florida USA, pp. 929–935.

[10] Brekke, H., "A Review on Oscillatory Problems in Francis Turbine," in New Trends in Technologies: Devices, Computer, Communication and Industrial Systems, 2010, InTech.

[11] Tanaka, H., 2011, "Vibration Behavior and Dynamic Stress of Runners of Very High Head Reversible Pump-turbines," International Journal of Fluid Machinery and Systems, vol. 4, no. 2, pp. 289–306.

[12] Tyler, J. M. and Sofrin, T. G., 1962, "Axial Flow Compressor Noise Studies," SAE International, Warrendale, PA, 620532.

[13] Kobro, E., 2010, "Measurement of Pressure Pulsations in Francis Turbines," Doctoral Thesis, Norwegian University of Science and Technology, Trondheim, Norway.

[14] Zobeiri, A., 2009, "Investigations of Time Dependent Flow Phenomena in a Turbine and Pump-Turbine of Francis Type: Rotor-Stator Interactions and Precessing Vortex Rope," EPFL, Lausanne.

[15] Hasmatuchi, V., 2012, “Hydrodynamics of a pump-turbine operating at off-design conditions in generating mode,” Doctoral Thesis, Ecode Polytechnique Federale de Lausanne, Lausanne, Switzerland.

[16] Lewis, B. J., Cimbala, J. M., and Wouden, A. M., 2012, “Investigation of distributor vane jets to decrease the unsteady load on hydro turbine runner blades,” IOP Conf. Ser.: Earth Environ. Sci., vol. 15, no. 2, p. 022006.

[17] Li, Z., Wang, Z., Wei, X., and Qin, D., 2016, “Flow Similarity in the Rotor–Stator Interaction Affected Region in Prototype and Model Francis Pump-Turbines in Generating Mode,” J. Fluids Eng, vol. 138, no. 6, pp. 061201–061201.

[18] Yan, J., Koutnik, J., Seidel, U., and Hübner, B., 2010, “Compressible simulation of rotor-stator interaction in pump-turbines,” IOP Conference Series: Earth and Environmental Science, vol. 12, p. 012008.

[19] Yonezawa, K., Toyahara, S., Motoki, S., Tanaka, H., Doerfler, P., and Tsujimoto, Y., 2014, “Phase Resonance in Centrifugal Fluid Machinery,” IJFMS, vol. 7, no. 2, pp. 42–53.

[20] Xia, L., Cheng, Y., and Cai, F., 2017, “Pressure Pulsation Characteristics of a Model Pump-turbine Operating in the S-shaped Region: CFD Simulations,” IJFMS, vol. 10, no. 3, pp. 287–295.

[21] Yan, J., Koutnik, J., Seidel, U., and Hübner, B., 2010, “Compressible Simulation of Rotor-Stator Interaction in Pump-Turbines,” IJFMS, vol. 3, no. 4, pp. 315–323.

[22] Trivedi, C., Agnalt, E., and Dahlhaug, O. G., 2018, “Experimental study of a Francis turbine under variable-speed and discharge conditions,” Renewable Energy, vol. 119, pp. 447–458.

[23] IEC, 1999, “NEK IEC 60193 Hydraulic turbines, storage pumps and pump-turbines Model acceptance tests.”

[24] Zobeiri, A., Ausoni, P., Avellan, F., and Farhat, M., 2012, “How oblique trailing edge of a hydrofoil reduces the vortex-induced vibration,” Journal of Fluids and Structures, vol. 32, pp. 78–89.

[25] Rayle, R. E., 1949, “An investigation of the influence of orifice geometry on static pressure measurements,” Master Thesis, Massachusetts Institute of Technology, Cambridge, Massachusetts, USA.

[26] Franklin, R. e. and Wallace, J. M., 1970, “Absolute measurements of static-hole error using flush transducers,” Journal of Fluid Mechanics, vol. 42, no. 01, pp. 33–48.

[27] Hessling, J. P., 2006, “A novel method of estimating dynamic measurement errors,” Measurement Science and Technology, vol. 17, no. 10, p. 2740.

[28] Physikalisch-Technische Bundesanstalt (PTB) and German Calibration Service (DKD), “Guideline DKD-R 6-1 Calibration of Pressure Gauges.” Mar-2014.

[29] White, F. M., 2005, Viscous Fluid Flow, 3 edition. New York, NY: McGraw-Hill Education.

[30] White, F., 2015, Fluid Mechanics, 8 edition. New York, NY: McGraw-Hill Education.

[31] Thapa, B. S., Trivedi, C., and Dahlhaug, O. G., 2016, “Design and development of guide vane cascade for a low speed number Francis turbine,” Journal of Hydrodynamics, Ser. B, vol. 28, no. 4, pp. 676–689.

[32] “Francis-99 NTNU.” [Online]. Available: https://www.ntnu.edu/nvks/francis-99. [Accessed: 10-Sep-2018].

"The lesson is that no matter how plausible a theory seems to be, experiment gets the final word"

(Robert L. Park. 2000. Voodoo Science. New York: Oxford University Press)

On the rotor-stator interaction effects of low specific speed Francis turbines

Einar Agnalt[1], Igor Iliev[1] Bjørn Winther Solemslie[1] and Ole Gunnar Dahlhaug[1]

[1]1Waterpower Laboratory, Norwegian University of Science and Technology
Alfred Getz v. 4, 7034 Trondheim, Norway,
einar.agnalt@ntnu.no, igor.iliev@ntnu.no, bjorn.w.solemslie@ntnu.no,
ole.g.dahlhaug@ntnu.no

Abstract

The rotor-stator interaction in a low specific speed Francis model turbine and a pump-turbine is analyzed utilizing pressure sensors in the vaneless space and in the guide vane cascade. The measurements are analyzed relative to the runner angular position by utilizing an absolute encoder mounted on the shaft end. From the literature, the pressure in the analyzed area is known to be a combination of two effects: the rotating runner pressure and the throttling of the guide vane channels. The measured pressure is fitted to a mathematical pressure model to separate the two effects for two different runners. One turbine with 15+15 splitter blades and full-length blades and one pump-turbine with six blades are investigated. The blade loading on the two runners is different, giving different input for the pressure model. The main findings show that the pressure fluctuations in the guide vane cascade are mainly controlled by throttling for the low blade loading case and the rotating runner pressure for the higher blade loading case.

Experimental study of the rotor-stator interaction in a low specific speed Francis turbine and a pump-turbine

1. Introduction

The rotor-stator interaction (RSI) is known to be the main source for pressure fluctuations in low specific speed turbines. The pressure from the rotating runner causes pressure fluctuations in the vaneless space, guide vane cascade and farther upstream in the spiral casing and the inlet conduit. This phenomenon has been thoroughly investigated for decades in hydraulic machinery. In the open literature, various terms are used to describe the effects of the RSI, such as throttling, blocking, potential interaction, rotating runner pressure field, squeezing, etc. The throttling and blocking are the effects creating the fluctuating pressure and velocity in the guide vane cascade. The source of the fluctuations is the downstream runner with high and low-pressure sides of the blades giving fluctuations in the downstream boundary condition of each guide vane passage. The potential interaction is the combination of the two pressure fields in the rotor and stator. The rotating pressure field is the high and low pressure onboard the runner due to the blade loading, seen from the stationary domain and the stationary pressure field is the high and low pressure around each guide vane.

Several studies focus on how the RSI fluctuations in Francis runners and pump runners effect the surroundings of the runner and how to predict the pressure fluctuations, but details about the RSI effects are not discussed[1–3]. Zobeiri et.al [4] focused on the pressure propagation of the RSI in the guide vane cascade and the spiral casing in a pump-turbine in generating mode. The presented results showed how the rotor-stator interaction created pressure fluctuations in the monitored area. By investigating the presented figures, the highest pressure was found when the high-pressure side of the impeller was near the measuring sensor. In the guide vane cascade, the highest pressure was found when the high-pressure side of the impeller was in the same location as the guide vane trailing edge stagnation pressure. In addition, an observation of a higher harmonic can be seen in the measurements without further discussion. Yonezawa et.al [5] showed how the RSI interacted with the penstock waves and created a resonance condition. The unsteady pressure propagating upstream the runner was strongly connected to the rotor-stator

interaction through the throttling effect. Qian [6], Ciocan and Kueny [7] and Hasmatuchi [8] did detailed studies of the velocity field in the vaneless gap and the guide vane cascade. Major findings were how the runner blades created a blockage of the flow in the guide vanes and thereby creating a velocity fluctuation in the entire guide vane cascade, and details about the velocity field in the guide vane cascade could be seen. Other explanations found in the literature for the RSI includes a "shock" created when the blade leading edge is in the vicinity of a guide vane trailing edge and the different amplitudes found in the vaneless space is explained with squeezing of water towards the guide vanes.

Based on the findings in the literature, the RSI in the vaneless gap and in the guide vane passages can be seen as a combination of two effects, namely the throttling of the flow in the guide vane passages and the rotating pressure field from the runner. Both effects originates from the rotating pressure field, but the throttling of the guide vane passages creates pulsations in the velocity field, in and upstream the guide vane cascade, which could create a hydro-acoustic resonance condition. The rotating pressure field would decay exponentially with the distance from the runner if there were no guide vanes, and the throttling of the guide vane channels is the effect creating upstream fluctuations[9].

The current paper presents pressure measurements in the vaneless space to investigate the physics of the RSI. To enable a detailed analysis, three sensors were utilized in the vanless space and one in the guide vane cascade to distinguish between the throttling and the rotating pressure field effects. The throttling effects were assumed to be in phase for the pressure sensors in the same guide vane channel, while the pressure field rotating with the runner was phase shifted corresponding to the position of the pressure sensors. From these assumptions, a mathematical pressure model was developed to analyse both effects. The purpose of the pressure model is to detect both the various amplitudes and the phase shifts measured in the pressure field in the vaneless space. The main objective of the current study is to decompose the measured pressure in the effect of throttling and the rotating pressure field to increase the details and the precision in the understanding of the rotor-stator interaction effects.

2. Methods

2.1. Experimental setup

The Francis test-rig available at the Waterpower Laboratory, Norwegian University of Science and Technology was used for the experimental studies[11]. The Francis test-rig was equipped with all required instruments to conduct model testing according to IEC 60193[12]. The number of guide vanes was 28 and the spiral casing was bolted through 14 stay vanes. The draft tube of the test rig was an elbow-type. The Francis turbine in the test-rig is shown in Figure 38

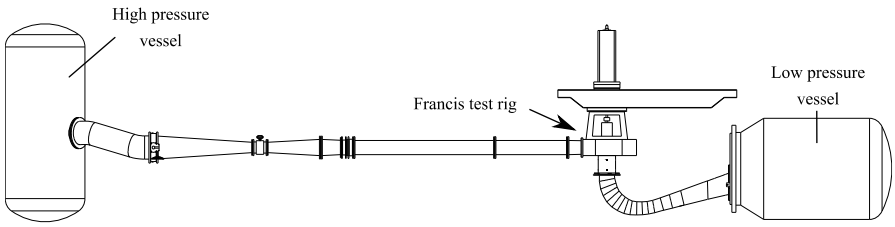

Figure 38 The Francis test-rig, including the high and low pressure vessel.

Measurements were performed on two runners in the Francis test rig. First a bolted design with 15+15 splitter and full-length blades utilized in the Francis 99 research project[11], denoted F99, and second a reversible pump turbine, denoted RPT, with six blades as shown in Figure 39. The F99 runner has dimensionless specific speed of 0.07 and the RPT 0.08. Both runners were designed to fit the same test-rig; hence main dimensions were equal. The F99 runner was based on the Tokke powerplant in Norway and was developed to provide measurements on an open geometry to the hydropower research community. The RPT was designed to study the instable behavior at part-load for low specific speed pump-turbines[13].

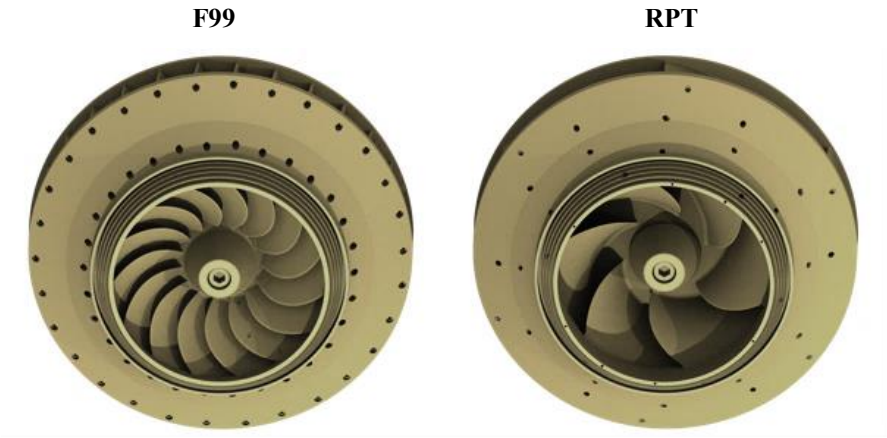

Figure 39 Three-dimensional view of the investigated runners.

Flush mounted sensors were selected to reduce uncertainty related to the mounting method[14]. Figure 41 shows the locations of the pressure sensor in the turbine (S1 to S4). All sensors were bridge sensors directly connected to the data acquisition (DAQ) system with excitation voltage from the DAQ module. The position sensor was installed on the end of the shaft, above the generator as shown in Figure 40. The signal was converted to analog +-10V before the DAQ system with a digital to analog converter (DAC) to utilize synchronized parallel sampling with the signals from the pressure sensors.

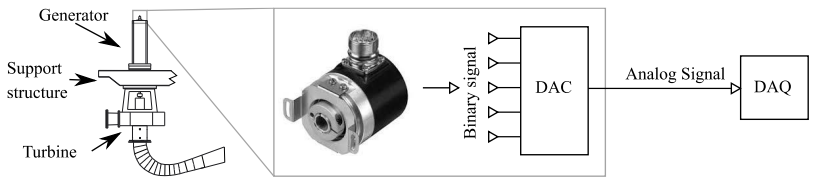

Figure 40 Absolute position sensor on the shaft end above the generator

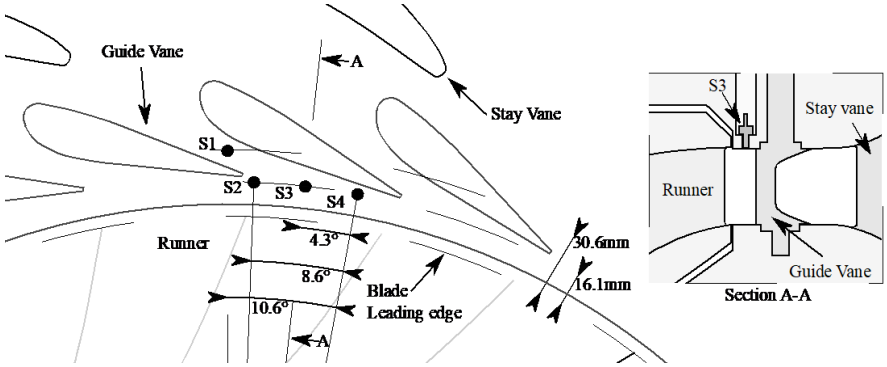

Figure 41 Pressure sensors in the vaneless space and in the guide vane cascade. The angular distance between sensor S2-S3 and S3-S4 is 4.3º. The sensors were flush mounted in the upper cover of the turbine as shown with sensor S3. The distance from the runner blades leading edges to the sensors are 16.1mm and 30.6mm.

2.2. Measurements

The results in this paper are based on the measurements conducted at the operational points presented in Table 10. Several guide vane openings were investigated, but the results were similar and the best efficiency point (BEP) for both runners were selected to have the best signal to noise ratio.

Table 10. Measurement summary. α is guide vane opening as defined in the IEC60193[12].

Description	n_{ED}	Q_{ED}	Head	α	Flow	Efficiency	Speed
F99, BEP	0.180	0.154	15.6m	10º	0.232m^3/s	92.2%	382.2 rpm
RPT, BEP	0.220	0.134	12.0m	11º	0.185m^3/s	89.1%	412.7 rpm

2.3. Calibration and uncertainty

Static calibration of the pressure sensors was initially done in an estimated pressure range for the measurements with a GE P3000 Series pneumatic deadweight tester as the primary reference. As evaluation of pressure amplitudes is a dynamic quantity, dynamic uncertainty must be addressed. All components in the current pressure measurement chain, from the sensors to the data acquisition, are stated to have resonance frequencies above 10kHz, hence the dynamic uncertainty is assumed to be neglectable and only repeatability and hysteresis from static calibration remain in the uncertainty evaluation. A repeatability test was conducted at 1 Hz with a pressure alternating between 100kPa and 90kPa absolute pressure. The uncertainty budget for the RSI blade passing amplitudes at BEP is shown in Table 11.

Table 11. Uncertainty budget for RSI first and second harmonic amplitudes, BEP F99

Sensor	1Hz Repeatability [kPa]	Amplitude RMS of first harmonic RSI [kPa]	Relative Uncertainty [%]	Amplitude RMS of second harmonic RSI [kPa]	Relative Uncertainty [%]
S1	0.002	0.404	0.50	0.028	7.2
S2	0.005	0.462	1.1	0.018	28
S3	0.002	1.218	0.16	0.064	3.1
S4	0.002	1.118	0.18	0.098	2.0

The uncertainty budget for the position sensor (Z) is summarized in Table 12. The uncertainties are based on the given data for the encoder and the DAC. A smoothing filter was utilized to filter the signal noise and the noise uncertainty was calculated from the difference in the raw signal and the filtered position signal used in the analysis[15]. Timing uncertainties were converted to angular offset with the average of the speeds given in Table 10

Table 12. Uncertainty budget of position sensor

Encoder linearity [º]	DAC conversion rate [º]	Noise [º]	Time delay [º]	Total absolute uncertainty [º]
0,05	0	0,4	0,2	0,45

The position accuracy was verified with several measurements at BEP, at different rotational speed and head. The angular shift of the pressure was calculated with cross-correlation and was found to be within the stated total absolute uncertainty.

2.4. Pressure model

All pressure values presented were calculated as percentage of specific hydraulic energy of the machine (E=gH) and denoted pE(%) as recommended by the IEC60193[11] where H is net head. The pressure fluctuations in the vaneless space and guide vane channels were assumed to be a linear combination of a rotating runner pressure field ($\tilde{p}_r$) and a variation in the guide vane cascade pressure due to throttling of the respective guide vane channel ($\tilde{p}_b$). The total pressure fluctuation measured in each location ($\tilde{p}_t$) were the superposition of the runner pressure and the guide vane channel pressure, hence a two way coupling was not considered. All measured pressures were modelled as a sum of sines and as a function of the runner position, *x.* The frequencies (*f)* were normalized to the runner rotational frequency and harmonics was denoted i for each sensor (*k).* A phase offset $\delta_{k,i}$ was introduced to set the start position of each harmonic. The amplitudes ($a_{k,i}$).were independent for each sensor and each harmonic.

$$\tilde{p}_{t,k} = \tilde{p}_{r,k} + \tilde{p}_{b,k} = \sum_i a_{k,i} \cdot \sin\left(i \cdot f \cdot x + \delta_{k,i}\right) \quad (1)$$

For the throttling pressure, the measurements in each sensor position were in the same guide vane channel, hence each harmonic of the pressure for all sensors were assumed to have the same phase. A harmonic phase offset (γ_i) was utilized for the start position of the pressure. The amplitudes ($b_{k,i}$).were independent for each sensor and each harmonic.

$$\tilde{p}_{b,k} = \sum_i b_{k,i} \cdot \sin(i \cdot f \cdot x + \gamma_i) \quad (2)$$

The runner pressure was assumed equal for each measurement position. Due to the rotation of the runner, the phases were set equal to the sensor angular offset (θ_k). An additional parameter (φ_i) was introduced to allow phase position adjustment of each harmonic. The amplitudes (c_i).were independent for each harmonic, but in common for each sensor.

$$\tilde{p}_{r,k} = \sum_i c_i \cdot \sin(i \cdot f \cdot x + \varphi_i - i \cdot f \cdot \theta_k) \quad (3)$$

The equation for the total pressure fluctuation was eq. (2) and (3) inserted into eq. (1)

$$\begin{aligned} \tilde{p}_{t,k} &= \sum_i b_{k,i} \cdot \sin(i \cdot f \cdot x + \gamma_i) \\ &\quad + \sum_i c_i \cdot \sin(i \cdot f \cdot x + \varphi_i - i \cdot f \cdot \theta_k) \\ &= \sum_i a_{k,i} \cdot \sin\left(i \cdot f \cdot x + \delta_{k,i}\right) \end{aligned} \quad (4)$$

The total number of unknowns were $i \cdot (2 \cdot k + 1)$ and the number of constants were $i \cdot (k + 3)$ as a function of the number of harmonics and the number of sensors calculated. However, eq. (4) with more than one harmonic gave more than one solution; hence, a stepwise calculation was performed. The first harmonic was solved initially, then the next harmonic with the previous as constants as shown in Table 13 .

Table 13. Stepwise calculation of pressure field

Fit	Formula	Fit coefficients	Constants
j=1	$c_{k,1} \cdot \sin(1 \cdot f \cdot x + \varphi_1 - 1 \cdot f \cdot \theta_k) + b_{k,i} \cdot \sin(1 \cdot f \cdot x + \gamma_1) = a_{k,1} \cdot \sin(1 \cdot f \cdot x + \delta_{k,1})$	$c_1, \varphi_1, b_{k,1}, \gamma_1$	$a_{k,1}, \delta_{k,1}, \theta_k$
j>1	$\sum_{i=1}^{j-1}[c_i \cdot \sin(i \cdot f \cdot x + \varphi_i - i \cdot f \cdot \theta_k)] + c_j \cdot \sin(j \cdot f \cdot x + \varphi_j - j \cdot f \cdot \theta_k) + \sum_{i=1}^{j-1}[b_{k,i} \cdot \sin(i \cdot f \cdot x + \gamma_i)] + b_{k,j} \cdot \sin(j \cdot f \cdot x + \gamma_j) = \sum_{i=1}^{j}[a_{k,i} \cdot \sin(i \cdot f \cdot x + \delta_{k,i})]$	$c_j, \varphi_j, b_{k,j}, \gamma_j$	$a_{k,1}, \delta_{k,1}, \theta_k, c_1, \varphi_1, b_{k,1}, \gamma_1, \ldots c_{j-1}, \varphi_{j-1}, b_{k,j-1}, \gamma_{j-1}$

3. Results and discussion

The following steps were performed:

1. Presentation of the measurement data
2. Analysis of the amplitude and phase information in the measured data wit least square fitting to a sum of sines, eq. (1)
3. Analysis of the effect from throttling and rotating pressure with least square fitting, eq. (4)
4. Compare the calculated throttling effect with the measurement S1.

The measurements were analysed relative to the position of the runner, which was discretised into 720 angular sectors and the data from 600 revolutions was analysed in

each sector. The details about the analysis method were published in a previous paper[14]. In order to compare the phase shifts with the position relative measurements, it was converted to runner angular position change. The relation between the runner angular position (θ) and the pressure phase shift (ϕ) of the harmonic (i) of a normalized frequency (f) is:

$$\phi = \theta \cdot i \cdot f \tag{5}$$

The pressure in the vaneless space was measured with sensors S2 to S4 and the pressure in one guide vane channel with the sensor S1. The sensor S1 was utilized as a reference for the throttling phase with the assumption of pure throttling effect inside a guide vane channel. The sensors S2-S4 were used for the calculations of the pressure model. The measurements were high pass filtered at half the blade passing frequency to remove the lower frequency effects.

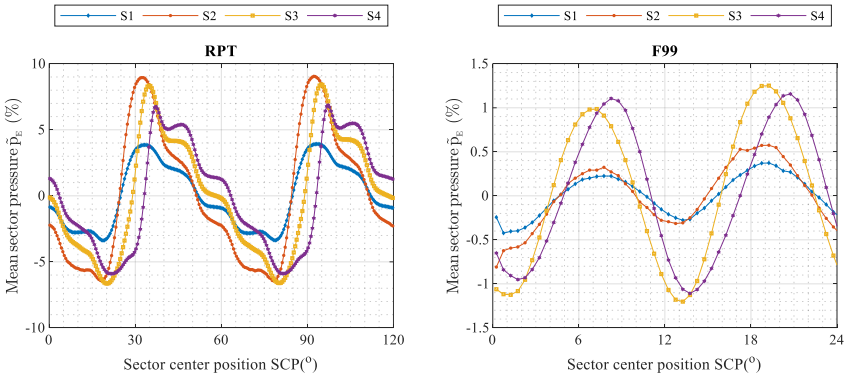

Figure 42 The mean sector pressure from the pressure sensors as percentage of head. The angular size of each sector was 0.5º, with 720 sectors in total. The mean sector pressure was calculated from 600 full revolutions.

In Figure 42, the pressure measured with sensor S1 and S2 fluctuated in phase for both the F99 and the RPT. This was similar to the results found in the literature described as

throttling. For the sensors S2 to S4, the measurements were not according to pure throttling, nor pure rotational pressure. In the F99 case, the pressure at S4 was lagging compared to S1 to S3, while the RPT measurements had a lagging close to the angular shift of the pressure sensors (θ). In addition, the amplitudes in the different sensor locations was varying for the F99, while the RPT amplitudes were in the same range, especially for S2-S4 in the vaneless space. From the measurements, the F99 seemed mostly effected by the throttling, while the RPT mainly effected by the rotating runner pressure field.

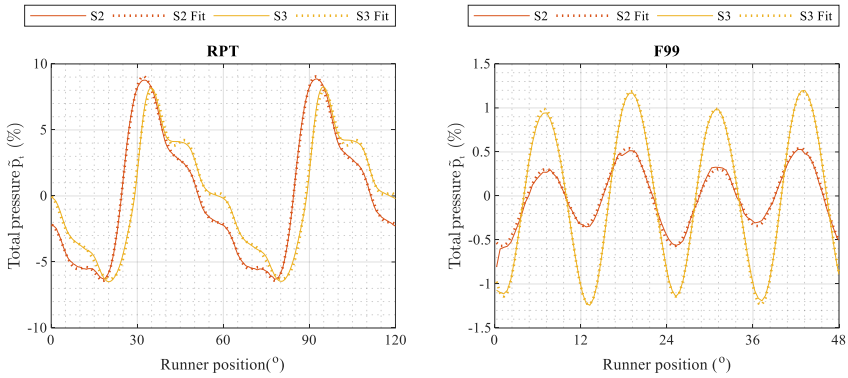

Figure 43 The measured signal and the fit represented with the measurements from sensor S2 and S3.

The amplitudes and phases of the measured signals were found by fitting the measured data to eq. (1). The fitting algorithm was a gradient based minimizer. The F99 measurements were fitted with half the blade passing frequency (the splitter effect), the first and the second harmonic. The RPT was fitted with the first harmonic blade passing frequency and up to and including the fifth harmonic. The highest fit accuracy for the RPT was achieved with eight harmonics, but only the first five were included to limit the results. The fitting results of the measured pressure for S2 and S3 are presented in Figure

43. It can be seen that the higher harmonics of the RTP have a small deviation between the fit and the measured signal, but the results were still found satisfactory. The F99 had good agreement between the fits and the measurements. Some deviation was expected since the fit acts as a filter, only keeping the RSI frequencies. The accuracy of the results for S1 was similar to S2 and the accuracy of the S4 results was similar to S3.

The calculated phases from the measurement fitting are presented in Figure 44. The sensor location shift is indicated with the stems and the measured phase shifts for each harmonic with the bars.

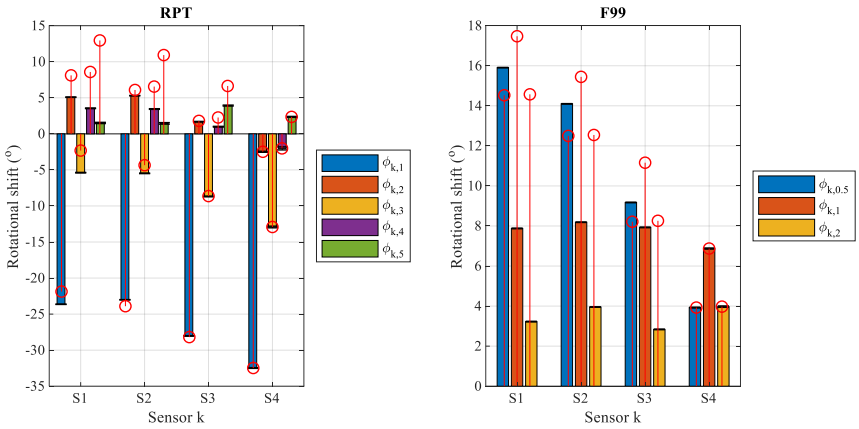

Figure 44 The angular shift from S4 to S1, S2 and S3 relative to runner rotation. The theoretical shift according to the sensor position as shown in Figure 41 is indicated with the red stems. The theoretical shift is normalized to sensor position S4. The subscript k is the sensor number S1 to S4.

A pure throttling effect would result in all measurements being in phase and a pure rotating pressure effect would give phases similar to the position of the pressure sensors. The phase results presented coincide with the observation in Figure 42

The difference between the sensor angular position and the measured phase is now discussed. For the pressure measured with the sensor S1, the difference was a consequence of the position inside a guide vane channel, and thereby mainly throttling was measured. For the RPT case, the fundamental and two next harmonics (k=1,2,3) were close to the theoretical shift, the fourth (k=4) had about half the theoretical shift and the fifth (k=5) was found with almost the same phase for all sensors. This gave reasons to believe that the first three (k=1,2,3) harmonics were controlled by throttling, the last (k=5) by the rotating pressure field and the fourth (k=4) controlled by both throttling and the rotating pressure field.

For the F99 case, the two blade passing frequency harmonics (k=1-2) were not following the sensor angular shift. Compared with the results from the RPT, the F99 seemed to be controlled by the throttling effect since the phase shift between the sensors was relatively small. The half blade passing frequency (k=0.5) had a phase difference close to the theoretical shift. The effect is known to be due to the splitter design causing slightly different flow conditions in two neighboring channels. As a result, the pressure changed for each second blade passing and the effect was therefore strongly connected to the runner position and the rotational shift.

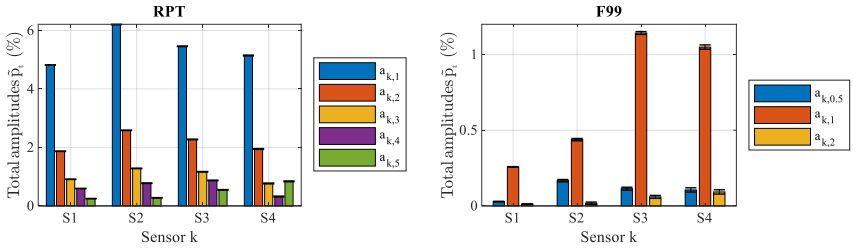

Figure 45 The blade passing frequency amplitude with 95% probability for each sensor. The amplitude is percentage of head. The subscript k is the sensor number S1 to S4.

The fitting results of the measured amplitudes are shown in Figure 45. The amplitudes from the throttling effect were unknown, as the velocity around the guide vanes were location dependent and thereby the pressure amplitudes location dependent also. For the rotating pressure, the assumption was to find same amplitude for all sensors at the same distance from the runner (S2-S4). The data in Figure 45 confirms the observations from the phase. The RPT had similar amplitudes for each sensor compared with the F99 with more variations, indicating most throttling for the F99 case.

The next step was to separate the two effects. The amplitudes and phases were used to solve eq. (4). The square error of the equation was minimized in five steps for the RPT and in three steps for the F99 according Table 13. The calculation results for each step are shown in Figure 46. The results are presented with the throttling, the rotating runner pressure and the comparison between the total modelled pressure and the measured pressure for S2-S3. For the RPT, Fit I is the blade passing frequency ($i=1, f=6$) and the last calculation was Fit V for the fifth harmonic. The rotating runner pressure was found to be the predominant effect with the highest amplitudes, as expected from the phase discussion. The throttling was highest when the blade passed the guide vane channel, and almost no effect was found before the next blade passing. This was expected since the throttling was driven by the sudden increase in the downstream pressure from the high-pressure side of a blade. Another observation is the harmonic content of the pressure. The throttling did only have the three first harmonics, while the rotating pressure field was found with all harmonics. This was in accordance to the observation of the phase where the higher harmonics seemed to be more influenced by the rotating pressure. Initially, all harmonics for the rotating pressure were fitted with phase shift according to the sensor location as previously described. However, with such assumption the Fit V did not change from Fit IV. Due to the low number of blades, the pressure fluctuations onboard the runner were expected to be found in the vaneless space measurements as seen in the literature[4]. In the current experiment with six blades and 28 guide vanes, four guide vane passing should occur with S1-S4 still in the same runner channel. The pressure effects onboard the runner from these passings should be in phase for all pressure sensors. The number of

blades and guide vanes made this pressure coincide with the fifth harmonic. In the initial fitting process, the fifth harmonic did not improve the fit when modelled with a phase shift according to eq. (3). In the Fit V in Figure 46, the fifth harmonic was assumed in phase for all sensors, significantly improving the fit. From this result, the onboard pressure fluctuations could be analyzed with sensors in the vaneless space. This should be analyzed in a future study, with both onboard sensors and sensors in the vanless space of a runner with sufficiently few blades.

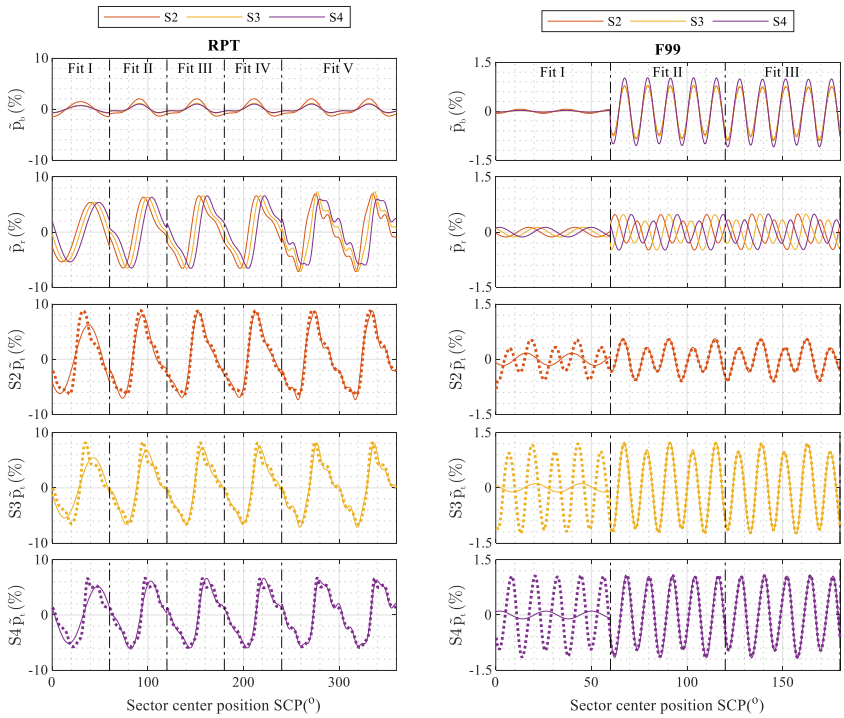

Figure 46 The fitting results. The results are divided into the throttling effect, the runner pressure effect and the total pressure in each location S2-S4.

The F99 was initially fitted with half the blade passing frequency (*i=0.5, f=30*) and then the first and the second harmonic. It can be observed that the fit improved for each step. The throttling in the F99 case was the most predominant part of the measurement, which also explained why the measurements S1-S4 were almost in phase. The splitter effect did have a small influence of the throttling, obviously because of the slightly different amplitude of the high pressure from the runner.

The position of the runner with the highest throttling and highest pressure for S2-S3 is shown in Figure 47 for the RPT case. The maximum pressure order was found to be first throttling, then S2, S3 and S4 i.e. in the order of the sensor position. This was as expected with the highest influence from the rotating runner pressure. The rotational shift of the blades for each peak can be observed. The runner does not rotate the same distance as the sensors position between each maximum. This difference is due to the throttling effect.

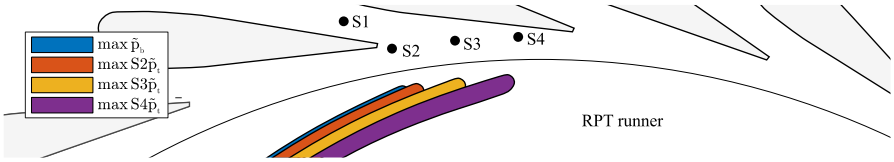

Figure 47 The blade positions for the RPT were the highest effect was found from throttling and the measured total pressure in the location S2-S4. The order was found to be first throttling, then S2, S3, S4

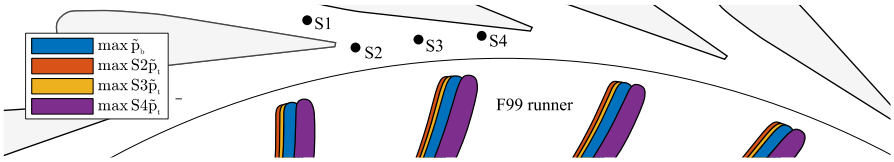

Figure 48 The blade positions for the F99 were the highest pressures were found. First S2, then S3, throttling and S4. The order is different from the RPT.

For the F99 case, the position of the runner for the highest pressure in throttling and each pressure measurements is shown in Figure 48. Interestingly, the order was first S2, then S3, throttling and last S4. The throttling effect is evident from the small rotational shift of the runner between the maximum pressures as seen from the position of the blades.

To verify the calculated phase for the throttling, the calculated throttling pressure was compared with the measurement S1 as shown in Figure 49. Both the RPT and the F99 had good agreement between the calculated throttling and the measurement at location S1. The amplitude was a function of location because of the pressure and velocity distribution in the guide vane cascade, thus they were not expected to be comparable and therefore normalized to max.

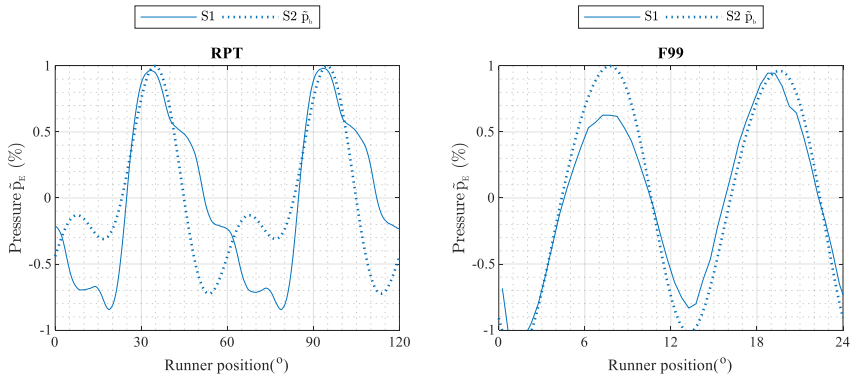

Figure 49 Comparison of the calculated throttling pressure and the measurements with sensor S1. All pressure values were normalized to signal max.

The RPT measurements, with high blade loading and few blades gave the most expected result. First, throttling of a guide vane channel was seen when the high-pressure side of the blade was in the vicinity of the stagnation pressure of the trailing edge of the first guide vane as shown in Figure 47. Next, the high pressure from the runner was measured in the same order as the position of the sensors in the vaneless space. The

throttling effect caused the phase shift of the measurements to be smaller than the actual distance between the sensors. In the case of the F99, the blade loading was smaller, giving amplitudes in the vaneless space of 1/5 of the RPT as seen in Figure 46. This is believed to be the main cause of the different order in Figure 48 compared to the RPT in Figure 47. The pressure in the guide vane cascade was much stronger compared to the rotating runner pressure, hence the main effect in the measurements was from the throttling, which was the fluctuation of the cascade pressure. The reason for the position of the highest effect of throttling was believed to be where the pressure difference between the runner and the guide vane is the highest, hence between two trailing edges as seen in Figure 48. From airfoil theory, a known strong connection between the pressure distribution around the airfoil and the velocity field exist[15]. The throttling effect is understood to be a consequence of increasing the pressure on the low-pressure side of the airfoil. By disturbing the pressure field, both velocity and pressure around that particular guide vane were disturbed.

4. Conclusion

Two runners with similar specific speed but different number of blades were investigated to find the effects from the rotor-stator interaction in the vaneless space. For the F99 case with lowest blade loading, the main influence of the pressure field in the guide vane cascade and vaneless space was found to be the pressure disturbance from the runner introducing a throttling effect in the guide vane channel, resulting in fluctuation in the potential pressure in the guide vane cascade. The findings are in accordance with previous studies found in the literature[7–9].

With higher blade loading and few blades, the pressure in the vaneless space were a direct measurement of the rotating pressure field from the runner and small influence from the throttling as with the RPT case.

The fifth harmonic in the RPT case was found to be the onboard pressure fluctuations because the wide channel gave the possibility to measure several guide vane passing with the sensors in the vaneless space.

The throttling effect were found in different locations for the two cases and is highly influenced by the blade loading. Higher blade loading gave highest throttling when the high pressure side of the blade was close to the guide vane channel outlet, while lower blade loading moved the throttling position closer to the low pressure area of the guide vanes.

The difference in the measured pressure amplitudes in the vaneless space was caused by the phase shift between the throttling effect and the rotating runner pressure and their amplitudes.

The results give more details about the physics in the rotor-stator interaction in a low specific speed turbine.

Acknowledgments

This work was founded by Energy Norway, Norwegian Research Council and the Norwegian Hydropower Center. The authors are grateful for all the support from the technical staff at the Waterpower laboratory which were invaluable to make the measurements possible.

Nomenclature

a	Amplitude total pressure
b	Amplitude throttling pressure
c	Amplitude runner pressure
f	Normalized frequency
i	Harmonic number
n_{ED}	Dimensionless speed factor

$\tilde{p}$ Fluctuating pressure

Q_{ED} Dimensionless discharge

x Runner angular position

γ Phase shift throttling pressure

δ Phase shift total pressure

θ Sensor angular location

φ Phase shift runner pressure

Subscripts

b Throttling (pressure)

i Harmonic number

k Sensor number

r Rotating (pressure)

t Total (pressure)

Reference

[1] Lais, S., Liang, Q., Henggeler, U., Weiss, T., Escaler, X., and Egusquiza, E., 2009, "Dynamic analysis of Francis runners-experiment and numerical simulation," IJFMS, vol. 2, no. 4, pp. 303–314.

[2] Yan, J., Koutnik, J., Seidel, U., and Hübner, B., 2010, "Compressible Simulation of Rotor-Stator Interaction in Pump-Turbines," IJFMS, vol. 3, no. 4, pp. 315–323.

[3] Xia, L., Cheng, Y., and Cai, F., 2017, "Pressure Pulsation Characteristics of a Model Pump-turbine Operating in the S-shaped Region: CFD Simulations," IJFMS, vol. 10, no. 3, pp. 287–295.

[4] Zobeiri, A., Kueny, J.-L., Farhat, M., and Avellan, F., 2006, "Pump-turbine rotor-stator interactions in generating mode: pressure fluctuation in distributor channel," in 23rd IAHR Symposium on Hydraulic Machinery and Systems.

[5] Yonezawa, K., Toyahara, S., Motoki, S., Tanaka, H., Doerfler, P., and Tsujimoto, Y., 2014, "Phase Resonance in Centrifugal Fluid Machinery," IJFMS, vol. 7, no. 2, pp. 42–53.

[6] Qian, R., 2008, "Flow field measurements in a stator of a hydraulic turbine," Ph. D., Laval University, Laval, Canada.

[7] Ciocan, G. D. and Kueny, J. L., 2006, "Experimental Analysis of Rotor-stator Interaction in a Pump-Turbine," in 23rd IAHR Symposium on Hydraulic Machinery and Systems, Yokohama, Japan.

[8] Hasmatuchi, V., 2012, "Hydrodynamics of a pump-turbine operating at off-design conditions in generating mode," Doctoral Thesis, Ecode Polytechnique Federale de Lausanne, Lausanne, Switzerland.

[9] Dörfler, P., Sick, M., and Coutu, A., 2013, Flow-Induced Pulsation and Vibration in Hydroelectric Machinery. London: Springer London.

[10] "Francis-99 NTNU." [Online]. Available: https://www.ntnu.edu/nvks/francis-99. [Accessed: 10-Sep-2018].

[11] IEC, 1999, "NEK IEC 60193 Hydraulic turbines, storage pumps and pump-turbines Model acceptance tests."

[12] Olimstad, G., 2012, "Characteristics of Reversible Pump-Turbines," Ph. D., Norwegian University of Science and Technology, NTNU, Trondheim.

[13] Franklin, R. e. and Wallace, J. M., 1970, "Absolute measurements of static-hole error using flush transducers," Journal of Fluid Mechanics, vol. 42, no. 01, pp. 33–48.

[14] Agnalt, E., Solemslie, B. W., and Dahlhaug, O. G., 2018, "Onboard measurements of pressure pulsations in a low specific speed Francis model runner," in 29th IAHR Symposium on Hydraulic Machinery and Systems, Kyoto, Japan, To be published.

[15] Schlichting, H. and Gersten, K., 2016, Boundary-Layer Theory, 9th ed. 2017 edition. New York, NY: Springer.

"A measurement result is complete only if it is accompanied by a quantitative expression of its uncertainty. The uncertainty is needed to judge whether the result is adequate for its intended purpose and whether it is consistent with other similar results."

(Ferson, S., et al. L. 2007. Experimental Unvertinaty Estimation and Statistics for Data Having Interval Uncertainty. SAND2007-0939. Albuquerque: Sandia National Laboratories)

Experimental study of a low specific speed Francis model runner during resonance

Einar Agnalt[1], Petter Østby[1,2], Bjørn W. Solemslie[1], Ole G. Dahlhaug[1]

[1]Waterpower Laboratory, Department of Energy and Process Engineering, NTNU - Norwegian University of Science and Technology, Trondheim, Norway

[2]Rainpower AS, Kjeller, Norway

Correspondence: Einar Agnalt; einar.agnalt@ntnu.no

Abstract. An analysis of the pressure in a runner channel of a low specific speed Francis model runner during resonance is presented, which includes experiments and the development of a pressure model to estimate both the convective and acoustic pressure field from the measurements. The pressure was measured with four pressure sensors mounted in the runner hub along one runner channel. The mechanical excitation of the runner corresponded to the forced excitation from rotor-stator interaction. The rotational speed was used to control the excitation frequency. The measurements found a clear resonance peak in the pressure field excited by the second harmonic of the guide vane passing frequency. From the developed pressure model, the eigenfrequency and damping were estimated. The convective pressure field seems to diminish almost linearly

from inlet to outlet of the runner, while the acoustic pressure field had the highest amplitudes in the middle of the runner channel. At resonance, the acoustic pressure clearly dominated over the convective pressure. As the turbine geometry is available to the public, it provides an opportunity for the researchers to verify their codes at resonance conditions.

1. Introduction

Power plants with recently installed Francis runner have experienced breakdown after few running hours[1]. Some breakdowns are related to vibration and resonance of the runner. A resonance condition for a runner is known to have a frequency and a related shape with diametral modes (DM)[2]. In low specific speed runners, the main excitation force is found to be the rotor-stator interaction (RSI). The RSI excites the runner with a distinct pattern dependent on the number of runner blades and guide vanes[3–6]. Due to the phase shift of the pressure fluctuations in each runner channel, the overall pressure fluctuations in the runner creates a pressure field with mean diametrical modes similar to the frequency response of the runner[7]. Hence, the verification of the frequency response of a runner is crucial to avoid operation at resonance.

The way of measuring frequency response found in the literature is with the use of accelerometers and strain gauges and the excitation methods found is pressure field excitation, impact excitation or excitation with various vibration mechanisms as electronic muscles and shakers. The surrounding structure of the runner has high impact on the natural frequencies and damping, hence the analysis should preferably be carried out with the runner mounted in the housing[3, 8]. Presas et.al analyzed the frequency response of a pump turbine while mounted in the housing, but the use of two electronic muscles were not sufficient to excite all modes[9]. Østby et.al did similar experiment but with six patches on a six bladed model with good results. Major findings included that the modes with large movement of the hub and shroud, the global modes, disappeared when the runner was mounted in the housing. The blade modes were minimally affected

by the housing[10]. Valentín et.al analyzed the natural frequencies of a prototype turbine through impact excitation in air, and later, pressure field excitation while in operation. Strain gauges and accelerometers were utilized to measure the frequencies and the modal shape. The results included natural frequencies excited during startup and frequencies excited by random phenomena's in part load and high load. By utilizing the excitation which naturally occurs in the operation of the runner, excitation complexity is reduced[11]. Several other studies focused on the frequency response and the added mass effect, mainly with measurements carried out with the runner not mounted in the turbine housing[12–17].

The objective of this paper is to investigate the use of pressure sensors to find the resonance frequency of a runner. RSI are used to excite a model of Francis turbine runner with forced excitations, and the mechanical response is measured with the pressure sensors mounted in one runner channel and one accelerometer mounted above one runner channel close to the inlet. In addition, to allow numerical researches to verify their calculations, a model which separates the convective pressure field from the incompressible flow field and the acoustic pressure field from the acoustic mechanical eigenmodes, has been developed. It produces useful estimates for the pressure fields, damping and eigenfrequency which can be evaluated individually against the numerical calculations. This is a significant advantage as the researcher can verify each step of the calculation process and not only the final resulting pressure field. The turbine geometry in current study is openly available through the Francis99 project and provides a unique opportunity for numerical researchers to verify their codes at resonance conditions[18].

2. Methods

2.1. *RSI excitation*

The guide vanes create lift to direct the flow and as a result, a circumferential repetitive pattern around the runner with zones of higher and lower pressure is created[19]. When the runner rotates, each runner channel is experiencing a varying pressure and velocity field depending on the position relative to the guide vanes. This variation of the inlet condition to the runner channels is the source of the fluctuation pressure found onboard

the runner. Due to different number of runner channels and guide vanes, the fluctuating pressure in different runner channels is phase shifted. As a result, the overall pressure onboard the runner, and thereby the forces acting on the runner, has a pattern of higher and lower pressure. Since the pressure in each channel fluctuates, the overall pressure pattern is rotating. This overall pressure field is known as the modal pressure field, or the pressure spinning mode and can be expressed with Equation (1) [3, 20].

$$mZ_b + nZ_b = k \tag{1}$$

where m and n is harmonic number for the runner pressure and guide vane pressure respectively. The number of diametral modes are k, number of blades are Z_b and number of guide vanes are Z_g.

The runner in the current study is equipped with $Z_g=28$ guide vanes and $Z_b=30$ runner blades. The excitation force for the fundamental guide vane passing frequency, $m=1$ and $n=1$, gives $k=2$ diametral modes in the pressure field and is illustrated by dividing a 28 period signal into 30 segments as shown in Figure 50.

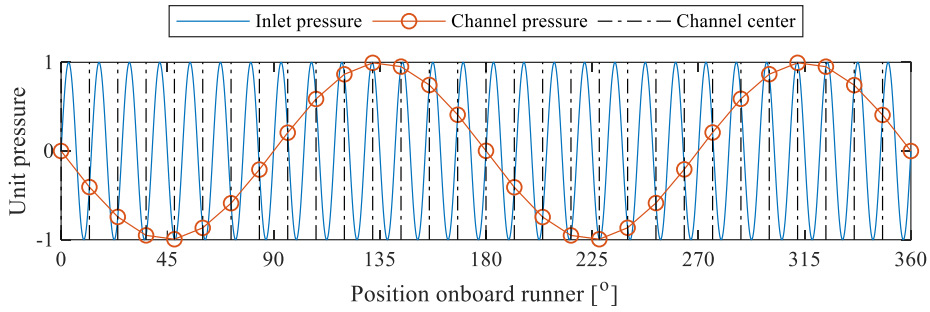

Figure 50 Instantaneous illustration of the DM2 excitation. A sinusoidal signal with 28 periods are divided into 30 equal segments. The intersection line for each segments represents the pressure in each of the 30 runner channels. By plotting a curve through the intersection points, the overall pressure with 2 diametral modes appears.

The second harmonic of the guide vane passing frequency, *m=1* and *n=2,* resulting in *k=4* and can be seen in Figure 51

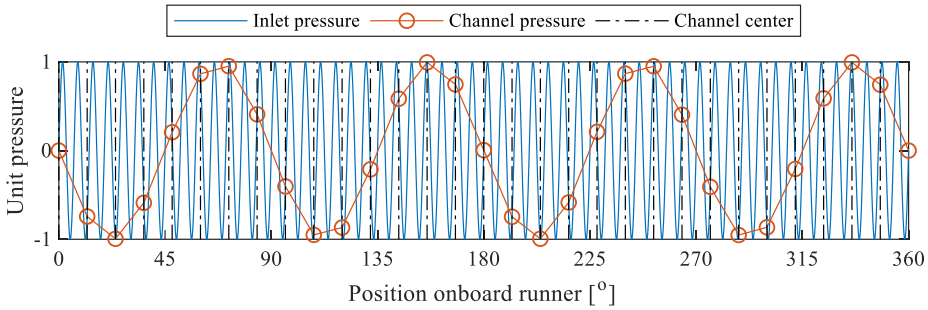

Figure 51 Instantaneous illustration of the DM4 excitation. A sinusoidal signal with 2*28 periods are divided into 30 equal segments. The intersection line for each segments represents the pressure in each of the 30 runner channels. By plotting a curve through the intersection points, the overall pressure with 4 diametral modes appears.

The deflection pattern of the runner is defined by the excitation from the pressure field. Each deflection pattern with diametral modes can have different deflections amplitudes for the blades, hub and shroud. The blade mode is a deflection pattern of the runner where the blades have the largest amplitude, while the disc mode is a deflection pattern of the runner where the hub and shroud have the largest amplitudes. Modes with high deflection of the hub and ring, disc modes, could have higher damping due to the surrounding water and structure in the housing compared to blade modes[10].

2.2. *Experimental setup*

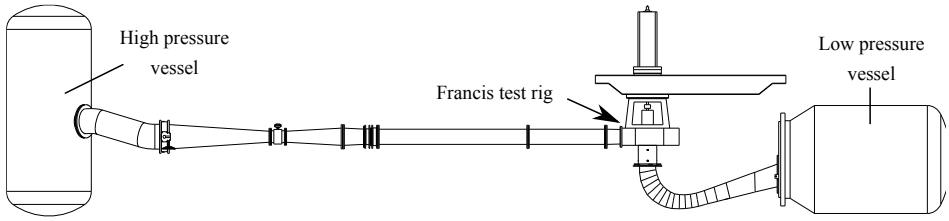

Figure 52 The Francis test-rig, including the high and low pressure vessel.

The Francis test-rig available at the Waterpower Laboratory, Norwegian University of Science and Technology was used for the experimental studies as shown in Figure 52. The Francis test-rig was equipped with all required instruments to conduct model testing according to IEC 60193[21]. The runner in the current study was a bolted design with 15+15 splitter and full-length blades. The number of guide vanes was 28 and the spiral casing was bolted through 14 stay vanes. The dimensionless specific speed of the runner was 0.07. The draft tube of the test rig was an elbow-type. The Francis turbine in the test section is shown in Figure 53 and the Hill diagram of the investigated runner is shown in Figure 54.

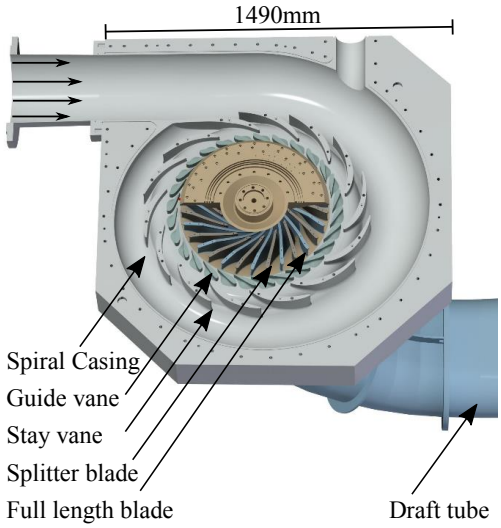

Figure 53 Three-dimensional view of the investigated Francis turbine.

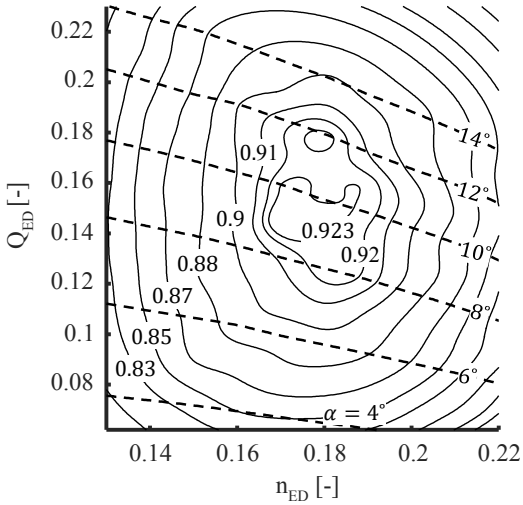

Figure 54 Hill chart of the investigated runner.

Measurements involving moving fluids can be severely influenced by the mounting method of the sensor [22]. For application where accurate flush mounting is possible, the uncertainty from mounting i.e. related to hole size, transmission tubes and cavities will be neglectable[23]. The time and frequency response for the measurements is then only related to the dynamic properties of the diaphragm and the data acquisition (DAQ) chain[24]. In the current measurements, flush mounted sensors were selected to reduce uncertainty related to mounting method.

Figure 55 shows the locations of the onboard pressure sensor in the turbine (R1 – R4) and the accelerometer (A). The pressure sensor sensing technology consists of a Wheatstone bridge with silicon strain gauges. The R1 and R2 sensors were Entran EPX sensors and the R3 and R4 sensors were Measurements Specialties XPM5. In addition to the pressure sensors, a Brüel & Kjær 4397 accelerometer was utilized for reference measurement of the runner vibration. All of the sensors were mounted in the runner's hub, and the signals were amplified onboard and then transmitted through a slip-ring before the connection to the DAQ system. The slip-ring was a Penlink SRH-series for through bore applications mounted on the shaft between the runner and the generator. A schematic presentation of the measurement system is shown in Figure 56 .

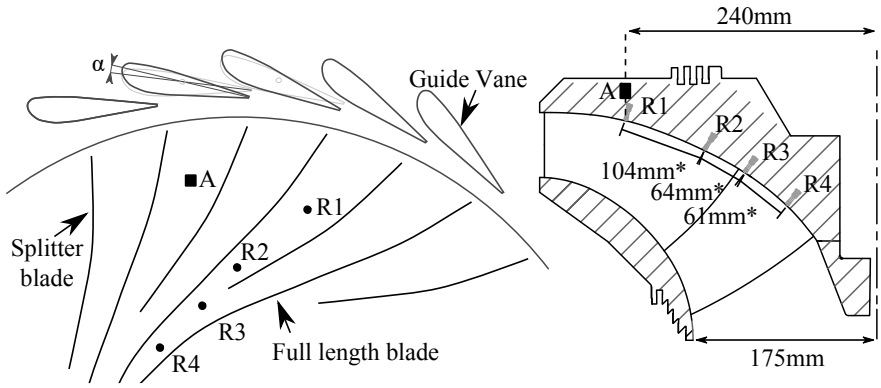

Figure 55 Onboard pressure sensors. The distance between the sensors are indicated. *Distance in $\mathbb{R}^3$

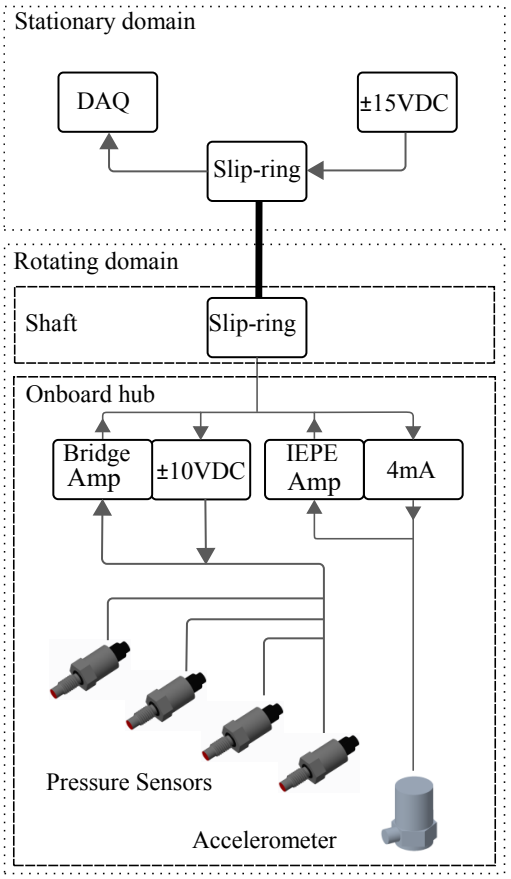

Figure 56 Overview of the measurement chain.

2.3. *Pressure model*

All pressure values presented were calculated as percentage of specific hydraulic energy of the machine (E=gH) and denoted $p_E(\%)$ as recommended by the IEC60193[21] where H is net head. Fluctuating quantities are denoted with a tilde (~). The pressure fluctuations in the runner channel are assumed to be a linear combination of a convective ($\tilde{p}_c$) pressure from the flow field and an acoustic pressure from an excited acoustic-mechanical eigenmode in the runner ($\tilde{p}_a$). The total pressure fluctuation ($\tilde{p}_t$) in the channel is the sum of the convective and acoustic pressure.

$$\tilde{p}_t = \tilde{p}_c + \tilde{p}_a \qquad [\%E] \tag{2}$$

Both the dynamic convective pressure ($\tilde{p}_c$) and the dynamic acoustic pressure ($\tilde{p}_a$) can be modelled as transient waves with a real and an imaginary component. The convective pressure amplitudes are assumed to be proportional to the turbine head and the relative phase angle between each sensor, *j*, is assumed unchanging even with a change in runner speed, thus

$$\tilde{p}_{c,j} = \tilde{p}_{cRe,j} + \tilde{p}_{cIm,j} \qquad [\%E] \tag{3}$$

The acoustic pressure was modelled as the response of a coupled acoustic mechanical 2DOF system to accommodate higher modes while still limiting the number of unknowns in the model. As the fluid at the wall acts with the effect of added mass the pressure has to be proportional to the frequency squared. A frequency proportionality $\omega_p = \omega/\max(\omega)$ factor is used, were $\max(\omega)$ is the highest measured frequency. The amplification of the acoustic mode can thus be described as:

$$D(\omega,\zeta) = \frac{\omega_p^2}{\left(1-\left(\omega/\omega_n\right)^2\right)+i\cdot\left(2\cdot\zeta\cdot\omega/\omega_n\right)} \qquad [-] \tag{4}$$

Where ω denotes the excitation frequency, ω_n is the natural frequency of the excited eigenmode and ζ is the relative damping factor. The acoustic pressure at each sensor, *j*, for the two normal modes in the system is thus described by the equation:

$$\tilde{p}_{a,j} = \left(\Phi_{Re,j} + i\cdot\Phi_{Im,j}\right)\cdot D(\omega,\zeta)\big|_1 + \left(\Phi_{Re,j} + i\cdot\Phi_{Im,j}\right)\cdot D(\omega,\zeta)\big|_2 \quad [\%E] \tag{5}$$

Here Φ_j is the acoustic mode with a value for each sensor, j. Based on the measurements by Bergan et.al[25] the damping is assumed to be proportional to the water velocity going through the runner.

$$\zeta = k\cdot\omega_p \qquad [-] \tag{6}$$

The model has a total of 28 unknowns, eight of which are for the complex convective pressure field, another 16 are for the complex acoustic pressure field, two for the eigenfrequencies and two for the scaling constants k for the damping.

$$\tilde{p}_{t,j} = \left(\tilde{p}_{cRe,j} + i\cdot\tilde{p}_{cIm,j}\right) \qquad Convective$$
$$+ \left(\Phi_{Re,j} + i\cdot\Phi_{Im,j}\right)\cdot D(\omega,\zeta)\big|_1 \quad Mode1 \tag{7}$$

$$+\left(\Phi_{Re,j}+i\cdot\Phi_{Im,j}\right)\cdot D(\omega,\zeta)\big|_2 \quad Mode\ 2$$

The accelerometer was modelled without the frequency squared in the amplification D, but with the same damping and natural frequencies giving another 6 unknowns. The convective part in the pressure was modelled as a constant part in the accelerometer.

$$D_a(\omega,\zeta)=\frac{1}{\left(1-\left({}^{\omega}/_{\omega_n}\right)^2\right)+i\cdot\left(2\cdot\zeta\cdot{}^{\omega}/_{\omega_n}\right)} \qquad [-] \tag{8}$$

$$\begin{aligned}\tilde{a} &= (a_{cRe}+i\cdot a_{cIm}) && Const\\ &+\left(\mathrm{A}_{Re,j}+i\cdot\mathrm{A}_{Im,j}\right)\cdot D_a(\omega,k)\big|_1 && Mode1\\ &+\left(\mathrm{A}_{Re,j}+i\cdot\mathrm{A}_{Im,j}\right)\cdot D_a(\omega,k)\big|_2 && Mode2\end{aligned} \tag{9}$$

With the accelerometer included in the fit, the total number of unknowns were 34.

2.4. *Measurements*

The frequencies for the forced excitation were controlled by changing the speed of the runner while changing the head to keep the speed factor (n_{ED}) around the best efficiency point (BEP). The results in this paper are based on the operational conditions shown in Table 14. To maintain similar flow conditions, all measurements were close to BEP. The flow was measured in the inlet pipe with an electromagnetic flow meter.

Table 14. Measurement summary. $\boldsymbol{\alpha}$ is guide vane opening.

Description	Flow [m^3/s]	n_{ED} [-]	Q_{ED} [-]	Efficiency [-]	Head [m]	α [°]	Speed [rpm]
BEP1	0.107	0.185	0.152	0.916	3.45	10.0	185.1
BEP2	0.134	0.179	0.154	0.916	5.2	10.0	219.8
BEP3	0.160	0.176	0.156	0.920	7.2	10.0	254.3
BEP4	0.183	0.178	0.154	0.919	9.6	10.0	297.8
BEP5	0.209	0.178	0.155	0.920	12.6	10.0	340.5
BEP6	0.232	0.180	0.154	0.920	15.55	10.0	381.7

α is guide vane opening as defined in the IEC60193 where 0º is closed position.

2.5. *Calibration and uncertainty*

The uncertainty of the measurements was calculated from calibrations, vibration sensitivity and repeatability of the measurements. Static calibration of the pressure sensors was initially done in an estimated pressure range for the measurements with a GE P3000 Series pneumatic deadweight tester as the primary reference. As the evaluation of the pressure amplitudes was a dynamic quantity, dynamic uncertainty was addressed. All components in the current pressure measurement chain, from the sensors to the data acquisition, were stated to have resonance frequencies above 10kHz, hence the dynamic uncertainty was assumed to be neglectable and only repeatability and hysteresis from static calibration remained in the uncertainty evaluation [26]. A repeatability test was conducted at 1 Hz with a pressure alternating between 100kPa and 90kPa absolute pressure. The uncertainty of the amplitudes measured by the accelerometer was stated in the documentation to be relative 1%.

A vibration test with the runner surrounded by air was conducted to analyze the pressure sensors vibration sensitivity. An unbalanced mass shaker was used to excite the runner from 0 to 850 Hz. The response was measured with the accelerometer and the pressure sensors to evaluate the vibration sensitivity of the pressure sensors. Four test points were selected from the frequency response with different acceleration amplitudes and repeated with constant frequency. The results are shown in Figure 57.

The highest vibration amplitudes measured by the accelerometer in the vibration test were 17ms^{-2}. The highest measured vibration amplitude for the second harmonic guide vane passing in the measurements BEP1 to BEP6 were 0.05ms^{-2} in BEP6. From the results shown in Figure 57, the first comparison point was with an acceleration of 0.12 ms^{-2}while the pressure sensors response was just above the noise band, with the highest amplitudes from the sensor R4 of 0.013kPa. The pressure sensors measured structural vibrations for higher acceleration values. Based on the current analysis, a conservative uncertainty estimate for the measured pressure amplitudes was 0.013kPa/0.12 ms^{-2} = 0.11kPa/ms^{-2}. Assuming the unbalanced shaker excited non-rotating modes, the accuracy of the analysis was dependent on which mode was being excited and the position of the sensors relative to the diametral modes. Unfortunately, such knowledge was not available in the measurements, but since the pressure sensors had different locations and showed similar frequency sensitivity trends, and the acceleration amplitudes in the measurements BEP1-BEP6 were small, the analysis were assumed to be conservative and valid.

To analyze the variation of the blade passing amplitude for each sensor, a short time fast Fourier transform (STFFT) was used. The analysis was performed with window length equal to 50 periods of the RSI signal with each window starting at the same relative position to the signal period. The amplitudes were found to be normally distributed, and a 95% confidence interval was calculated. The uncertainty budget for the RSI amplitudes is presented in Table 15. For the input to the pressure model, Equation (10) was used to find the uncertainty in the complex domain where ϵ is the 95% error estimate.

$$\begin{aligned} \epsilon_{re} &= \sin(\varphi) \cdot \epsilon \\ \epsilon_{Im} &= \cos(\varphi) \cdot \epsilon \end{aligned} \tag{10}$$

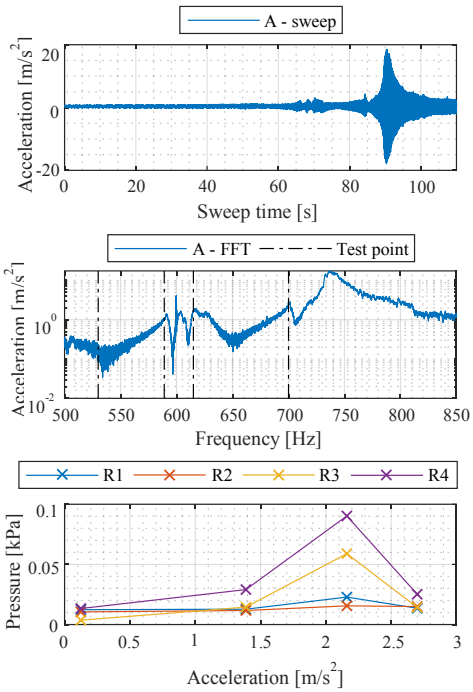

Figure 57 Vibration sensitivity test of the pressure sensors. The runner were excited in air with a frequency sweep with an unbalanced mass shaker. Four test points were repeated with constant frequency. The response were measured with the accelerometer and the pressure sensors.

2.6. Noise reduction

Anti-aliasing filters according to the Nyquist-Shannon sampling theorem were used on all measurement channels. To reduce the noise sensitivity, amplification of the measured signals was done close to the sensors inside the runner hub.

Table 15. Uncertainty budget for the fundamental RSI amplitudes, BEP5. The vibration sensitivity was calculated as 0.13 times the acceleration amplitude.

Location	Amplitude RMS of fundamental frequency RSI	Calibration repeatability ϵ_r	Vibration sensitivity ϵ_v	Repeatability of the measurements ϵ_m	Total relative uncertainty f_t
R1	0.94 kPa	0.01 kPa	0.003 kPa	0.015 kPa	1.9%
R2	0.70 kPa	0.01 kPa	0.003 kPa	0.011 kPa	2.2%
R3	0.53 kPa	0.006 kPa	0.003 kPa	0.010 kPa	2.3%
R4	0.30 kPa	0.006 kPa	0.003 kPa	0.012 kPa	4.6%
A	0.028ms^{-2}	1%	-	0.002 m/s^{-2}	7.1%

3. Results and discussion

3.1. Measurement results

For the accelerometer measurements, no normalization recommendations could be found in the literature. The goal of the normalization was to compare the acceleration as if the frequencies and the driving force were the same for each step in rotational speed and head. A speed ratio coefficient c was defined as the ratio between the investigated speed and the speed of the first measurement $c = n/n_{BEP1}$, and a driving force coefficient b was defined as the ratio between investigated head and head of first measurement $b = H/H_{BEP1}$. Assuming a sinusoidal fluctuating movement $\tilde{s}(t)$:

$$\tilde{s}(t) = b \cdot \sin(c \cdot t) \qquad [m] \qquad (11)$$

The acceleration is:

$$\frac{\partial^2 s}{\partial^2 t} = \tilde{a}(t) = -b \cdot c^2 \cdot \sin(c \cdot t) \qquad \left[\frac{m}{s^2}\right] \qquad (12)$$

Rearranged to achieve constant acceleration amplitude independent of speed and head:

$$\tilde{a}_{nH}(t) = \frac{\tilde{a}(t)}{b \cdot c^2} = -1 \cdot \sin(c \cdot t) \qquad \left[\frac{m}{s^2}\right] \qquad (13)$$

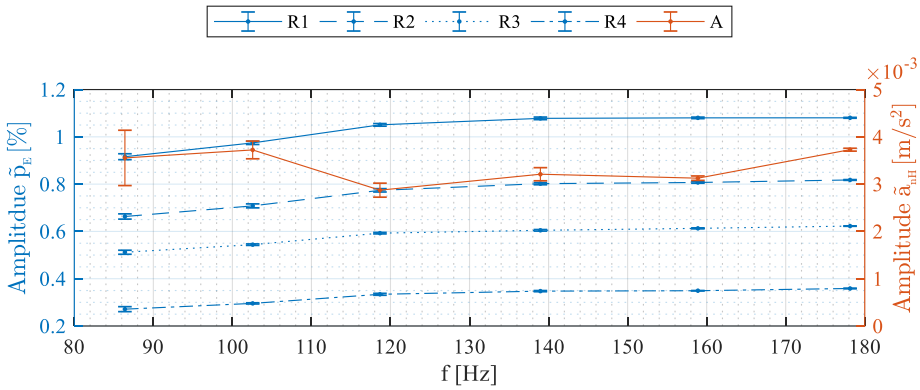

Figure 58 The RSI fundamental frequency. The error bars represents the uncertainty from calibration and the experimental repeatability of the amplitudes.

The amplitudes of the fundamental guide vane passing frequency is shown in Figure 58. The pressure amplitudes show a small increasing trend which may be to some extent related to Reynolds effects[27, 28]. The IEC 60193[21] recommends the Reynolds number (Re_{D2}) to be above $5{\cdot}10^6$ to avoid Reynolds dependencies in the model measurements. The Reynolds number range for the measurements BEP1 to BEP6 was $8 \cdot 10^5 - 2.5 \cdot 10^6$; hence the measurements were in a range were the friction losses in the turbine was expected to be dependent on the Reynolds number. By examining the efficiency for each of the measurements in Table 14, a similar trend as the pressure amplitudes in Figure 58 is found, hence the increased losses in the turbine at low flow could reduce the fluctuating pressure amplitudes. The accelerometer amplitudes were almost constant with the proposed scaling for the fundamental frequency. The excitation force from the RSI has two diametral modes for the fundamental frequency. There is no

evidence of a resonance condition in the measured frequency range as presented in the Figure 58.

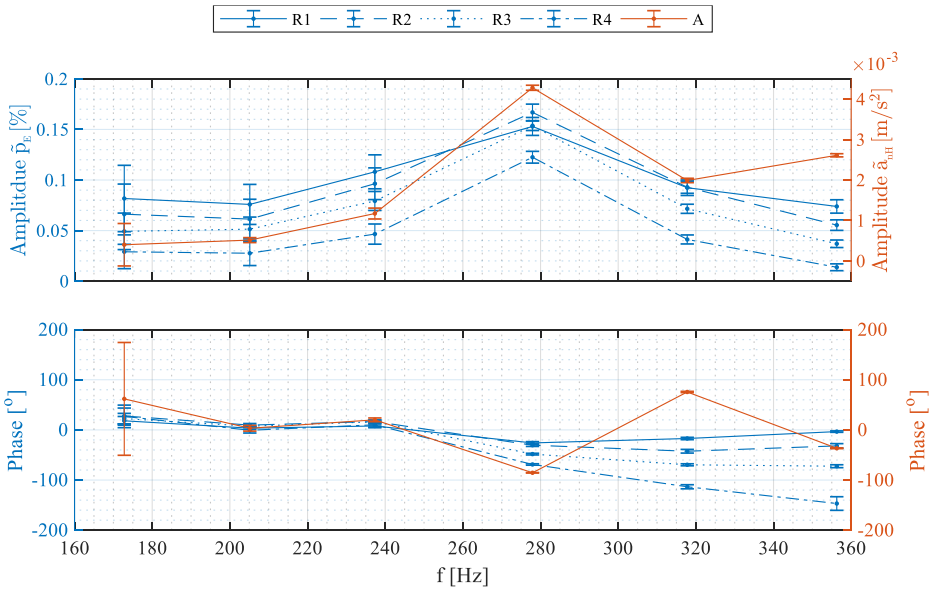

Figure 59 The RSI second harmonic frequency. Pressure amplitudes are normalized to the potential energy. The error bars represents the uncertainty from calibration and the experimental repeatability of the amplitudes.

The second harmonic of the RSI guide vane passing frequency had an increasing trend towards the measurement at 280Hz as shown in Figure 59. The higher pressure amplitudes indicate a resonance condition. The accelerometer measurements were similar to the pressure measurements until the last measured point. The deviation on the last measured point is a clear indication of a higher mode, not visible in the pressure measurements. The number of diametral modes is four, since the forced excitation from the second harmonic of the pressure field has four diametral modes.

3.2. Fitted model parameters

The following steps were performed for the fitting of the measured data:

1. An appropriate mathematical model were selected as described in the pressure model section.
2. A merit function were defined as the sum of square error, Equation (14).
3. The parameters were adjusted for the best fit by minimizing the merit function with a constrained nonlinear minimizing routine.
4. The goodness of fit were evaluated with the coefficient of determination, R^2, and the distribution of the residuals.
5. The accuracy of the best fit parameters were estimated with Monte-Carlo simulation.

The number of data points from the measurements were 60. Six measurements with five sensors with amplitude and phase information. The number of model parameters was required to be less than the number of measurements to limit the degree of freedom in the fitting and avoid overfitting. The measurements were fitted to a model with convective pressure and acoustic pressure with two acoustic modes, giving 34 model parameters. The merit function was calculated as the sum of the weighted square errors:

$$m = \sum_{i=1}^{n} w_i \, (y_i - \hat{y}_i)^2 \qquad (14)$$

where the weights were the inverse standard deviation of the data points, $w_i = 1/\sigma^2$. The goodness of fit R^2 was calculated as shown in Table 16. The solution of the modes in the fit was restricted to be within the frequency range of the measurements.

Table 16. Goodness of fit R^2

	Amplitude	Phase
R1	0.903	0.933
R2	0.986	0.961
R3	0.994	0.990
R4	0.996	0.984
A	0.991	0.894

The R^2 was relatively good for al curves, but since the analysis of R^2 cannot determine the quality of the fit, the residuals were analyzed. A good model fit should produce residuals normally distributed around zero with no systematic trends. The residuals for amplitudes and phases are shown in Figure 60. With one measurement for each sensor and a total of five points for each frequency, the distribution was not available. For accurate determination of the model fit accuracy to the measured values, more measurement points were needed. However, the residuals for the phase were, with the exception of one outlier at the first frequency, symmetrical around the zero line. The amplitude residuals were more scattered, especially for the low frequencies but the values were relatively small. Based on the residuals the model fitted the measurements well.

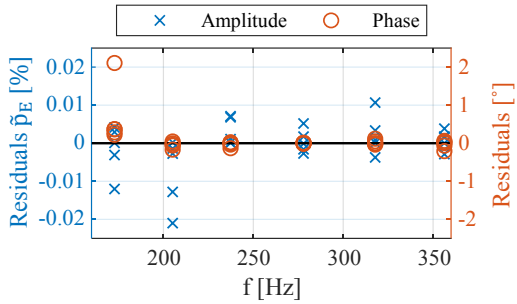

Figure 60 Residuals for the calculated model with two degrees of freedom in the acoustic pressure.

The uncertainty of the fitting coefficients was calculated from Monte Carlo Method simulation (MCM). The calibration uncertainties in each measurement point was not independent as required in the MCM simulation. The input to the calculation was therefore generated from normally distributed random numbers in the uncertainty interval for the calibration, combined with a normally distributed random number from the measurement uncertainty as shown in Equation (15). X is a normally distributed random number, σ_c and σ_m the standard deviation of the calibration and the measurement repeatability. The input for one iteration of the MCM simulation is shown in Equation

(15). The calculated range for pressure sensor R1 amplitudes with 10 000 MCM iterations is shown in Figure 61.

$$\tilde{p}_{t,jMCM} = \tilde{p}_{t,j} + \left(X_c \cdot \sigma_{c,j}\right) + \left[\left(X_m \cdot \sigma_{m,j}\right)\right]_{m=BEP1}^{BEP6} \quad (15)$$

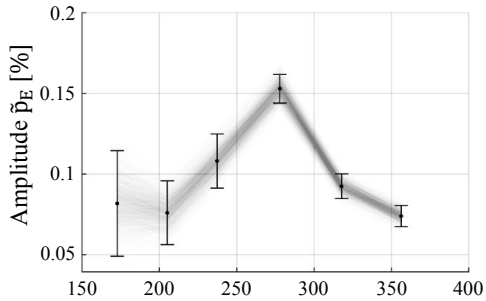

Figure 61 The 1000 first inputs to the MCM simulation of the amplitude data from pressure sensor R1. Each line is plotted with light color, darker color is coinciding lines. Measurement data is indicated.

The distribution of the coefficients from the MCM simulation was analyzed, and the 95% confidence interval was found with the empirical cumulative distribution function. Two example calculations are shown in Figure 62 for coefficient $\tilde{p}_{cRe.1}$ and ω_{n1}.

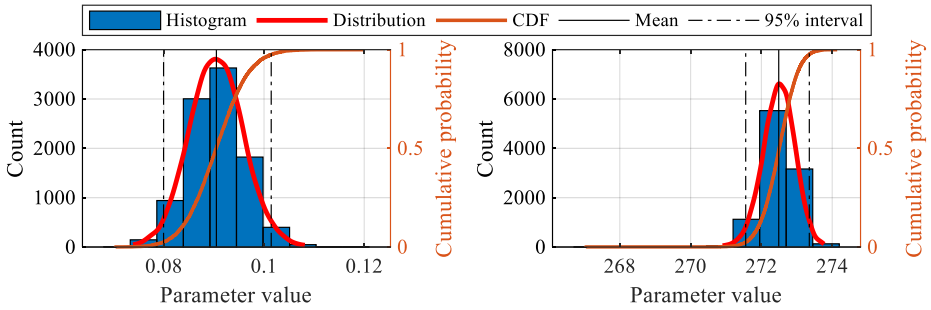

Figure 62 Two examples of the histogram, the distribution and the cumulative probability of the coefficients $\tilde{\boldsymbol{p}}_{\boldsymbol{cRe.1}}$ and $\boldsymbol{\omega_{n1}}$.Mean and 95% confidence interval is indicated.

Figure 63 shows the pressure fitting results and the measured pressure data while the accelerometer fit is shown in Figure 64. The coefficients from the fitting results are presented in Table 17 in the appendix for the comparison to numerical results. For the visualization of the calculated pressure at resonance condition, the convective, acoustic1 and acoustic2 amplitudes is shown in Figure 65. The convective part of the pressure were found to diminish almost linearly relatively to the distance between the sensors. The acoustic1 part of the pressure was found with highest amplitudes for R3, close to the middle of the runner channel, while the acoustic2 pressure were found with a more flat amplitude response in the runner channel.

With the use of eq. (1.6) and $\max(\omega) = 356.25Hz$, the damping for mode1 was found to be $\zeta_1 = 3.9(\pm 0.4)\%$ at $\omega_{n1} = 272(\pm 1)Hz$ and mode2 was found to be $\zeta_2 = 7.4(-1.2 + 1.5)\%$ at $\omega_{n2} = 326(\pm 3)Hz$. The accelerometer measurement were most influenced by the second mode, thus there is reasons to believe the mode includes more disc deflection and thus possible higher damping.

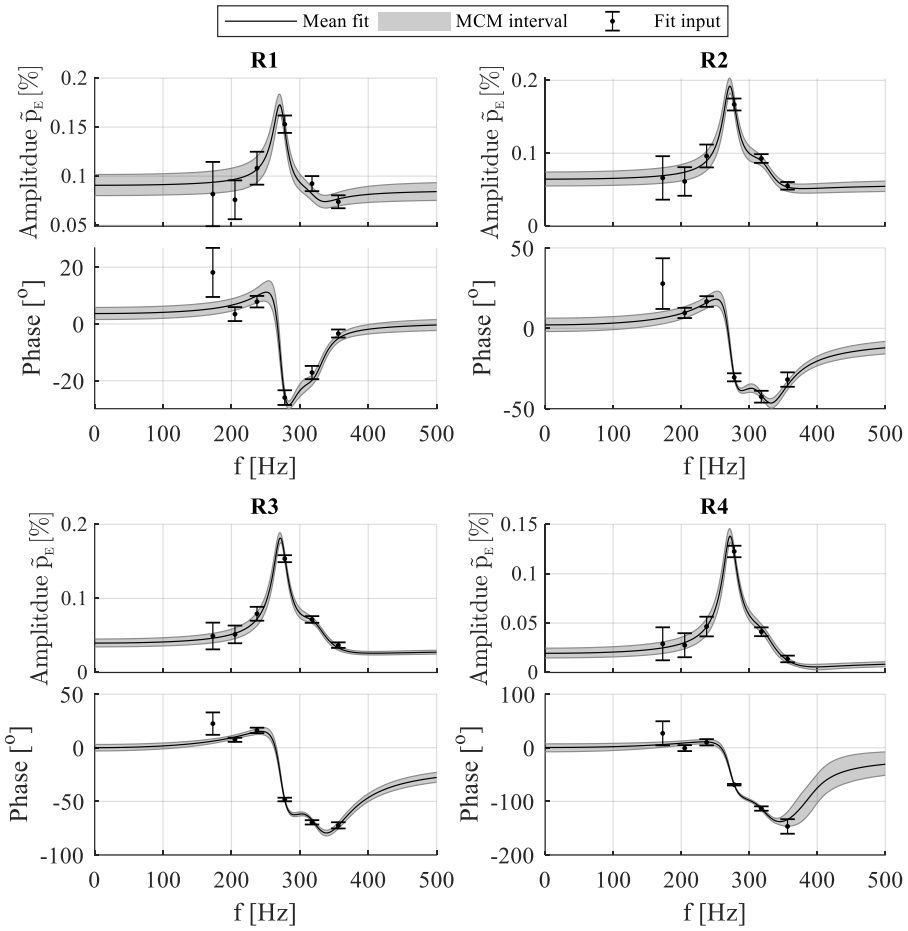

Figure 63 Least square fitting of the pressure measurements.

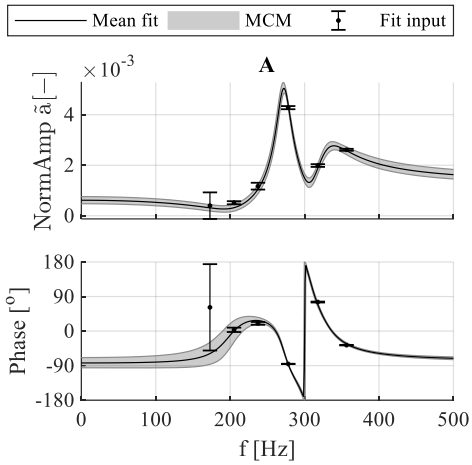

Figure 64 The accelerometer fit.

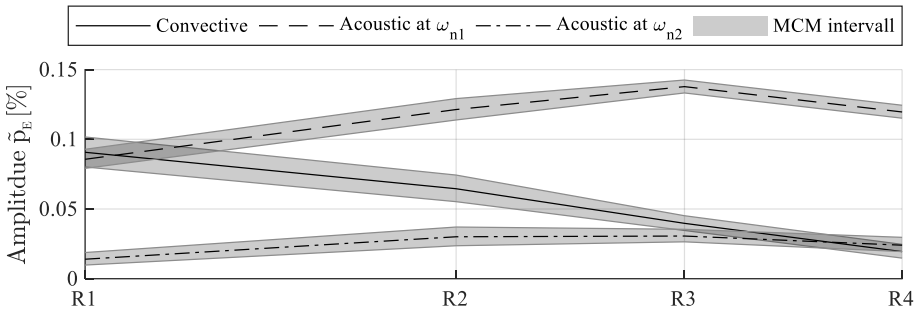

Figure 65 The calculated amplitudes from the fitting coefficients in Table 17 for R1-R4. The distance between the sensors is according to Figure 55

The first measurement point (BEP1) had the highest uncertainty and the proposed pressure model did not fit the phase in any of the pressure measurements, while the accelerometer model was within the range of the uncertainty. The amplitudes in the BEP1 were low and also the test rig was operated at a very low Head, giving the high uncertainty. For the higher frequencies the fit was very good for all sensors giving reasons to believe the proposed model is valid. Questions can be raised about the number of

measurements and the frequency step, and the accuracy would likely be better. The analysis method can separate experimental pressure data into convective and acoustic pressure. The convective pressure represents the pressure field not influenced by the vibrating structure while the acoustic pressure represents the pressure from the fluid structure interaction.

4. Conclusion

The pressure measurements were able to find a resonance and the proposed pressure model was able to calculate the convective and acoustic parts of the pressure for the investigated runner. By separating the measured pressure amplitudes into an acoustic and a convective pressure field, their individual shapes together with the eigenfrequency and the damping were estimated. The convective pressure field diminishes almost linearly from the inlet to the outlet, while the acoustic pressure field had the highest amplitudes in the middle of the runner channel. At resonance the acoustic pressure clearly dominates over the convective. For the acoustic1 mode, the estimated eigenfrequency was 272 Hz while the damping was in the range of 2.5% to 5.1% depending on the runner speed. The acoustic2 mode was estimated to 326 Hz with the damping in the range of 4% to 8%. It is shown that the analysis method can separate experimental data corresponding to the different results of numerical analyses. The convective pressure represents the output from computational fluid dynamics (CFD) and the acoustic pressure, resonance frequency and damping represents the output from simulations as modal and flutter analysis.

Abbreviations

2DOF	Two degrees of freedom
Amp	Amplifier
BEP	Best efficiency point
CFD	Computation Fluid Dynamics
DAQ	Data acquisition
IEC	International Electrotechnical Commission
IEPE	Integrated Electronics Piezo-Electric
MCM	Monte Carlo method
DM	Diametral mode
RSI	Rotor-stator interaction
STFFT	Short Time Fast Fourier Transform
VDC	Volt direct current

Nomenclature

A	Accelerometer mode
α	Guide vane opening
a	Fluctuating acceleration
ε_r	95% repeatability from calibration
ε_v	95% vibration sensitivity
ε_m	95% repeatability of the measurements
ε_t	95% total uncertainty
ζ	Damping coefficient
σ	Standard deviation
σ_r	Standard deviation of the calibration
σ_m	Standard deviation of the measurement
Φ	Acoustic pressure mode
ω	Frequency
ω_p	Frequency proportionality

H	Head of machine
k	Damping proportionality constant
n_{ED}	Dimensionless speed factor
p	Fluctuating pressure
Q_{ED}	Dimensionless discharge

Subscripts for the pressure symbols

a	Acoustic pressure
c	Convective pressure
E	Specific hydraulic energy of machine
j	Sensor identification
Im	Imaginary part
Re	Real part
t	Total pressure

Data Availability

The measurement data and geometry used to support the findings of this study are available at the Francis99 website[28].

Funding statement

This work was founded by Energy Norway, Norwegian Research Council and the Norwegian Hydropower Center.

Acknowledgments

The experiments were conducted under the HiFrancis research project. The authors are grateful for all the support from the technical staff at the Waterpower Laboratory to make the measurements possible.

Appendix

Table 17. Fitting coefficients

Convective		Acoustic1	
Description	Value and 95% interval	Description	Value and 95% interval
$p_{cRe,1}$	0.0905 (-0.0105,0.0109)	$\Phi_{\mathrm{Re},1}$	0.0057 (-0.0020,0.0019)
$p_{cRe,2}$	0.0644 (-0.0093,0.0098)	$\Phi_{\mathrm{Re},2}$	0.0061 (-0.0022,0.0021)
$p_{cRe,3}$	0.0397 (-0.0051,0.0055)	$\Phi_{\mathrm{Re},3}$	0.0111 (-0.0021,0.0019)
$p_{cRe,4}$	0.0194 (-0.0047,0.0052)	$\Phi_{\mathrm{Re},4}$	0.0123 (-0.0021,0.0019)
$a_{c,Re}$	0.0002 (-0.0001,0.0001)	A_{Re}	0.0003 (-0.0001,0.0000)
$p_{c\,\mathrm{Im},1}$	0.0058 (-0.0033,0.0033)	$\Phi_{\mathrm{Im},1}$	0.0099 (-0.0014,0.0014)
$p_{c\,\mathrm{Im},2}$	0.0024 (-0.0046,0.0048)	$\Phi_{\mathrm{Im},2}$	0.0150 (-0.0018,0.0018)
$p_{c\,\mathrm{Im},3}$	0.0001 (-0.0020,0.0022)	$\Phi_{\mathrm{Im},3}$	0.0146 (-0.0015,0.0015)
$p_{c\,\mathrm{Im},4}$	0.0002 (-0.0025,0.0025)	$\Phi_{\mathrm{Im},4}$	0.0102 (-0.0013,0.0014)
$a_{c,\mathrm{Im}}$	-0.0012 (-0.0002,0.0002)	A_{Im}	0.0003 (0.0000,0.0000)
	Acoustic2		Other
$\Phi_{\mathrm{Re},1}$	0.0013 (-0.0010,0.0011)	ω_{n1}	272.4895 (-0.9329,0.8634)
$\Phi_{\mathrm{Re},2}$	0.0053 (-0.0016,0.0020)	$k1$	0.0510 (-0.0051,0.0045)
$\Phi_{\mathrm{Re},3}$	0.0052 (-0.0013,0.0018)	ω_{n2}	325.5277 (-2.6368,2.7486)
$\Phi_{\mathrm{Re},4}$	0.0013 (-0.0011,0.0013)	$k2$	0.0813 (-0.0125,0.0153)
A_{Re}	-0.0005 (-0.0001,0.0001)		
$\Phi_{\mathrm{Im},1}$	-0.0020 (-0.0014,0.0011)		
$\Phi_{\mathrm{Im},2}$	-0.0006 (-0.0014,0.0014)		
$\Phi_{\mathrm{Im},3}$	-0.0015 (-0.0011,0.0009)		
$\Phi_{\mathrm{Im},4}$	-0.0041 (-0.0017,0.0012)		
A_{Im}	0.0003 (-0.0001,0.0001)		

References

[1] Østby, P. T. K., Billdal, J. T., Sivertsen, K., Haugen, B., and Dahlhaug, O. G., 2016, "Dynamic Stresses In High Head Francis Turbines," Hydropower Dams, no. 3.

[2] Presas, A., Valentin, D., Egusquiza, E., Valero, C., Egusquiza, M., and Bossio, M., 2017, "Accurate Determination of the Frequency Response Function of Submerged and Confined Structures by Using PZT-Patches†," Sensors, vol. 17, no. 3, p. 660.

[3] Tanaka, H., 2011, "Vibration Behavior and Dynamic Stress of Runners of Very High Head Reversible Pump-turbines," Int. J. Fluid Mach. Syst., vol. 4, no. 2, pp. 289–306.

[4] Rodriguez, C. G., Egusquiza, E., and Santos, I. F., 2007, "Frequencies in the Vibration Induced by the Rotor-stator Interaction in a Centrifugal Pump Turbine," J. Fluids Eng., vol. 129, no. 11, p. 1428.

[5] Kubota, Y., Susuki, T., Tomita, H., Nagafugi, T., and Okamura, C., 1983, "Vibration of Rotating Bladed Disc Excited by Stationary Distributed Forces," Bull. JSME, vol. 26, no. 221.

[6] Rodriguez, C. G., Mateos-Prieto, B., and Egusquiza, E., 2014, "Monitoring of Rotor-Stator Interaction in Pump-Turbine Using Vibrations Measured with On-Board Sensors Rotating with Shaft," Shock Vib., vol. 2014, pp. 1–8.

[7] Bertini, L., Neri, P., Santus, C., Guglielmo, A., and Mariotti, G., 2014, "Analytical investigation of the SAFE diagram for bladed wheels, numerical and experimental validation," J. Sound Vib., vol. 333, no. 19, pp. 4771–4788.

[8] Valentín, D., Ramos, D., Bossio, M., Presas, A., Egusquiza, E., and Valero, C., 2016, "Influence of the boundary conditions on the natural frequencies of a Francis turbine," IOP Conf. Ser. Earth Environ. Sci., vol. 49, no. 7, p. 072004.

[9] Presas, A., Valero, C., Huang, X., Egusquiza, E., Farhat, M., and Avellan, F., 2012, "Analysis of the dynamic response of pump-turbine runners-Part I: Experiment," IOP Conf. Ser. Earth Environ. Sci., vol. 15, no. 5, p. 052015.

[10] Østby, P. T. K., Sivertsen, K., Billdal, J. T., and Haugen, B., 2019, "Experimental investigation on the effect off near walls on the eigen frequency of a low specific speed francis runner," Mech. Syst. Signal Process., vol. 118, pp. 757–766.

[11] Valentín, D., Presas, A., Bossio, M., Egusquiza, M., Egusquiza, E., and Valero, C., 2018, "Feasibility of Detecting Natural Frequencies of Hydraulic Turbines While in Operation, Using Strain Gauges," Sensors, vol. 18, no. 1, p. 174.

[12] Lais, S., Liang, Q., Henggeler, U., Weiss, T., Escaler, X., and Egusquiza, E., 2009, "Dynamic analysis of Francis runners-experiment and numerical simulation," Int. J. Fluid Mach. Syst., vol. 2, no. 4, pp. 303–314.

[13] Kurosawa, S., Matsumoto, K., Miyagi, J., He, L., and Wang, Z., 2015, "Fluid-Structure Interaction Analysis for Resonance Investigation of Pump-Turbine Runner," p. V01AT12A002.

[14] Kushner, F., 2004, "Rotating Component Modal Analysis And Resonance Avoidance Recommendations."

[15] Egusquiza, E., Valero, C., Liang, Q., Coussirat, M., and Seidel, U., 2009, "Fluid added mass effect in the modal response of a pump-turbine impeller," in *ASME 2009 International Design Engineering Technical Conferences and Computers and Information in Engineering Conference*, pp. 715–724.

[16] Rodriguez, C. G., Egusquiza, E., Escaler, X., Liang, Q. W., and Avellan, F., 2006, "Experimental investigation of added mass effects on a Francis turbine runner in still water," J. Fluids Struct., vol. 22, no. 5, pp. 699–712.

[17] Valentín, D., Presas, A., Egusquiza, E., Valero, C., and Bossio, M., 2017, "Dynamic response of the MICA runner. Experiment and simulation," J. Phys. Conf. Ser., vol. 813, no. 1, p. 012036.

[18] "Francis-99 NTNU." [Online]. Available: https://www.ntnu.edu/nvks/francis-99. [Accessed: 10-Sep-2018].

[19] Antonsen, Ø., 2007, "Unsteady flow in wicket gate and runner with focus on static and dynamic load on runner," Doctoral Thesis, Norwegian University of Science and Technology, Trondheim, Norway.

[20] Tyler, J. M. and Sofrin, T. G., 1962, "Axial Flow Compressor Noise Studies," SAE International, Warrendale, PA, 620532.

[21] IEC, 1999, "NEK IEC 60193 Hydraulic turbines, storage pumps and pump-turbines Model acceptance tests."

[22] Rayle, R. E., 1949, "An investigation of the influence of orifice geometry on static pressure measurements," Master Thesis, Massachusetts Institute of Technology, Cambridge, Massachusetts, USA.

[23] Franklin, R. e. and Wallace, J. M., 1970, "Absolute measurements of static-hole error using flush transducers," J. Fluid Mech., vol. 42, no. 01, pp. 33–48.

[24] Hessling, J. P., 2006, "A novel method of estimating dynamic measurement errors," Meas. Sci. Technol., vol. 17, no. 10, p. 2740.

[25] Bergan, C. W., Solemslie, B. W., Østby, P., and Dahlhaug, O. G., 2018, "Hydrodynamic Damping of a Fluttering Hydrofoil in High-speed Flows," Int. J. Fluid Mach. Syst., vol. 11, no. 2, pp. 146–153.

[26] Dunn, P. F., 2014, Measurement and Data Analysis for Engineering and Science, Third Edition. CRC Press.

[27] Ida, T., 1990, "Analysis of scale effects on performance characteristics of hydraulic turbines," J. Hydraul. Res., vol. 28, no. 1, pp. 93–104.

[28] Østby, P. T. K., Billdal, J. T., Haugen, B., and Dahlhaug, O. G., 2017, "On the relation between friction losses and pressure pulsations caused by Rotor-stator interaction on the Francis-99 turbine," J. Phys. Conf. Ser., vol. 782, no. 1, p. 012010

Part III – Additional Papers

“The Patent Committee has considered your communication of February 20, 1939, relating to Resistance Strain Gages, Wire Type. … while this development is interesting, the Committee does not feel that the commercial use is likely to be of major importance”

(Letter from the M.I.T Patent Committee to Professor Arthur C. Ruge, inventor of the resistance strain gage, March 22, 1939)

Paper 1

Investigations of unsteady pressure loading in a Francis turbine during variable-speed operation.

Trivedi, Chirag; Agnalt, Einar; Dahlhaug, Ole Gunnar

Renewable Energy
Volume 113, December 2017, Pages 397-410

Abstract

Current study was aimed to investigate the unsteady pressure loading in a model Francis turbine under variable-speed configurations. Focus was to investigate the time-dependent characteristic frequencies and the pressure amplitudes. Detailed analysis of both stochastic and deterministic pressure loading in the vaneless space, runner and draft tube was conducted. Total 12 pressure sensors were integrated in the turbine, including four sensors in the runner. The runner rotational speed was changed by ±30% of the rated speed, and the guide vanes were at a fixed aperture. Total four operating conditions were investigated. The measurements showed that, in the vaneless space and runner, amplitudes of unsteady pressure fluctuations increase with the runner angular speed. Pressure field at the blade trailing edge is strongly influenced by the draft tube flow at part load and low load. The variable-speed configuration allowed power generation under the stable condition, where the vortex rope effect is low. However, this led to high-amplitude stochastic frequencies in the runner and draft tube. Overall, the pressure measurements indicated that not only efficiency but also detailed study on pressure

fluctuations inside the turbine is vital before designing a runner for the variable-speed configurations.

Relevance to the current thesis

The measurement setup developed in the current thesis was utilized for the measurements, and the measurements were performed during the same measurement campaign. The paper is focused on the pressure loading in the vaneless space runner and draft tube. As the measurements are with variation of the runner rotational speed, the analysis could highlight details in the rotor-stator interaction not clearly visible with the steady-state analysis in the current thesis.

My contribution to the paper was the design and performance of the measurements.

Paper 2

Experimental study of a Francis turbine under variable-speed and discharge conditions

Trivedi, Chirag; Agnalt, Einar; Dahlhaug, Ole Gunnar.

Renewable Energy
Volume 119, April 2018, Pages 447-458

Abstract

This work investigates the unsteady pressure fluctuations in a hydraulic turbine that are observed during steep ramping. Although hydraulic turbines are expected to operate seamlessly during steep ramping, the resulting pressure amplitudes are so significant that they take a toll on a machine's operating life. Objective of the present study is to investigate time-dependent pressure amplitudes in the vaneless space, runner and draft tube during power ramping-up and -down under variable-speed configuration. Novelty is to vary both discharge and rotational speed of a runner. The measurements are performed on a high-head model Francis turbine. The investigations revealed that amplitudes of characteristics frequencies, especially rotor-stator interaction, are small during steep ramping however, at the end of transient cycle, the amplitudes quickly increased 30-fold. During steep ramping, blade passing frequency was appeared in the runner, which is uncommon phenomenon in high-head Francis turbines. Strong reflection of pressure waves towards runner from vaneless space (guide vane walls) may be one of the causes for the appearance of blade passing frequency in the runner.

Relevance to the current thesis

The measurement setup developed in the current thesis was utilized for the measurements, and the measurements were performed during the same measurement campaign. The analysis of pressure amplitudes in the vaneless space, runner and draft tube during the variation of both rotational speed and guide vane position could highlight more details about the rotor-stator interaction. The thesis focuses on the steady-state operation, while the paper focus on highly transient operational conditions.

My contribution to the paper was the design and performance of the measurements.

Paper 3

Experimental investigation of a Francis turbine during exigent ramping and transition into total load rejection

Trivedi, Chirag; Agnalt, Einar; Dahlhaug, Ole Gunnar

Journal of Hydraulic Engineering
Vol. 144, Issue 6 (June 2018)

Abstract

This study investigates the unsteady pressure fluctuations in a hydraulic turbine observed during a dangerous case of steep ramping interrupted by an unexpected transition into total load rejection. Although hydraulic turbines are expected to experience such events only a few times over their lifetime, the resulting pressure amplitudes are so significant that they take a toll on a machine's operating life. The focus of the present study is to experimentally measure and numerically characterize time-dependent pressure amplitudes in the vaneless space, runner, and draft tube of a model Francis turbine. To this end, 12 pressure sensors were integrated into a turbine, including four miniature sensors mounted in the runner. Steep ramping was performed by changing the rotational speed using a frequency controller. After a few seconds, as the load increased, total load rejection was initiated. This resulted in the generation of strong vibrations throughout the entire structure and strong pressure fluctuations in the turbine. The data analysis shows that pressure amplitudes are in the order of 10–20% of hydraulic energy in the vaneless space and runner, with high-amplitude fluctuations occurring at expected characteristic frequencies, including those associated with rotor-stator interactions, water hammer

travel times, and standing waves in the turbine. Various stochastic frequencies were also observed, especially at the runner outlet.

Relevance to the current thesis

The measurement setup developed in the current thesis was utilized for the measurements, and the measurements were performed during the same measurement campaign. The measurements in the paper are focused on the variation of the runner speed and total load rejection. Since the measurements were including the same positions as the current thesis, the data could give insight to phenomena in the operation of hydropower not found in measurements with steady-state

My contribution to the paper was the design and performance of the measurements.

Paper 4

Pressure Pulsation in a High Head Francis Turbine Operating at Variable Speed

Sannes, Daniel B.; Iliev, Igor; Agnalt, Einar; Dahlhaug, Ole Gunnar

Journal of Physics, Conference Series
vol. 1042 (1).

Abstract

This paper presents the preliminary work of the master thesis of the author, written at the Norwegian University of Science and Technology. Today, many Francis turbines experience formations of cracks in the runner due to pressure pulsations. This can eventually cause failure. One way to reduce this effect is to change the operation point of the turbine, by utilizing variable speed technology. This work presents the results from measurements of the Francis turbine at the Waterpower Laboratory at NTNU. Measurements of pressure pulsations and efficiency were done for the whole operating range of a high head Francis model turbine. The results will be presented in a similar diagram as the Hill Chart, but instead of constant efficiency curves there will be curves of constant peak-peak values. This way, it is possible to find an optimal operation point for the same power production, were the pressure pulsations are at its lowest. Six points were chosen for further analysis to instigate the effect of changing the speed by ±50 rpm. The analysis shows best results for operation below BEP when the speed was reduced. The change in speed also introduced the possibility to have other frequencies in the

system. It is therefore important avoid runner speeds that can cause resonance in the system.

Relevance to the current thesis

The measurement setup developed in the current thesis was utilized for the measurements, and the measurements were performed during the same measurement campaign. The analysis in the paper focuses on the pressure pulsations in variable speed configuration. The physics of the rotor-stator interaction in the current thesis can be utilized to describe some of the observed trends in the paper.

My contribution to the paper was the design of the measurement system and support during the measurements.

Paper 5

Signature analysis of characteristic frequencies in a Francis turbine

Trivedi, Chirag; Agnalt, Einar; Dahlhaug, Ole Gunnar; Brandåstrø, Bård Aslak

29th Symposium on Hydraulic Machinery and Systems
IAHR-2018

Abstract

This work investigates the unsteady pressure fluctuations in a model Francis turbine that are observed during steady state operation. Focus of the present study is to correlate pressure fluctuations between stationary and rotating components in the turbine. It is challenging and expensive to perform pressure measurements inside the rotating parts of the turbine. Pressure measurements at the runner upstream and downstream can help to understand the signature of pressure pulsations in the blade passages. To this end, one pressure sensor in the vaneless space, four pressure sensors in the runner and two pressure sensors in the draft tube cone were integrated to acquire pressure data. Detailed analysis of the acquired pressure data was carried out including statistical analysis, spectral analysis and coherence analysis. Further, stochastic and deterministic analysis of the pressure fluctuations in the turbine was carried out. The results showed that pressure data in the vaneless space and the draft tube could be used to understand the signature of pressure fluctuations existed in the runner.

Relevance to the current thesis

The measurement setup developed in the current thesis was utilized for the measurements, and the measurements were performed during the same measurement campaign. The discussion in the paper is focused on the signature of the runner pressure pulsations upstream and downstream the runner. Such understanding can only be achieved with detailed knowledge about the rotor-stator interaction and the pressure onboard the runner as presented in the current thesis.

My contribution to the paper was the design and performance of the measurements.

Paper 6

Variable-speed operation and pressure pulsations in a Francis turbine and a pump-turbine

Iliev, Igor; Trivedi, Chirag; Agnalt, Einar; Dahlhaug, Ole Gunnar.

29th Symposium on Hydraulic Machinery and Systems
IAHR-2018.

Abstract

The paper presents result from model measurements of the efficiency and pressure pulsation intensities for two low-specific-speed hydraulic turbines operated at variable speed, namely, one splitter-bladed Francis turbine marked with "F99" and one reversible pump-turbine marked with "RPT" and operated in a turbine mode. Both turbines have similar specific speeds, i.e. ($F99$)=21.88 and $nQH(RPT)$=27.26, and for their best efficiency points, both have similar guide-vane opening angles but different operating parameters (i.e., speed factor and discharge factor). Pressure pulsation measurements were conducted for a wide operating range and at specific locations in the (1) vaneless space and (2) draft tube. Histogram method was used to obtain the peak-to-peak amplitudes of the fluctuating pressure for all operating points used to construct the performance hill-charts of the turbines. To the best of the authors' knowledge, very little or no effort has been made so far to explore the amplitudes of pressure pulsations in the turbine when operated at rotational speeds specifically optimized for maximization of the hydraulic efficiency. Results show that operation of Francis turbines at optimized

rotational speeds can increase the hydraulic efficiency of the turbine, while decreasing or maintaining the same pressure pulsation amplitudes in the entire operational range. Also, it was found that the level of efficiency gain and reduction of the pressure pulsations is greatly dependent on the hydraulic design of the turbine and should be investigated individually for each case.

Relevance to the current thesis

The measurement setup developed in the current thesis was utilized for the measurements, and the measurements were performed during the same measurement campaign. The paper is focused on the benefits of variable speed operation seen with the efficiency and the pressure fluctuations in the vaneless space. The pressure fluctuations are strongly connected to the rotor-stator interaction discussed in the current thesis.

My contribution to the paper was the design of the measurement system and support during the measurements.

Paper 7

Pressure Pulsations and Fatigue Loads in High Head Francis Turbines

Solemslie, Bjørn Winther; Trivedi, Chirag; Agnalt, Einar; Dahlhaug, Ole Gunnar

29th Symposium on Hydraulic Machinery and Systems
IAHR 2018

Abstract

The Norwegian power system today includes a relatively large percentage of Francis turbines with a head of above 300m, in the world. This leads to a need to maintain and develop the national competence regarding the challenges connected to this type of turbine. The importance of this competence is increased by the fact that these turbines have a high installed capacity and are therefore crucial to the production stability. In the later years the old runners in Norwegian high head power plants have begun to show signs of fatigue. Taking the average age of these runners, which is approaching 45 years, into account, this may not be surprising. The surprising fact is that the same signs of fatigue, and in some cases total breakdown due to cracks, also occur in new and modern Francis runners. This leads to a hypothesis that the problem stems from sources other than the turbine runners themselves. The suspected cause of this reduction in the expected lifetime is the change the pattern of turbine operation to accommodate new intermittent energy in the power system and progress in the manufacturing technology enabling thinner blades. As an example the Horizon2020 project HydroFLEX initialised by the European Union aim to produce technology that allows for 30 start-stops per day for Francis runner. A

research project funded by the Norwegian Research Council and the Norwegian Hydro Power Industry, aim to increase the available knowledge regarding these high head Francis turbines. The research is done both on a basic and applied level where the focus is to increase the knowledge of the phenomena and to produce validation data for numerical simulations of said phenomena. The fundamental research focus on the hydrodynamic dampening applied on a hydrofoil within a high velocity water flow. The applied research is focused on the Francis-99 runner, a model runner of a High Head Francis turbine, which has been instrumented in order to study the Rotor-Stator-Interaction(RSI) and the structural response of the runner. The research areas both consist experimental and numerical studies, where the experimental results are used to validate the numerical. This paper presents the background of the project, the different activities and some preliminary results from selected activities. The aim of the paper is to introduce the project, participants and the participants view on the future of High Head Francis runners that do not crack due to RSI.

Relevance to the current thesis

The work in this thesis is connected through the HiFrancis research project. The measurement campaign were used for both purposes, the discussion for the thesis and the gathering of experimental data for the numerical verification in the project. The thesis is a part of the results in the HiFrancis project.

Paper 8

Fluid structure interaction of Francis-99 turbine and experimental validation

Østby, Petter T K, Agnalt, Einar, Haugen, Bjørn, Billdal, Jan Tore

Third Francis-99 workshop 2019

Abstract

The ability to predict a Francis runner's dynamic response to the exciting forces is paramount to avoid unwanted disintegration of the turbines components. In this article, each of the principal factors contributing to the dynamic response of the runner; eigenfrequency, mode shape, damping and pressure force, is individually examined and compared to the measured values from the Francis-99 runner. Even though the runner is made with a bolted connection between the blades and crown/band, and thus severely increasing the complexity, quite accurate predictions are possible using methods previously validated for massive and symmetric runners. All calculations are conducted on the best efficiency point and with eigenmodes corresponding to Nodal Diameter 4 as excited by the second harmonic of the guide vane passing frequency. The calculated natural frequency for the first two ND4 eigenmodes is within 5% of the measured values. Further are the calculated eigenmodes, forcing pressure field and hydrodynamic damping all within measurement tolerances with some minor exceptions.

Relevance to the current thesis

The experimental data used for the verification of the numerical calculations in the paper is the data published in Paper D. All the steps in the numerical calculations are directly connected to the different outputs from the pressure model in the paper D.

My contribution to the paper was the provided data for the experimental validation and some effort with the CFD calculations.

2019:219

Einar Agnalt

Rotor Stator Interaction in Low-Specific Speed Francis Turbines

Doctoral Thesis

Einar Agnalt

ISBN 978-82-326-4034-8 (printed version)
ISBN 978-82-326-4035-5 (electronic version)
ISSN 1503-8181

NTNU
Norwegian University of
Science and Technology

NTNU
Norwegian University of
Science and Technology

NTNU
Norwegian University of
Science and Technology
Faculty of Engineering
Department of Energy and Process Engineering

2019:219

NTNU